SPECTRAL ANALYSIS OF OUTPUT DEVICES, FROM PRINTING TO PREDICTING

by

Behnam Bastani
MSc. Computer Science, Simon Fraser University, 2005
BSc. Computing Science, Simon Fraser University, 2003

THESIS SUBMITTED IN PARTIAL FULFILLMENT OF
THE REQUIREMENTS FOR THE DEGREE OF

DOCTOR OF PHILOSOPHY

In the
School of Computing Science

SIMON FRASER UNIVERSITY

Summer, 2009

APPROVAL

Name: **Behnam Bastani**

Degree: **PhD**

Title of Thesis: **Spectral Analysis of Output Devices, from printing to predicting**

Examining Committee:

Chair: **Dr. Torsten Möller**
Associate Professor of Computing Science

Dr. Brian Funt
Senior Supervisor
Professor of Computing Science

Dr. Tim Lee
Supervisor
Computer Scientist, Cancer Control Research, BC Cancer Agency

Assistant Professor, Dermatology and Skin Science, UBC

Adjunct Professor, Computing Science, SFU

Dr. Ghassan Hamarneh
Internal Examiner
Assistant Professor of Computing Science

Dr. Raja Bala
External Examiner
Principal Color Scientist at Xerox

Date Defended/Approved: June 29, 2009

Declaration of
Partial Copyright Licence

ABSTRACT

The focus of this thesis is to develop and introduce algorithms that extend traditional colour reproduction from three dimensions to higher dimensions in order to minimize metamerism. The thesis introduces models that can accurately predict interactions between the primaries for non-linear output devices in spectral colour space. Experiments were designed and performed to aid in understanding how optimized the spectral characteristics of existing printer inks and display primaries are, and how the inks and primaries should be designed so that the accuracy of the reproduction is optimized.

The time and space computational complexity of the reproduction algorithms grows exponentially with the number of input dimensions. The algorithms for finding the best combinations of inks or primaries matching a given input reflectance become more challenging when the inks interact with each other non-linearly, as is usually the case in printers. A number of different methods are introduced in this thesis to handle gamut mapping and the colour reproduction process in higher dimensions. An ink-separation algorithm is introduced to find the ink combination yielding a chosen gamut-mapped spectral reflectance. Experiments with real inks for spectral colour reproduction were performed to compare the results of the reproduction against trichromatic colour reproduction on a 9-ink printer system. Finally, a new application of reflectance analysis in higher dimensions is introduced.

Keywords:
Spectral Reproduction, Spectral Printing, Modelling, Gamut Size, Bronzing, Gamut Mapping

Subject Terms:

DEDICATION

I would like to dedicate this work to my father and my mother, Bijan and Mahnaz and my lovely wife Parinaz.

ACKNOWLEDGEMENTS

I would like to thank Dr. Jeffrey Dicarlo, Dr. Jan Morovic and Dr. Tim Lee for assisting me through this research. I also thank Dave Hunt, Rick Becker and Amy Van Liew for their financial and management support at Hewlett-Packard Company.

Last, but not the least, I would like to express my heartfelt gratitude to my senior supervisor, Dr. Brian Funt, for his encouragement and for patiently supervising and guiding me for the past four years.

TABLE OF CONTENTS

LIST OF FIGURES

LIST OF TABLES

GLOSSARY

ΔE_{94}	DeltaE is a measurement of distance in $CIELAB_{94}$ space. A value of one indicates a just noticeable difference in colour.
$\Delta E_{CIECAM02}$	Changes in CIECAM02 colour space. A value of one does not necessarily represent one noticeable change.
CMYK	cyan, magenta, yellow, black. In some cases, K is used to represent the grey axis
$CIELAB_{94}$	International Commission On Illumination L a* b* colour space. This is a perceptually uniform colour space, where a unit of distance anywhere in the space is intended to represent the same amount of perceptual difference
LUT	Look Up Table
SVR	Support Vector Regression
XYZ	Used to refer to the CIEXYZ tristimulus space, where X and Z represent chroma and Y represents luminance.
TPS	Thin Plate Spline Interpolation

CHAPTER 1: SPECTRAL REPRODUCTION

Introduction

In comparison to standard colour reproduction, spectral reproduction aims to reproduce a given reflectance spectrum rather than produce a metameric reflectance spectrum that simply matches a given colour. This approach attempts to reduce the problem that can arise in metameric colour printing or display, which is that the reproduced colour may match under one illuminant, but not match well under some other illuminant. Clearly, if the reproduced output reflectance matches the input reflectance, the reproduced colour will match the input colour under all illuminants.

Spectral reproduction has application in many fields. In fine art reproduction, it is important to reproduce a painting in spectral space as closely as possible to minimize metamerism. Bastani et al. [60]) showed that if the reflectances of a given set are optimized, fine art reproduction accuracy can be improved by as much as 30%.

Another application is in high-end photography where professional photographers would like to capture their subjects as accurately as possible and in some cases reproduce them accurately. Soft proofing is another area where the end-user requires the displayed image to look as a close as possible to the real target under a range of illuminations.

Spectral colour reproduction becomes feasible when there is more than one possible primary combination to match a colour. In this paper, primaries refer to inks in a printer, phosphors or colour channels in a monitor or filters in a projector. To have a more accurate colour reproduction, a larger number of primaries are needed that are fairly independent from each other in their wavelength coverage. However, the larger the number of primaries, the higher the computational complexity of printing or displaying algorithms in terms of both time and space. In particular, standard gamut-mapping algorithms map colours within a 3-dimensional space and their computational complexity increases rapidly with dimension. For example, a gamut-mapping algorithm that relies on the computation of the convex hull of the measured gamut will not work for spectral data with, say, 11 dimensions since computing a d-dimensional convex hull of n points requires order $O(n^{floor(d/2)+1})$ operations.

Survey and Proposal Layout

The first complication in spectral reproduction is modelling the output of a device accurately in spectral space. The modelling becomes more complex when the primaries interact non-linearly such as in a printing environment. A naïve approach is to measure all primary combinations and store them in a database. This means if each ink dimension is sampled N times and there are D inks in the system, then there are N^D primary combinations to measure. This means that in order to measure ramps of 255 samples along each primary axis with 8 primaries in the system, there are $1.8x10^{19}$ patches to measure and store, which is not practical.

The non-linear interaction of the inks with each other and with the paper (medium) makes modelling the printer output an important component of the research. Since the complexity of the proposed algorithms grows exponentially with the number of inks, spectral modelling of an N-ink printer system is a particularly significant topic. Two possible opportunities are discussed in thisthesis: The first is to reduce the necessary number of patches to measure by considering constraints such as ink limiting (amount of the ink that a medium can accept). The second path considers lowering the complexity of the printer gamut space before applying any interpolation method.

Spectral characteristics of the primaries and their interaction types, whether linear or non-linear, have the largest effect on an output device gamut size and the spectral reproduction accuracy of the devices. For instance, the optimum selection of a set of inks for a printer may have less overlap or be more spectrally independent of each other. The second part of this report presents methods for optimizing the spectral characteristics of the primaries to improve the spectral reproduction of a given system. It also presents how the effect on the output device gamut and spectral gamut space of a variation in a primary reflectance characteristic can be evaluated.

Given a set of ink reflectances and a device output model, the next challenge is gamut mapping in spectral space. The traditional gamut mapping algorithms work in three dimensions (CIELAB or CIEXYZ space) and they typically assume that the gamut shape is convex. The complexity of calculating the convex hull is another challenge that grows exponentially with the

dimensionality of the data. Two different gamut mapping approaches are considered in this paper.

To evaluate how the spectral colour reproduction can help professional users, an experiment is conducted to understand whether the proposed algorithms are feasible in real life, given the available set of inks and printer technology.

The last part of this study proposes other applications of spectral colour analysis beside spectral colour reproduction.

CHAPTER 2: MATHEMATICAL PRELIMINARIES

In this section we introduce some mathematical concepts and notation that will be used throughout the thesis.

Thin Plate Spline Interpolation

Thin Plate Spline, or TPS, is an interpolation method that finds a "minimally bended" smooth surface that passes through most input data points. The name "thin plate spline" came from the observation of bending a thin sheet of metal. In the physical setting, the bending of the plate is known to be orthogonal to the original plane structure. In order to apply this idea to the problem of coordinate transformation in a 2 dimensional space, the lifting of the plate can be interpreted as a displacement of the x or y coordinates within the plane. This means, two thin plate spline functions (basis) are needed to specify a two-dimensional coordinate transformation. The basis functions for TPS are the Radial basis functions [13].

A radial basis function (RBF) is a function that its output value depends on the Euclidean distance from the neighbouring input points, referred to as center points. For TPS, a smoothness constraint is added to the fitting, where the smoothness constraint minimizes the derivative variation between the output points.

Xiong et al. extended the TPS model to N-Dimensions and applied it to illumination estimation successfully [61].

For spectral printer modeling, TPS is used to find a set of continuous function that each maps between the set of inks and oneof the output dimensions. For instance if the output spectral reflectance of an 8-ink printer is measured from 380nm to 730nm with a 10 nm sampling, TPS is used to create 36 separate functions mapping from the 8 input dimensions to each reflectance wavelength 380nm, 390nm, …. to 730nm, separately.

Principal Component Analysis

Principal Component Analysis (PCA) [10] is a mathematical technique to discover correlation behaviour between a set of variables. The method uses the correlation information to break down the set of variables into subsets that are relatively independent of one another. Variables in each subset are correlated with one another and are largely independent of other subsets.

PCA is based on the orthogonal linear transformation of variables into a new coordinate system such that in this new coordinate system, the largest variance by any projection of the data falls on the first coordinate. Similarly, the second largest variance is on the second coordinate and so on.

PCA is widely used in many fields including signal processing, statistics and computer vision.

Least Square and Non-Negative Least Square Method

Least Squares regression, [11], is a mathematical method to solve systems that have more equations than unknowns. Least Squares regression finds the best-fitting curve to a given set of points by minimizing the sum of the squares of the offsets (residuals).

Non-negative least squares finds the best fitting curve using the Least Squares method with the additional constraint that all the coefficients of the fitting should be non-negative. In this study the non-negative least square implementation from Matlab is used [92].

ISOMAP and Multi-Dimensional Scaling

Multidimensional scaling (MDS) is a classical technique for mapping the input data to a lower dimensional space, subject to the constraint that pair-wise distances between data points are preserved as much as possible. The latter is accomplished via minimization of a cost function. The classical technique uses the Euclidean distance metric.

ISOMAP or complete isometric feature mapping is a variant of MDS that replaces the Euclidean distance with the geodesic distance.. For certain types of data, ISOMAP can be more effective in uncovering the underlying structure and dimensionality. Geodesic distance can be computed with a number of techniques, a common one being Dijkstra's algorithm. **Error! Reference source not found.**[62] [88].

Dijkstra's algorithm finds the shortest path between the vertices in a graph with nonnegative edge cost. This algorithm will be used to compute the geodesic distance between a pair of points (detailed below). The time complexity of the algorithm is $O(N^2)$, where N is the number of nodes (vertices) in a graph.

Specifically, the geodesic distances represent the shortest paths along the curved surface of the manifold. This can be approximated by a sequence of short steps or “hops” between neighbouring sample points. Since the manifold is not known ahead of time, some heuristic should be used to define the neighbours of a given point. In this thesis, the neighbours of a given point are defined as those points whose path length to the given point are smaller than a threshold. The threshold may vary based on how the points in a database are placed relative to each other. If the threshold selected is too large then almost all the points are selected as neighbours of each other and the ISOMAP technique may not be able to map the space into an optimal low-dimensional space. On the other hand, too small a threshold can cause a break in the space with the result that ISOMAP may map the input space into multiple low-dimensional spaces.

In this study, a search is done to find a threshold that optimizes the dimensionality reduction while stillincluding all the measurements points from the printer gamut in a single space.

After selecting the neighbourhood threshold, ISOMAP then applies MDS to the geodesic, rather than straight line, distances to find a low-dimensional mapping that preserves these pair-wise distances.

The Swiss Roll is a common example used to visualize the difference between geodesic and Euclidean distances. Figure 1 shows a Swiss Roll in 3 dimensions where points A and B have a small Euclidean distance (dotted line). Figure 2 shows the Swiss Roll after the ISOMAP transformation into 2 dimensions. The figure shows that the two points have a large Geodesic distance despite a small Euclidean distance relative to the other neighbouring points.

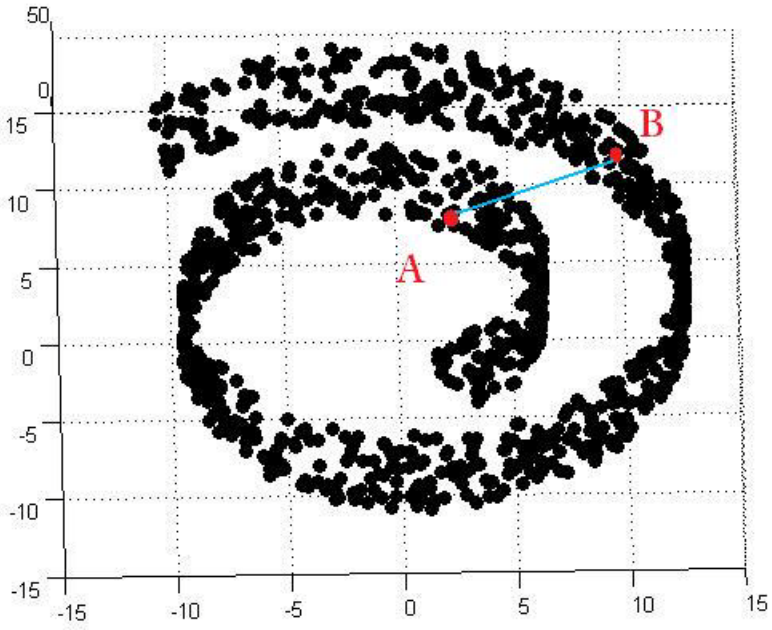

Figure 1: Swiss Roll representation in 3 Dimensions [86]

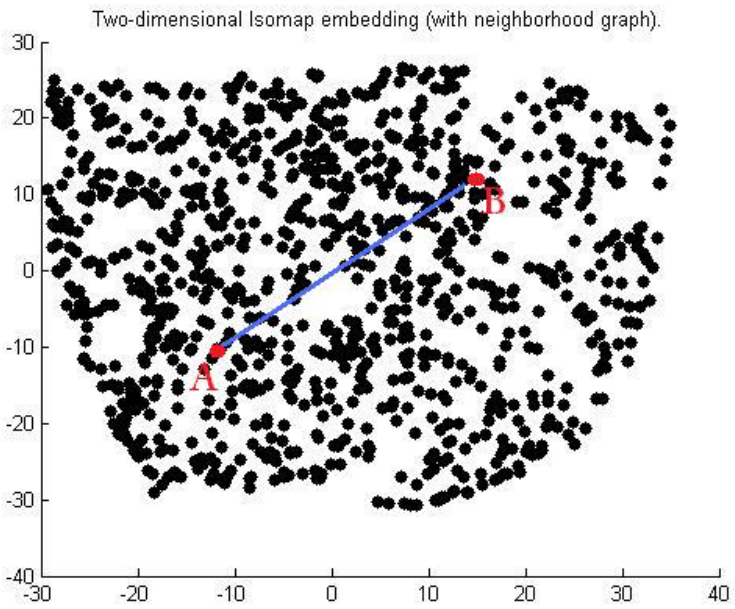

Figure 2: Un-folded Swiss Roll data into 2 dimensions using ISOMAP. [86]

CHAPTER 3: PRINTER MODELLING

As discussed earlier, modelling a device's output accurately in spectral space is essential to enabling spectral reproduction. In electronic displays, since the light is added quite linearly, simple linear approaches are used to model the displays' outputs [1][2][3][4]. The situation is quite different in a printer where inks behave in a non-linear fashion.

In this section, some basic background on printing systems and some well known printer models are presented. In addition, two possible methods to simplify and improve the accuracy of printer modelling are proposed.

Light and Media Interaction and the Dot Gain Phenomenon

When light hits a surface (medium), a percentage of the light gets reflected and the rest is absorbed. These two percentages are referred to as the scattering and absorption coefficients. Figure 3 illustrates this effect.

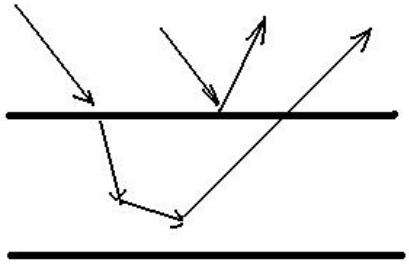

Figure 3: Primary Interactions between Light and Medium (paper) are scattering and absorption ([75]).

The reflectance behaviour for a material is different. For a fluorescent material , the material (molecules) absorbs a photon (UV) and then emits a photon (visible) of lower energy (longer wavelength). The effect of fluorescent materials was not considered in the research reported here.

In the printing environment, when a drop of ink is put on the medium, there are several physical and chemical interactions that happen which add to the complexity of the system. The most common way of reproducing images on a print is by half toning. Half toning produces different levels of grey or colours by small dots with maximum colour density but with varying local fractional area coverage, printed on a white substrate [12]. Whenever such a reproduction is used, an effect that is referred to as dot gain happens, which makes the actual image appear darker than what would have been expected from a perfect reproduction. There are two parts to dot gain: physical dot gain and optical dot gain. Physical dot gain occurs because the dots gain in physical size due to imperfections in the image transfer from the original to the print (Figure 4). A typical reason for physical dot gain is ink smearing and spreading in the printing process which is normally referred to as ink and media interaction.

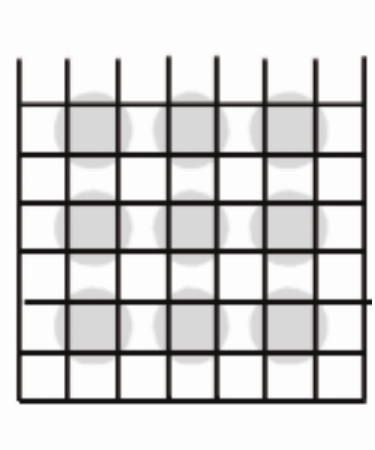

Figure 4: Physical dot gain causes a drop of ink to cover a larger area that expected from a perfect linear production.

Optical dot gain is the effect of a dot appearing larger than its actual size. Optical dot gain occurs because the half tone dots are printed on a scattering substrate (medium in printing systems) (Figure 5). The spread of light in the medium causes a shadow around the rim of the dots which, in turn, causes the dots to appear larger, represented as Δa_{opt} in Figure 5.

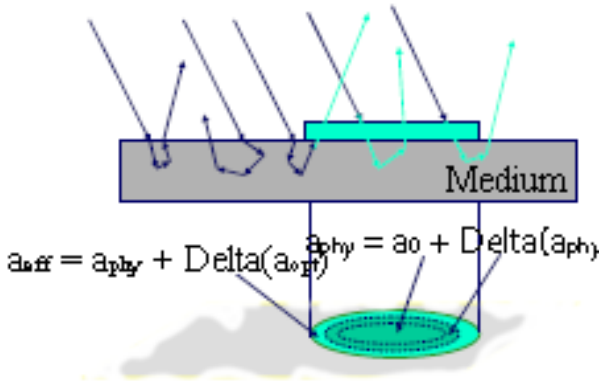

Figure 5: Optical dot gain occurs because the halftone dots are printed on a scattering substrate. a_0 shows the original drop size, Δa_{phy} is the physical dot gain and Δa_{opt} is the optical dot gain.

Figure 4 shows the dot gain curve relative to the ink density. It shows that the maximum dot gain occurs around 50% ink density, where there is enough

space left for physical dot gain and optical dot gain without interacting with neighbouring dots.

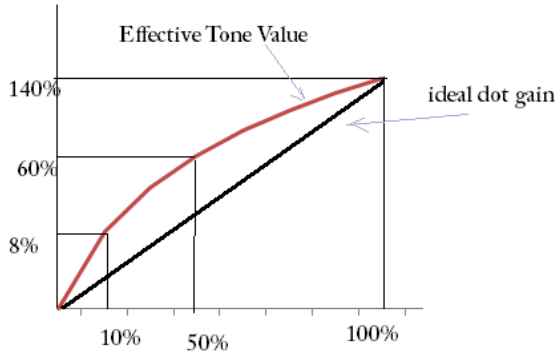

Figure 6: Dot gain curve. Maximum dot gain occurs around 50% of area coverage, where there is enough space left for physical dot gain and optical dot gain without interacting with neighbouring dots.

Modelling Ink and Medium interaction

In this section, performance of the three best known approaches for modelling printer output are summarized and compared.

Linear Model (Murray Davies) [15], [9], [17]

The Murray-Davies model is based on the assumption that the reflectance of a half tone cell adds up linearly. This model estimates a single ink reflectance on a medium using the following linear equation:

$$R_\lambda = aR_{\lambda,100\%} + (1-a)R_{\lambda,paper} \quad \textbf{(1)}$$

where *a* is a function of dot area coverage and $R_{\lambda,100\%}$ is the spectral reflectance of ink at 100% dot area coverage. $R_{\lambda,paper}$ is the reflectance of the white paper.

The Murray-Davies algorithm depends on the assumption of linear interaction between ink dot area coverage and the medium. As discussed earlier, because of some physical (dot gain) and chemical interaction between ink and medium, this assumption does not always hold.

Kubelka Munk Model [15], [16]

The Kubelka Munk model is the most popular method for modelling printer output. Kubelka Munk has a relatively simple equation. Its two parameters (K and S) represent reflectance and transmission from a surface. Kubelka and Munk examined the reflectance of a material having a thin layer of colorant in contact with the opaque surface of the material [14], [15]. Kubelka-Munk theory is based on the assumption that a colorant can be broken into a large number of thin layers with equal optical properties (Figure 7). Figure 7 shows a colorant of thickness X and two diffuse light fluxes I and J. The fluxes represent the overall light that each layer receives or passes through each layer. The idea is that once a colorant ink is broken into smaller layers, fluxes for each layer can be summed to obtain the overall flux of the colorant.

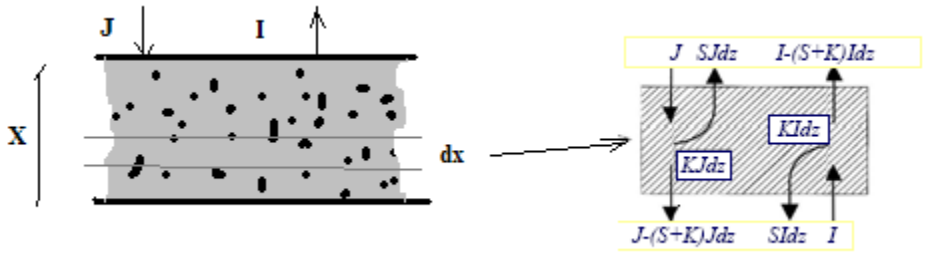

Figure 7: Kubelka Munk absorption and scattering theory.

In this theory, as the light goes farther down the colorant layer, the magnitude of downward flux (J) is decreased due to absorption and scattering of the layers. The scattered portion of downward flux (J) will be added to upward flux I. Similarly a portion of upward flux I is absorbed and added to downward flux (J). Using differential equations, the downward and upward fluxes can be represented as:

(2)

$$d_i = -(S + K)\, I\, d_x + S_j\, d_x$$

$$dj = -(S+K)\, J\, d_x + S_i\, d_x$$

where K represents the absorption coefficient and S represents the scattering coefficient. If P is the ratio of J to I, the above equation can be re-written as:

(3)

$$\frac{dp}{dx} = \frac{d(J/I)}{dx} = \frac{I(dJ/dx) - J(dI/dX)}{I^2}$$

Re-arranging the above equation and applying boundary conditions results in:

(4)

$$\int_0^x dx = \int_{Rg}^{R} \frac{dp}{S - 2(K+S)\,p = Sp^2}$$

By solving the above equation for R, the famous Kubelka Munk equation

(5)

$$R_\lambda = \frac{1 - R_{\lambda,g}[a_\lambda - b_\lambda \coth(b_\lambda S_\lambda X)]}{a_\lambda - R_{\lambda,g} + b_\lambda \coth(b_\lambda S_\lambda X)}$$

is obtained, where *a* equals 1+K/S and *b* equals $(a^2 - 1)^{1/2}$. To solve for the two unknowns (K and S) in the above equations, two equations are solved by measuring two ink reflectance samples.

Measurement Requirements: the Kubelka Munk model only requires measurement of individual inks and the blank medium. If there are N inks in the system, this model requires only N+1 measurements. The model assumes that ink and media interactions are homogenous. This model is widely used in the paint industry.

The accuracy of the model is fairly good in predicting hue; however, it has problems in predicting chroma of two or more inks overlapped [15].

Neugebauer Model ([18], [20], [21], [15])

The monochrome Murray–Davies model was extended to work for colour cases and to handle multiple inks by the 1937 landmark work of H. E. J. Neugebauer ([18]). The Neugebauer model predicts the reflectance of multiple colorants by summing the products of the fractional area coverage of each colorant and its reflectance at full area coverage:

(6)

$$R_\lambda = \sum_{i=1}^{N} a_i R_{\lambda,i}$$

N represents the n Neugebauer primaries at maximum ink coverage. For instance, for a 3-colorant system, CMY, there are 8 primaries: medium, single separations (C, M, Y), two-colour overlap (CM, MY, CY), and three-colour overlap (CMY=K). a_i is the area coverage of each primary. There are two common assumptions used when calculating the area coverage. The Demichel model, [19], assumes that the half tone dots are printed randomly on the medium. For instance, the area coverage of two inks in a 3-ink system is no more than the joint probability of these two inks. The equation below shows the area-coverage calculation using the Demichel model. C represents the percentage of cyan ink from maximum coverage. Similarly, M and Y are defined as the maximum area coverage of the magenta and yellow.

(7)

$$
\begin{aligned}
a_w &= (1-C)(1-M)(1-Y) \\
a_c &= C(1-M)(1-Y) \\
a_m &= (1-C)M(1-Y) \\
a_y &= (1-C)(1-M)Y \\
a_{cm} &= CM(1-Y) \\
a_{cy} &= C(1-M)Y \\
a_{my} &= C(1-M)(1-Y) \\
a_{cmy} &= CMY
\end{aligned}
$$

The second dot area coverage, Dot-on-Dot, assumes perfect dot placement overlap.

Similar to the Murray-Davies model, the linear interaction assumption fails for the Neugebauer model because of optical and physical dot gain. In 1951,

Yule and Nielsen introduced a method to model nonlinear interaction of ink and medium [20]. They showed that the nonlinear relationship between measured and predicted reflectance could be well described with a power function. Based on their result, they introduced a modification to the Murray-Davies model as:

$$R_{\lambda}^{1/n} = a_i R_{\lambda,100\%}^{1/n} + (1-a_i) R_{\lambda,paper}^{1/n} \quad \textbf{(8)}$$

where n is a parameter to describe the behaviour of light spreading in the medium. Typically, a nonlinear optimization is used to find the best Yule-Nielson value. By applying Yule-Nielson theory to the Neugebauer model, the Yule-Nielson Neugebauer Model is obtained:

$$R^{1/n}{}_{\lambda} = \sum_{i=1}^{N} a_i R^{1/n}{}_{\lambda,i} \quad \textbf{(9)}$$

To improve on the accuracy of the Yule-Nielson Neugebauer model, the ink space can be measured at a higher resolution (larger number of cells). This extension is referred to as the Yule-Nielson Cellular Neugebauer (YNCN) Model [24].

Measurement Requirement: If there are K colorants (inks) in the system there are 2^K Neugebauer primaries and, thus, 2^K measurements are needed. By adding a larger number samples to the system (r samples), there will be r^K

measurements required. This model assumes a linear relationship between reflectance and coverage percentage in a space similar to log space.

Challenges of Ink Modelling and Printer Characterization

The Yule Nielson Cellular Neugebauer (YNCN) model is the most accurate model for characterizing the printer gamut in spectral space. However, as was discussed earlier, if there are K inks in the system with r samples along each ink dimension, there will be r^K samples to be measured. This means the number of measurements required for this model grows exponentially as we add more inks or try to increase the number of samples.

For spectral reproduction purposes, there is a need for a large number of inks in the system (around 9 or 12) and Tzeng et al. [26] have only extended the YNCN model to a 6-ink system accurately. One challenge would be to be able to extend this model to an N-ink printer system where N can be as large as 9 or 12 dimensions.

To reduce the complexity of the model, three concepts are considered in this paper. First, linearization of each ink before printing the training patches can be used to keep the Neugebauer cells in uniformly spaced locations and further reduce the necessary number of steps per colorant. Second, the physical constraints of the paper, such as the amount of ink it can reliably absorb, can be used to reduce the potential patches to only the patches that are physically possible to be printed. The third approach is based on a smarter transformation

of the printer gamut before interpolations are applied. This approach is a sophisticated version of the linearization method discussed in the first approach.

Smarter Sampling: Uniform Sampling in Perceptual Colour Space

In essence, the Cellular Neugebauer model is a piecewise linear model, and the Yule-Nielsen correction reduces nonlinearity related to dot gain, but does not capture all of the possible curvature caused by ink interactions, etc. One method to capture all the curvatures is to increase the sampling range. Using Taylor series expansion, we can expect that, if we increase the sampling size of the gamut indefinitely (distance between neighbours → 0), the correlation between two very close neighbours (ink combinations) can be represented linearly.

As discussed earlier, increasing sampling size is not practical, so another method can be to find a better process to capture the non-linearity between input ink combinations and output spectral reflectances.

Linearization is a common transformation method used to improve accuracy of characterization methods for the output of electronic displays, such as CRT and LCD devices [1]. The intent of this method is to remove some of the non-linearity between input channels and output performance by linearizing input channels against the output performance of the desired device.

The original design of YNCN model calculates the weights used for the interpolation based on variation in the input (ink density) and not what the variation in the input channels (ink densities) can cause in the output spectral

reflectance. By linearizing the input channels against the output reflectances, the weights for YNCN interpolation can be better adjusted so that fewer points are required to be used in interpolation. Raja Balasubramanian [87] introduced a method of linearizing the YNCN sampling to improve the modeling performance and reduce number of prints required.

Physical Constraint: Ink Limiting

Printing substrates commonly have a certain ink limit beyond which the page is too saturated to print. In the inkjet realm this leads to issues such as cockle, bleed, dry time and gloss non-uniformity. It is not reasonable to print and measure patches that violate the ink limit of the substrate medium. This observation can be used to significantly reduce the number of patches required to measure for the YNCN model. By imposing the constraint that it is not necessary to print or measure patches that violate the ink limit, the number of data points to measure for the model can be reduced by up to 97%. The following is a mathematical analysis of the effect of ink limiting on the number of training data points that can be printed without exceeding the physical ink limitation of the paper.

In an inkjet printer, the maximum dispensable weight-per-unit-area W^i for each colorant *i* is defined by factors such as drop size, nozzles per inch, and number of passes. This value varies for each ink, and is generally between 50% and 100% of the overall ink limit of the medium. The "percent under limit" for each ink *i* is defined as $U_i = W_i / InkLimit$.

Given the number of colorants, *k*, the number of steps per colorant, *n*, and the percent under limit, U_i, the complexity subject to the ink-limit constraint can be computed. For simplicity, it is assumed that $U = min(U_i)$ for all inks, which will error on the side of over-estimating the complexity.

In the case where $U = 1$, the printer is capable of delivering exactly the media ink limit with each ink individually. In two dimensions, the valid sample space is a triangle defined by (0,0), (n,0), (0,n) as shown in Figure 8.

In general, the space of printable patches can be represented by a k-simplex (hyper-simplex) defined by the origin and the points along each colorant axis at a distance of n. The area of such a region is [80] :

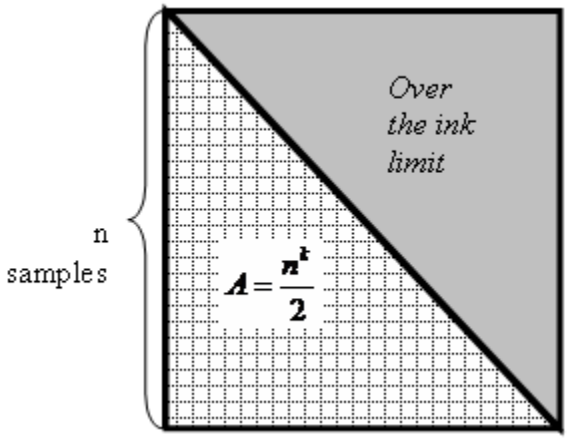

Figure 8: Valid Patches for 2 inks with U=1.

(10)

$$A_{U=1} = \frac{n^k}{k!}$$

In the case where U_i is between 0.5 and 1, the valid space is a hyper-cube with sides of length n, and one corner removed by the ink-limit hyper-plane, as shown in Figure 9.

The volume of this region can be computed by calculating the area of the k-simplex formed by the ink-limit hyper-plane and subtracting the corners that are outside the printable hypercube, resulting in the following equation:

(11)

$$A_{U=(0.5,1)} = \frac{\left(n/U\right)^k}{k!} - k\left(n/U - n\right)^k$$

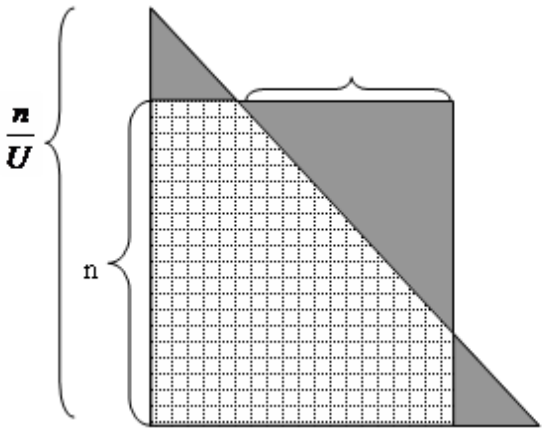

Figure 9: Valid Patch Space for ½ < U < 1.

For values of U less than 1/k, the ink-limited hyper-plane does not intersect the dispensable ink hyper-cube, so the complexity reverts to n^k. Computations for 1/k < U > 1/2 are more complex, and are not generally needed since the colorants are generally defined with $U \geq 1/2$.

To determine how effective this constraint is on reducing the number of measurement points required for the YNCN model, this constraint was implemented on two training sets, one on glossy photo media and the other on plain media. In the case of glossy media, 4 steps along the primaries on an 8-ink

printer required 6048 patches – a reduction of 91% over n^k. On plain media, the same test required 2175 patches – a reduction of 97%.

The cause for the difference in savings between glossy and plain media was related to a difference in the definition of the primary ink axes on those two media. One of the inks was not intended for use on glossy media, so its linearization table on glossy media was defined such that very little ink would be dispensed even at 100% fill. As a result, the U-value for that ink was very low and no clipping occurred in that dimension.

By applying these constraints, the number of training data points is reduced substantially, which can cause some points in the printer gamut not to have all the neighbours required for interpolation. The next section discusses how the YNCN model can be modified to handle cases that do not have all the points for the interpolation.

Handling the Missing Points (Neighbours)

The YNCN model is based on interpolation between neighbouring primaries, some of which may have missing data because of the ink-limit constraint. This poses a challenge for the interpolation operation.

To enable the YNCN model for *N* inks with missing neighbours, the weights for all neighbours are computed, the sum of weights for the missing neighbours is recorded as a "missing score" or M-score value for each interpolated point. The missing weights are then set to zero and the remaining

weights redistributed using a factor of *1/sum(weights)* to re-normalize the sum back to 1.

To redistribute the weights more accurately, the original Neugebauer model is modified so that weights are calculated based on the linearized distance of the neighbours in CIELAB colour space. For instance, if the variation along the yellow primary is smaller than the gray primary, neighbours of the gray primary will get a larger portion of the weights from missing neighbours.

The second method that was considered handling the missing points was to extrapolate Neugebauer primaries so that the training data set is populated enough to cover missing neighbours for a given data set. The idea is that if the printer spectral gamut is extrapolated slightly, some of the missing points might be recovered and redistribution of interpolation weights avoided.

The complexity of typical extrapolation algorithms grows rapidly as the dimensionality of the input data grows. A linear extrapolation method, applied to one ink at a time, was used in this investigation. For a missing neighbour, P, in an N ink printer system, N separate interpolations are calculated considering one of the N inks at a time, resulting in N separate spectral predictions. For each wavelength, weighted sums of the N predicted reflectances are used to calculate the predicted reflectance at the same wavelength for the missing neighbour.

Smarter Transformation and More Advanced Interpolation Method

One of the other constraints of using the YNCN model, besides requiring a large number of training points, is the requirement for uniform sampling along each axis.

Also, as it was discussed earlier, the Yule-Nielson factor was introduced to remove some of the non-linear interaction of ink and medium. Other techniques such as ISOMAP can be considered to better capture any nonlinearity in the ink and medium and thus improve the accuracy of the interpolation.

Improving Printer Characterization using TPS interpolation based on Manifold Transformation

One method considered in this study was to use a printer model based on Thin Plate Spline (TPS) interpolation. This model has the advantage that the number of training points and the computational requirements grow much more slowly than in the case of the YNCN model. In addition, TPS does not require training data to be sampled on an evenly spaced grid.

TPS can be used to find a continuous function that maps between the set of inks and each of the output dimensions. For instance if the output spectral reflectance of an 8-ink printer is measured from 380nm to 730nm with a 10 nm sampling, TPS is used to create 36 separate functions mapping from N input dimensions (if there are N inks in the system) to each reflectance wavelength in 10mm increments from 380nm to 730nm,

Many spaces appear to have a high dimensionality in a linear space, but actually have lower intrinsic dimensionality as the Swiss Roll example discussed earlier. It is possible that the lower dimensional space has a more linear correlation with the input values that created the space.

One approach that is examined was to improve the printer modeling algorithms by transforming the output space (printer gamut) to a space that has a simpler correlation to the input data (ink densities). After the transformation is applied, TPS interpolation is used to interpolate between input ink densities and transformed printer gamut data points.

The new interpolation method has the following steps:

1. Find the geodesic distances of spectral reflectances in a printer gamut
2. Map the printer gamut into a new space (typically of lower dimension) using the geodesic distances (ISOMAP Technique)
3. Create continuous functions between input ink combinations and transformed gamut space

Data Collection

An 8-ink printer with the following inks was used to study performance of the model: cyan, magenta, yellow, light cyan, light magenta, black, gray, and light gray. The results are based on 6048 patches for training and 939 patches for testing. The patches were printed on glossy media with an ink limit of either 1.5 or 2 drops of ink (depending on the ink type).

A GretagMacbeth Spectralino [5] was used to measure the spectrum reflectance of the printed patches consisting of 10nm sampling from 380nm to 730nm. The Spectralino has an accuracy of around 0.30 ΔE_{94} between two different sets of measurements under the D50 illuminant. The printer has an average 0.75 ΔE_{94} page-to-page variation (including instrument variation).

Implementation

Drops of inks which are intended to fall on top of each other during the printing process can fall on top of each other (Dot-on-Dot), beside each other (dot-by-dot) or have a more random placement (Demichel). There are modeling methods to capture each scenario.

In this section, both Demichel [23] and Dot-on-Dot [81] models were implemented. The Dot-on-Dot model assumes perfect dot placement during printing, whereas the Demichel equations assume a more random dot placement, which is more suited to ink-jet printers with a half toning process done to redistribute the dot placement.

Three different methods for handling missing points in the model (missing neighbours) were implemented and studied. The three models are as follows: Distributing weights for missing neighbours with and without some linearization or extrapolating Neugebauer primaries to fill in missing neighbours as much as possible. These three approaches are referred to as Lin=0, Lin=1, Extrap=1.

In order to find the proper Yule-Nielson correction factor, a search was done to find the best value. The search used starts with incrementing the Yule-

Nielson factor and stops if the prediction accuracy is within 0.10 ΔE_{94} for the subsequent Yule-Nielsen values.

Results

Results: Modified YNCN (Smarter Sampling and Dealing with Missing Neighbours)

Table 1 shows the accuracy of the model for both Dot-on-Dot and Demichel dot placement approaches. The results are shown both in ΔE_{94} for D50 illumination and spectral difference calculated as Root Mean Squared (RMS) difference between prediction and input reflectances.

Table 1 shows that the Demichel model is more accurate than the Dot-on-Dot model for predicting reflectance of multi-ink systems and modeling. The data also shows that YNCN performance is improved by linearizing the training data before calculating the interpolation points. Figure 10 shows that the main error in the YNCN prediction comes from the data points that have too many missing neighbours. Table 2 also shows that correlation of the error with the missing neighbours when different methods are used to redistribute weights of the missing neighbours. The important conclusion taken from Table 1 is that a simple linear extrapolation of the training data point to recover as many as missing neighbours is more effective than redistributing the YNCN weights for the missing neighbours.

Table 1: YNCN Performance for an 8-ink printer with missing Neighbours. Mean, Max and Std represent average, maximum and standard deviation of the error respectively [68]

		ΔE_{94}	**RMS**
Demichel, YN=5.2, Lin=0	Mean	2.43	0.0072
	Max	10.92	0.048
	Std	1.49	0.0057
Demichel, YN=5.1, Lin=1	Mean	2.31	0.0064
	Max	10.73	0.0613
	Std	1.34	0.00542
Demichel, YN=4.1,Extrap=1	Mean	1.48	0.0047
	Max	5.12	0.0284
	Std	0.81	0.00299
Dot-on-Dot, YN=7.5, Lin=0	Mean	8.54	0.0363
	Max	37.46	0.2848
	Std	5.42	0.0367
Dot-on-Dot, YN=7.3, Lin=1	Mean	7.87	0.0313
	Max	29.38	0.257
	Std	5.08	0.0326
Dot-on-Dot, YN=7.1,Extrap=1	Mean	3.00	0.00584
	Max	11.75	0.0471
	Std	1.56	0.00465

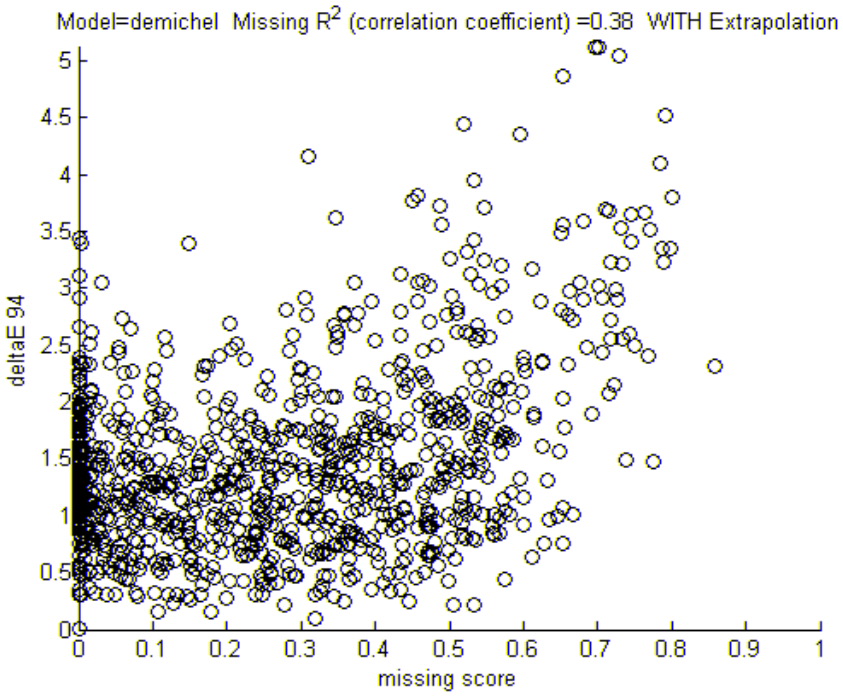

Figure 10: Correlation of missing neighbours and error for Extrap=1 method, R2=.38.

Table 2: Correlation between missing score (percentage of missing neighbours) and error in the model (ΔE94)

Method	Correlation
No Extrapolation, No Linearization (Lin=0)	0.63
No Extrapolation, with Linearization (Lin=1)	0.48
Extrapolation, No Linearization (Extrap=1)	0.38

Result: Manifold Based Printer Model

All the existing printer modeling algorithms including the YNCN model are based on different interpolation techniques. The accuracy of most interpolation techniques is improved if the input data has a simple correlation with output data. For this reason, the Yule-Nielson factor is used in the YNCN model to transform the spectral output to a space that has a more linear relation to the input ink densities.

Figure 11 shows a dimensionality analysis of the printer spectral gamut of the 8-ink printer system before and after applying a Yule-Nielson value of 2 (Note: Using a Yule-Nielson factor of 2 is effectively applying logarithmic transformation of base 2). Principal Component Analysis (PCA) is applied to the data set, and residual variance between reconstructed data from PCA basis and original data is plotted in the Y axis. The X axis represents the number of bases used to reconstruct the input data.

The figure shows that, after applying a non-linear transformation to the printer gamut, the dimensionality of the gamut is reduced to almost 4 rather than 6 dimensions.

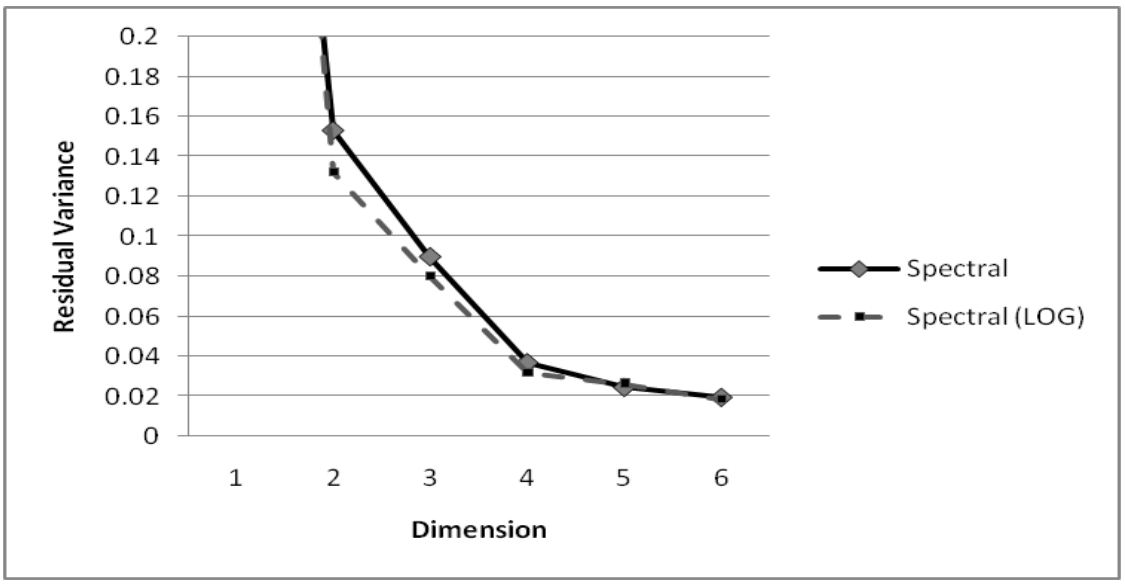

Figure 11: Residual error of spectral recovery as a function of reflectance dimensions. The data is for spectral measurement and spectral measurement after a logarithmic transformation.

Knowing that the Yule-Nielson transformation was effective in reducing the dimensionality of the printer gamut, the ISOMAP transformation was used to test whether this transformation can be optimized and, thus, improve the printer modeling algorithms. Figure 12 shows that after the ISOMAP transformation is applied to the printer spectral gamut, the dimensionality of the system is reduced to 3 dimensions. The figure also shows that applying a Yule-Nielson transformation after ISOMAP transformation does not help with the dimensionality reduction.

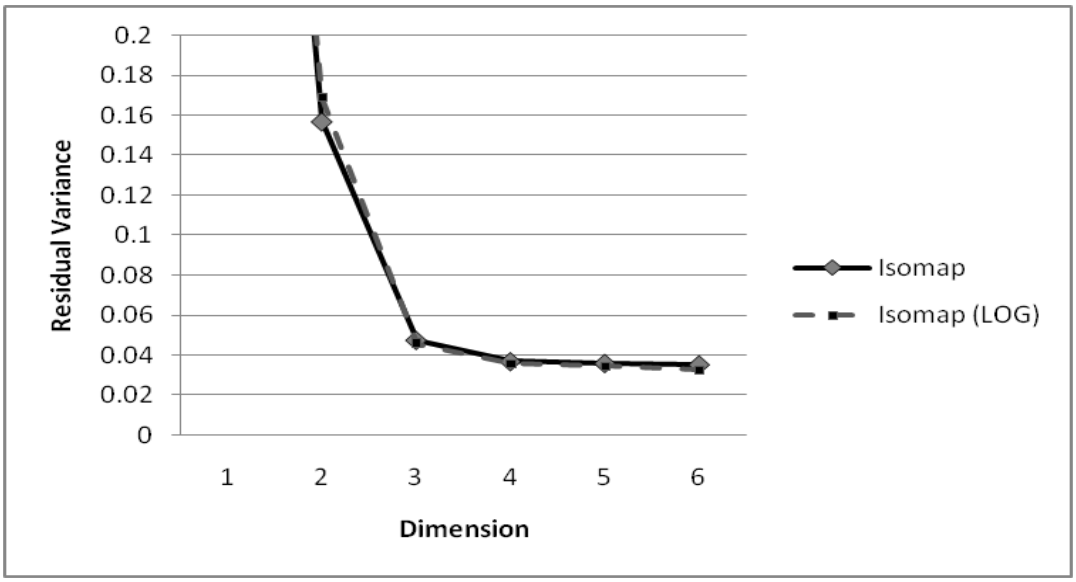

Figure 12: Residual error for spectral recovery of the 8-ink printer spectral gamut after ISOMAP transformation. ISOMAP (LOG) shows when a Yule-Nielson of value 2 is applied to the ISOMAP transformed gamut data.

The first important observation that can be drawn from this comparison is that the printer spectral gamut may not be as complex as it has been observed by looking at the gamut space directly. Knowing how neighbouring points that created the printer spectral gamut are connected to each other can be used towards space complexity reduction of the printer gamut. The second observation is that knowing which ones are the true neighbours of a point on the printer gamut and how they are connected to the point of interest, more accurate weights than those yielded by the YNCN model should be calculated for the printer model.

To evaluate the accuracy of the new modeling algorithm, TPS interpolation was used to interpolate between ink density and output spectral reflectance before and after the ISOMAP transformation. Since the ISOMAP calculation has higher time complexity than the YNCN algorithm, the training

sample size was reduced to half of the training sample size used for the YNCN model in order have a similar or slightly faster modeling algorithm. The samples were selected randomly from the ones used in the YNCN model.

Figure 13 and Table 3 present the performance of the TPS interpolation to predict the spectral gamut directly and after ISOMAP transformation. The results are compared against the YNCN model. The data shows that applying TPS interpolation to predict the spectral printer gamut directly, given ink densities, has poor performance. The performance is slightly improved if the interpolation is applied after the printer gamut data has gone through a logarithmic transformation. This can be explained by knowing that the transformed space has a lower dimensionality (as presented in Figure 11).

On the other hand, applying TPS interpolation after the ISOMAP transformation is as accurate as the YNCN model, when only half of the training data points were used for this new model.

Table 3: Performance of Geodesic (ISOMAP) and Linear based modelling of the 8-ink printer system using TPS (Thin Plate Spline) interpolation. ISOMAP (LOG) and Spectral (LOG) represents TPS interpolation applied to each space after they have gone through a logarithmic transformation (which is similar to having the Yule-Nielson factor equal to 2).

	RMS		**ΔE_{94}**	
	Mean	**Max**	**Mean**	**Max**
YNCN	0.0047	0.0284	1.48	5.12
Spectral	0.0097	0.1027	3.1	47
Spectral (LOG)	0.0086	0.09	2.1	23
ISOMAP	0.005	0.0629	1.99	6.71
ISOMAP (LOG)	0.0049	0.068	2.1	7.2

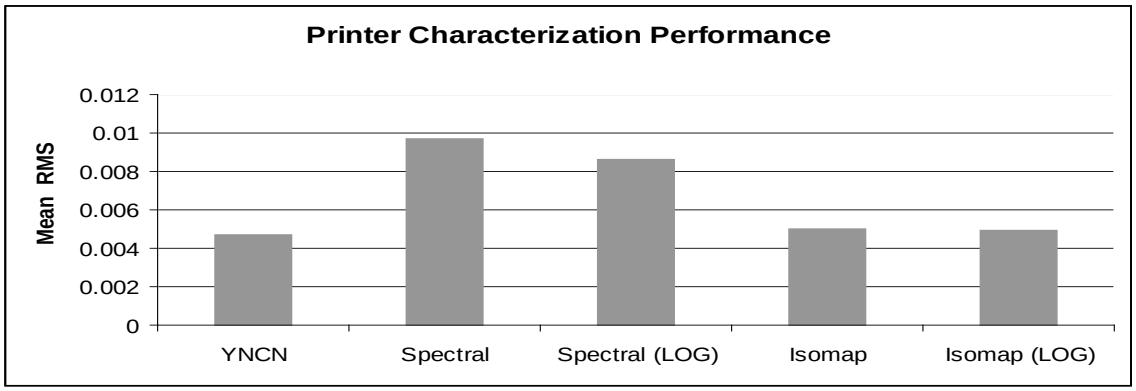

Figure 13: Performance of Geodesic (ISOMAP) and Linear based modelling compared against the YNCN model. The vertical axis represents the average error calculated as the Root Mean Square difference between predicted reflectance and measured values.

CHAPTER 4: NUMBER OF PRIMARIES

One of the main goals in spectral reproduction is to reduce metamerism by matching each input spectrum as closely as possible, while requiring the minimum number of primaries. In the printing industry, to make a good spectral match, the printer gamut is expanded by adjusting the chemistry of the inks, and especially by increasing the number of the inks used in the printer [28], [29], [30]. Similarly, in cameras and display technologies, it is now common to make the system with more than the traditional three primaries (sensors, LEDs, filters or phosphors) to further reduce the degree of metamerism [32], [33], [34]. The focus of this section is to determine a lower bound on the number of primaries needed to do a reasonable job in spectral printing.

Calculating Data Set Complexity

A simple approach to measuring the complexity of a data set is to assume that the number of channels needed in a system is limited and relates to the underlying dimensionality of the captured data in a linear space. Approaches such as Principal Component Analysis (PCA) and Independent Component Analysis (ICA) are widely used in research-related spectral data dimensionality where it is agreed that a small number of basis functions is adequate to represent a high dimensional data set accurately.

For instance, in studies of Munsell Colours, Eem et al. [35] proposed four, Maloney [36] proposed five to seven, Burns [32] suggested five to six, Parkinnen et al. [37] and Wang et al. [38] proposed eight, and Hadeberg et al. [39] recommended as many as 18 basis functions to represent the data accurately. Even though there are variations in their findings -- because of having different thresholds for measuring the similarity between the original and matched spectral data -- all the authors used similar techniques to analyze the complexity of a data set.

Recently the focus of the research has been on proposing the number of needed basis functions plus their reflectance characteristics [27][30]. The advantage of these approaches is that the proposed basis functions have similar reflectance or sensitivity characteristics to physically available solutions. Using these methods, researchers can optimize the characteristics of the primaries in a system to better capture or reproduce a reflectance with a minimum number of primaries.

Rotated PCA Basis

PCA provides a method to determine the dimensionality of the spectral sample population [40]. PCA has been widely used in colour-related applications [41], [42]. The main assumption of this technique is that the set of sampled vectors ($\underline{A}$) is multivariate normally distributed in the original dimensionality (typically 31 dimensions for spectral analysis). The linear combinations of the first p eigenvectors should describe the entire set of $\underline{A}_\lambda$ if the original was created by p linear basis, i.e.:

(12)

$$A_{\lambda,sample} = \sum_{i=1}^{p} b_i e_{\lambda,i} = \mathbf{EB}$$

Where $e_{\lambda,I}$ is the i^{th} eigenvector and b_i is the corresponding coefficient to reconstruct a sample.

One of the drawbacks of using techniques such as PCA is that the returned basis functions do not necessarily correlate to the physical dimensionality of the data. For instance Di-Yuan et al. [27] observed that the PCA basis functions representing a set of painting reflectances have negative values which do not correspond to the actual ink amounts (Figure 14).

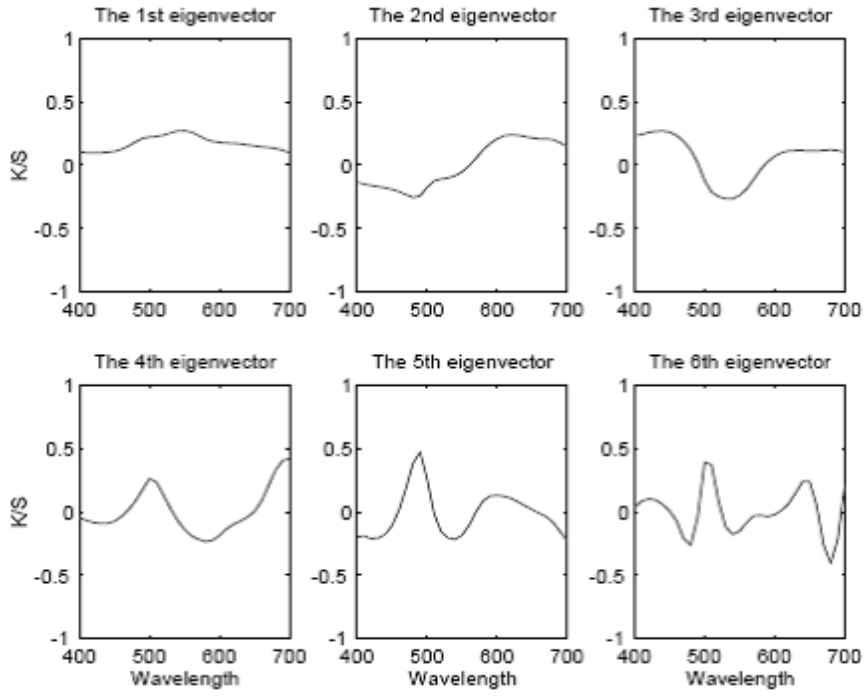

Figure 14: The six eigenvectors obtained from the still life painting by Di-Yuan [27].

One approach to overcome the negative values of the basis function is to develop a linear transformation of the basis functions so that the new functions

have all positive values. Ohta [43] proposed running a regression search method to find the best transformation of the PCA basis functions that reconstructs the spectral data set accurately and which has two main properties: all the basis functions have positive values and the concentration matrix should have all non-negative entries. After the transformation is applied to the PCA basis, the bases are not necessarily orthogonal to one other.

PCA Eigenvector without Sample Mean

Di-Yuan et al. [27] proposed eigenvector reconstruction of PCA without removing the sample mean to find basis functions that are closer to realistic primary characteristics. Using PCA basis functions a spectrum can be reconstructed as:

(13)

$$A_{\lambda,sample} = \sum_{i=1}^{p} b_i e_{\lambda,i} + A_{\lambda,samplemean}$$

The sample mean used in PCA is only a statistical parameter which specifies the average data set behaviour. The sample mean does not represent any physical colorant. Also, since the eigenvectors are the only clue leading to a set of possible colorants, the sample mean must be excluded to maintain the transformation relationship between eigenvectors and the set of possible colorants which is specified by the above equation.

Di-Yuan et al. ran an experiment on a data base of paintings created by six independent acrylic-paints. 126 samples were measured. Figure 15 shows the properties of the 6 paints.

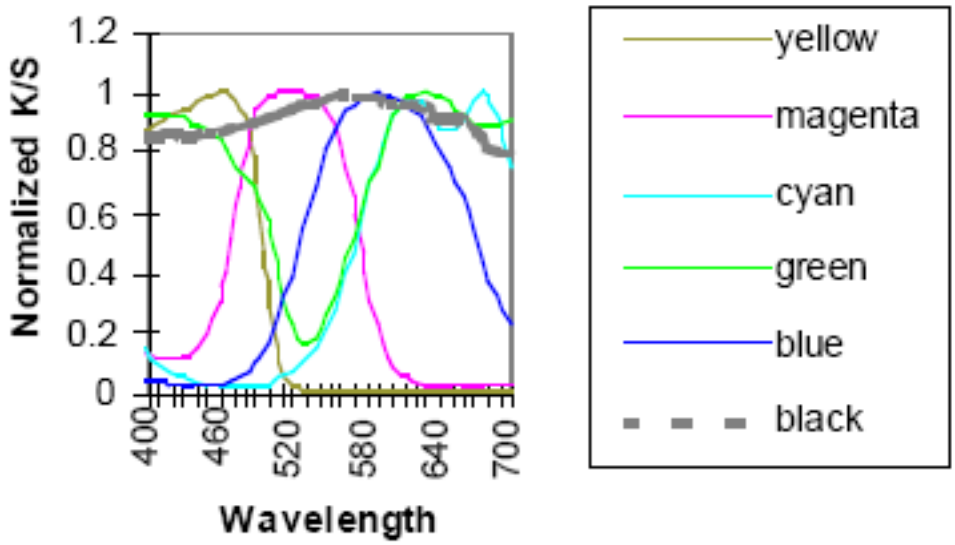

Figure 15: The six acrylic-paints used for generating the sample population. The vertical axis shows the K/S factor of Kubelka Munk theory, a representation of reflectance (absorption/scattering).

The initial six rotated eigenvectors without removing the mean are shown in Figure 15.

Table 4 shows the accuracy of using the first 6 basis functions of PCA in reconstructing spectral reflectance. The data shows that the 6-basis-driven analysis using the described method can reproduce the intended set of data quite accurately.

Table 4: Colorimetric accuracy of the six estimated colorants for the painting database

	DeltaE$_{94}$
Mean	0.22
STD Deviation	0.16
Maximum	0.92
Minimum	0.02

As shown in Figure 15, the estimated colorants are not similar to the measured reflectance of the 6 paints. There is also a colorant spectrum (thick dotted line) with various absorption bands across the visible spectrum. None of the predicted colorants represents a flat (neutral) spectrum either. The neutral colorant with an approximately flat spectrum can be approximated using a linear combination of the other five estimated colorants. To include the neutral colorant in the predicted basis, a new constraint was proposed to first estimate the neutral colorant using linear regression to fit the perfectly flat spectrum by the six eigenvectors. Then, the most significant fix eigenvectors were rotated individually to a non-negative representation. The curves of the new 6 reflectances are shown

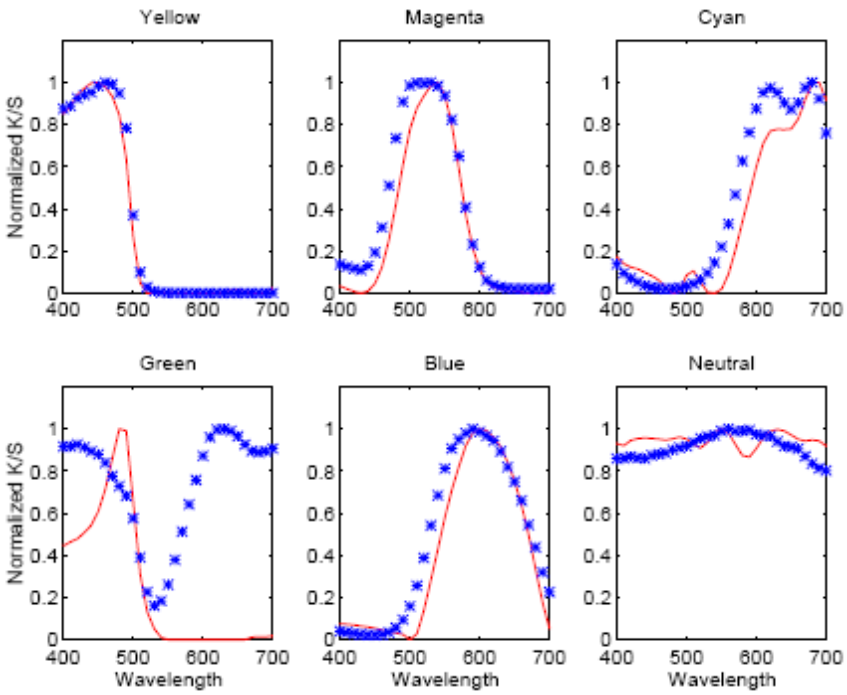

Figure 16: The estimated colorants (solid lines) and the original colorants (marked as start) used in the painting data base.

Multi-Peak Primaries [30]

As discussed earlier, in order to match the characteristics of predicted primaries to those of real primaries, a constrained search was used to guarantee positive reflectances or sensitivities [27][43].

Previous approaches worked with reasonable accuracy in lower dimensions. However, the modulation of the characteristics of the primaries is proportional to their order, i.e., additional vectors have an increasing number of peaks. It is preferred that, as the number of primaries increases, the algorithm can find the primaries that have non-negative values so that their individual sensitivities can be concentrated in distinct regions of the visible spectrum [30].

For example, in a trichromatic camera, the sensors are commonly chosen to be red, green and blue so the peaks are almost evenly spaced in the visible wavelength. Finally, it is preferred that the transformed vectors should ideally span the same space as the original.

Hardeberg et al. [30] proposed a search algorithm based on varimax rotation preferences [31] to develop a transformation that meets the above preferences. This transformation can be represented as a matrix transformation B, such that matrix B takes an initial basis to a non-negative basis. The algorithm searches for an orthogonal rotation to B that maximizes the preferences (varimax) criterion. The preference (varimax) metric is a combination of distance of the peaks plus width of the peaks. For instance, it can include the preference that the peaks of sensors in a camera system be spaced equally and have similar widths. The preference metric can also be more specialized. For instance, it can be adjusted to allow wider peaks at lower wavelengths.

Hardeberg also emphasizes that most of the synthetic analysis that is done on the number of primaries and their characteristics does not consider the noise that exists in the real system. Adding more primaries improves metamerism if the system is noise free. However, if each primary has noise in reproducing or capturing a reflectance, more primaries means a higher noise level and thus lower reproduction accuracy. He created the data base by adding two types of noise to the modelled reflectances:

(14)

$$A_{\lambda,sample} = \sum_{i=1}^{p} b_i e_{\lambda,i} + n_{shot} + n_{quant}$$

N_{shot} represents the noise in generation and reflection of light, and N_{quant} is the noise associated with quantising the simulated responses. Figure 17 compares the effect of noise in a camera system plus the effect of imposing preferences on sensor characteristics. Piche and varimax are two ways of imposing the preference that Hardeberg considered on a data base of 1269 Munsell reflectances.

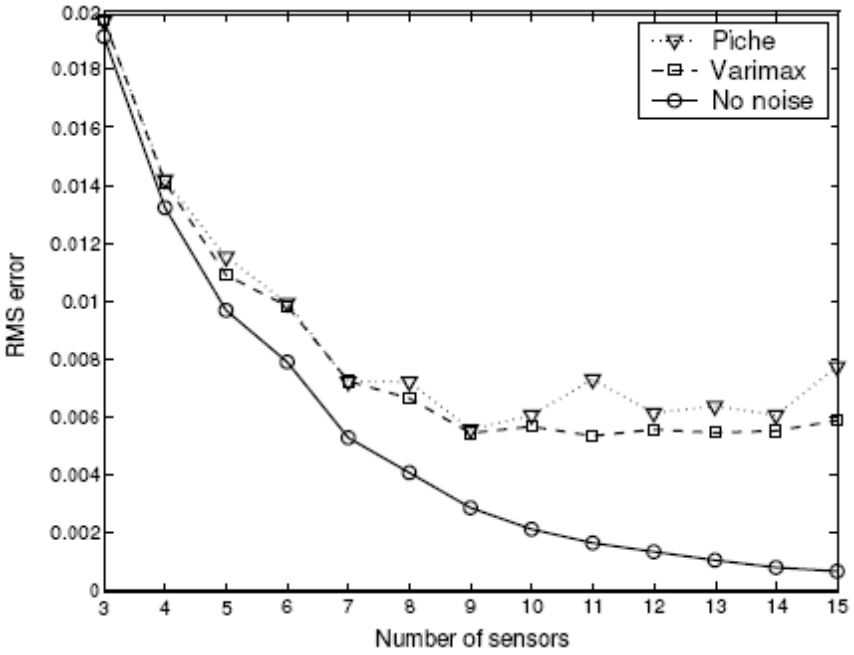

Figure 17: The effect of increasing the number of sensors with 12-bit quantization and 1% shot noise.

Compared to synthetic noise-free systems, Hardeberg found that when the real physical constraints of a system are considered, many fewer sensors are required to get the maximum reconstruction from the system.

Analysis of Primary Characteristics

In this section, a method is proposed to evaluate the extent to which spectral reproduction accuracy is improved as more and more primaries are used. The effect of primary reflectance characteristics on device output gamut performance in spectral space is also considered.

Primary Selection

One purpose of this experiment was to understand the effect of primary reflectance characteristics on the accuracy of spectral reproduction. This data can help better define what changes can be done with respect to a given set of primaries in order to optimize the accuracy of spectral reproduction and reduce metamerism in a system. Reflectance characteristics that will be discussed are the effects of variations in the number of primaries, percentage of overlap between each primary and degree of smoothness of each primary reflectance.

To compare the performance of the available primaries in the industry against what can be used as an optimal set, two general sets of primary characteristics were used in this study. One set was based on reflectances of real inks, and the other set was synthetic primaries (ink or filter light reflectance depending on the device model used). Both synthetic and actual measurement data were used to make the result less dependent on a specific ink selection. The real ink reflectance measurements were based on actual prints of pigmented inks. The following 9 inks were used: orange (O), cyan (c), magenta (m), yellow (y), Green (Gr), violet (V) and black (K), light magenta (LM) and light cyan (LC).

Three types of synthetic primaries were also used. The first type of reflectance used was based on square-wave reflectance as shown in Figure 18 where the edges are sharp, and thus resembles sub-sampling of the spectral reflectance. The 3 inks, as shown in Figure 18, cover the visible wavelengths 380 to 730, and are non-overlapping. The 6 inks were created by subdividing each ink in the 3-ink model into two separate square waves. The set of 9 and 12 non-overlapping inks were created similarly. The white of the print medium was taken to be the ideal white with 100% reflectance at all wavelengths.

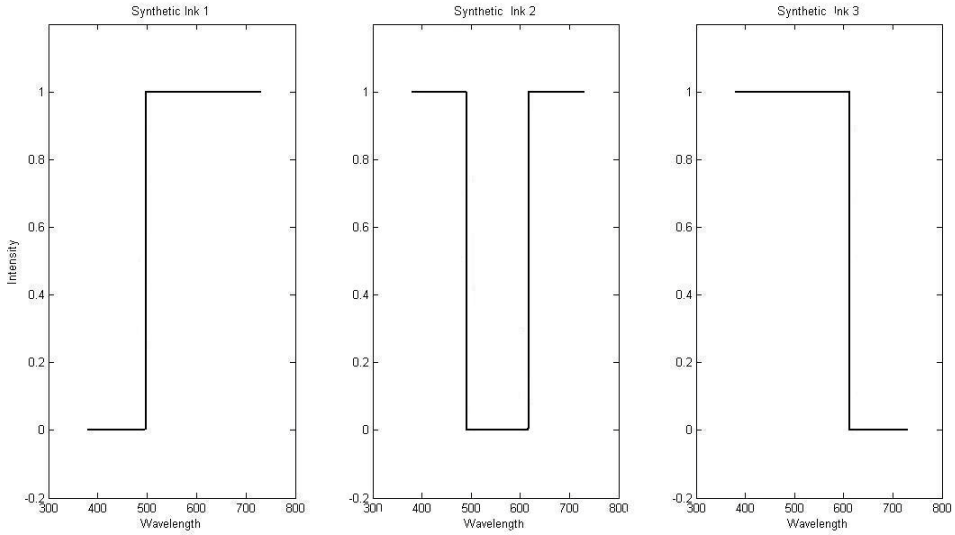

Figure 18: 3 Square wave synthetic ink reflectances covering 380 to 730 nm equally.

The second set of primaries studied has a more gradual transition from a non-absorbance region to the area of reflectance absorbance. This set of reflectances was used to compare the effect of having a tail (gradual transition between the absorptive and non-absorptive regions of each primary) on the accuracy of spectral reproduction.

Two sets of primaries with tailed overlap were considered as shown in Figure 19 and Figure 20. One set was based on modified square-wave reflectances with longer tails with the other set more sinusoidal (Figure 20).

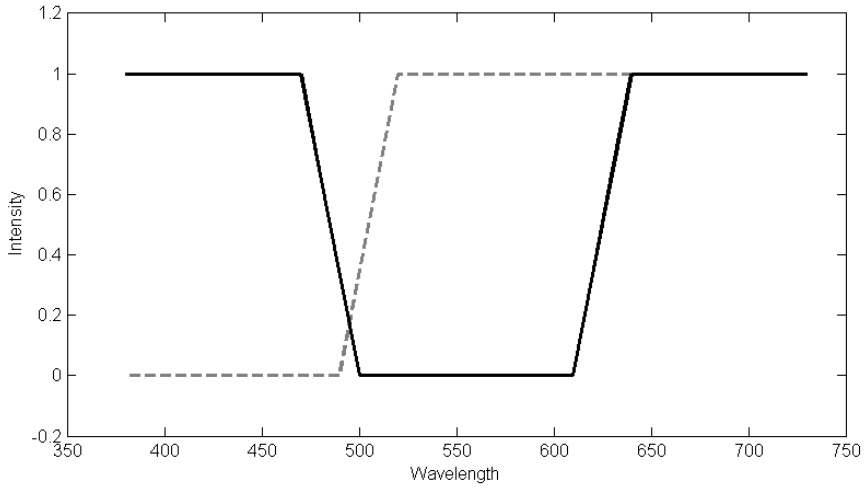

Figure 19: Two primaries with non-smooth tailed endings. The reflectances of these primaries have a gradual transition between absorptive and non-absorptive regions.

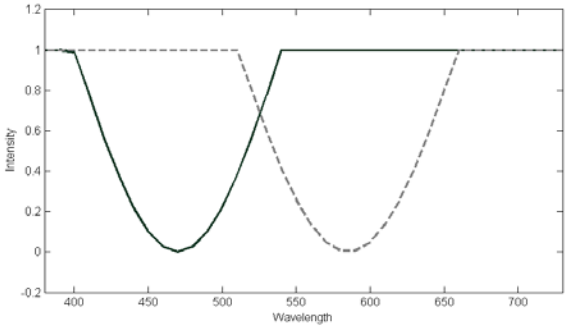

Figure 20: Two primaries with smooth tailed endings. The reflectances of these primaries have a smooth gradual transition between absorptive and non-absorptive regions.

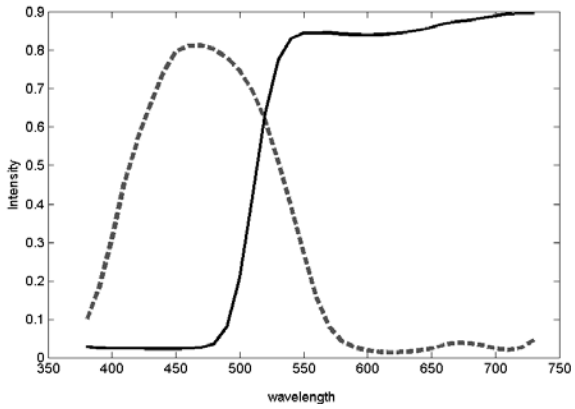

Figure 21: Reflectance of real inks measured. The curves show the smooth and long tails that are common for real reflectances.

Another contributing spectral reflectance characteristic of primaries studied was the percentage of spectral reflectance overlap. To evaluate the possible benefits of overlap for each type of reflectance, a set of 4 different reflectances in each reflectance type with 0%, 10%, 20% and 40% overlap was used. Figure 22 and Figure 23 compare two different sets of square-wave functions with different degrees of overlap.

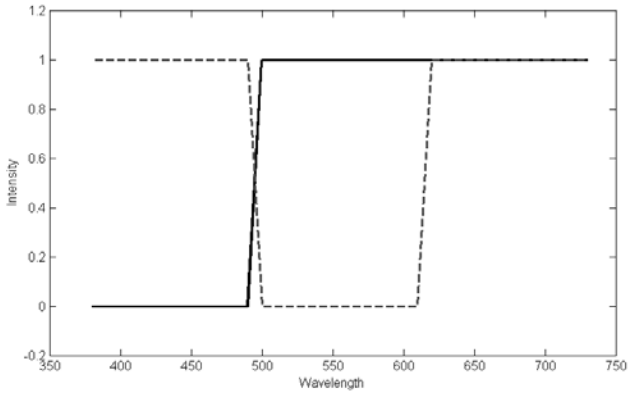

Figure 22: Square-wave reflectance functions with 0% overlap.

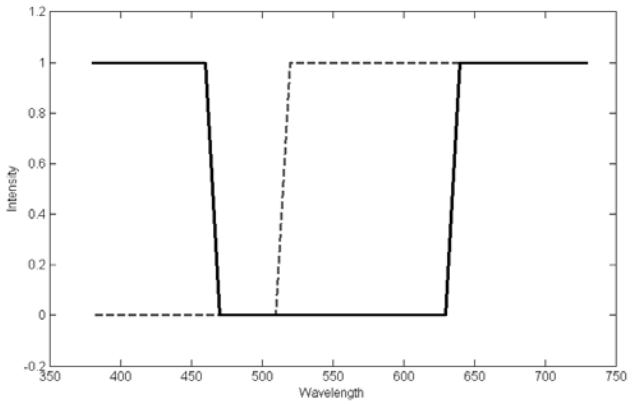

Figure 23: Square-wave reflectance functions with 20% overlap.

Device Characteristics

To evaluate the effect of the interactions between the primaries on the spectral reproduction accuracy, two types of device models were considered. Two device models, denoted LP (linear projector) and TK (Tzeng simple-Kubelka Munk), were used to predict the spectral reflectance resulting from printing or displaying a given primary combination. For LP, the displayed reflectance was assumed to be a linear combination of the primary reflectances. The equation below expresses how the model works:

(15)

$$R_\lambda = [\Sigma c_i R_{\lambda,i}] = C_{(1xn)} R_{\lambda(nx1)}$$

$R_{\lambda,i}$ is the reflectance of primary i at 100% density, and c_i is the area coverage. $R_{\lambda(nx1)}$ represents a matrix of size $nx1$ of reflectances at wavelength λ.

The LP model assumes that the primaries mix linearly in a subtractive colour mixing system and there is no non-linear interaction between the primaries [64]. The advantage of LP is that the ink separation algorithm to reproduce an input reflectance becomes a straightforward linear algebraic operation. In

addition, this model is quite similar to how output for displays (e.g., monitors and projectors) is modelled [1] and, because of that, the data from the LP model can also be used to evaluate the performance of displays using different primary characteristics.

The printer model, TK, introduced by Tzeng et al. [27], [29], was used to mimic the real ink and media reflectance. The following equations were used to predict the reflectance of multi-ink printing system:

$$R_\lambda = (R_\lambda^{1/w}{}_{paper} - \psi_{\lambda,mixture})^{w} \quad \textbf{(16)}$$

$$\psi_{\lambda,\,mixture} = \Sigma c_i R_{i\lambda}$$

$$\psi_\lambda = R_\lambda^{1/w}{}_{paper} - R_{\lambda,i}^{1/w}$$

where w is the non-linearity weight similar to Yule-Nielsen factor [21] and R_λ,i is the reflectance of the i^{th} ink as a function of wavelength.

Evaluation Method

To determine how the number of primaries affects the accuracy of spectral reproduction in terms of reproducing spectra, spectral matches for 3-, 6-, 9- and 12-primary devices (LP and TK models) were calculated. The performance of these synthetic primaries was compared against real ink spectral reflectances in order to understand how optimized the reflectances of the existing inks are. For case of the reflectance of actual inks, the 3 inks considered are the most common 3 inks used in practice, namely, cyan, magenta, and yellow. For the 6-

ink case, the initial 3 inks are retained, and 3 more complementary inks are added, namely, orange, green, and violet. light cyan, black and light magenta are added to these 6 for the 9-ink case.

However, the complexity of the conventional methods for evaluating gamut performance of a printer grow exponentially as the dimensionality of the input data increases (The analysis is discussed in more detail in Chapter 4). One method to indirectly evaluate spectral gamut size of a printer system which includes a set of primaries and a printer model is to evaluate how accurately the printer system can reconstruct a database of input reflectances. This method depends on spectral gamut mapping algorithms to estimate the printer gamut size.

For the LP (Linear Projector) model -- since the primaries interact linearly with each other -- gamut mapping becomes a simple linear projection operation. The equation below shows the process of deriving the closest primary combination to reconstruct an input reflectance:

$$R_\lambda = [\Sigma c_i R_{\lambda,i}] = \mathbf{C}_{(1xn)}\mathbf{R}_{\lambda(nx1)} \qquad \textbf{(17)}$$

$$\boldsymbol{C}_{(1xn)} = (\mathbf{R}_{\lambda(nx1)})^{-1} \; R_\lambda$$

However, when the primaries interact non-linearly, gamut mapping becomes more complicated.

Hierarchical Search (HS) Gamut Mapping Algorithm

For the TK printer model -- since the primaries interact with each other and the media non-linearly -- the gamut mapping process cannot be done using a linear projector operation. There are some proposed methods to handle gamut mapping in spectral space that will be discussed in Chapter 4. However, most of these spectral gamut mapping algorithms try to improve their time or space complexity at the expense of accuracy.

To understand the effect of each primary characteristic on gamut performance independent of the gamut mapping algorithm performance, results were based on a search-based mapping algorithm. This algorithm is based on hierarchical search in ink space where the search is done in subdivisions of ink combinations. Let the set of the subdivisions of ink space be M, where there is a spectral reflectance associated with each ink combination, m_i, in M. The algorithm is as follows:

1. Find the closest m_i spectrum to a given input point p in spectral space.

2. Create a grid of ink subdivisions around m_i with smaller ink variation.

3. Go back to step 1 until the grids are small enough. Then go to the next step.

4. Return the spectral reflectance of m_i as the closest point.

The main drawback of the search algorithm is that its accuracy highly depends on the sampling resolution of the system. Because of the exponential growth in the sampling as a function of the number of inks in the system, a modification to the search algorithm is needed for printer systems with 9 or more inks. The modification involves breaking the spectral wavelength range into segments and running the search for each segment independently. The premise is that if the reflectance wavelength of interest is segmented into T subsections, each section can be analyzed separately. To account for inks that have absorption sensitivity on more than one segment, the neighbouring segments have 30% overlap in their wavelength. For example working with spectral reflectances ranging from 380 to 730 wavelengths with 3 segments, the first segment covers 380 to 520, the second one covers 470 to 640 and the third one covers 590 to 730 nm in wavelengths.

For each segment, the algorithm only considers the inks that have absorption sensitivity in that segment wavelength range. Applying this second filter reduces the number of inks that need to be considered, thus enabling the search method to have similar sampling rate as for printer systems with fewer number of inks.

Optimizing the HS Parameters

For the HS algorithm, there are two sets of parameters to optimize. The first set of parameters represents the maximum number of iterations allowed during the search and the number of samplings to have along each dimension.

The second set of parameters represents the number of segments that the input reflectance will be divided into and the percentage of overlap between neighbouring segments. The higher the number of segments, the fewer the number of primaries in each segment and, thus, the faster the search algorithm will be. However, smaller segments means more segments that the search has to deal with. Also, if the segments are too small (cover small range of wavelength) and the overlap percentage is kept the same, the accuracy of the model can be low. As a result, a balance needs to be made between the number of segments and the overlap percentage.

The output of the HS algorithm was evaluated on an output system with LP primary interaction (linear interaction). Doing so enabled a comparison of HS performance against linear projection, as well as optimization of the parameters to get the lowest error from the HS search algorithm.

In this experiment, the first parameter, which is the number of search iterations, was kept constant for 3, 6, 9 and 12 ink printer systems. For 3 and 6 ink systems, based on the comparison to the LP output model, it was enough to use only one segment. For 9 and 12 ink printer systems, 1, 2, 3 and 4 segments in spectral space with 10, 15 and 20 percent overlap for each were tested and the best parameter was selected. Table 5 represents the performance of the HS algorithm against projection method for square type inks. The table shows that after selecting the right search parameters, the HS search method finds results that are very similar to the direct linear projection method. The parameters are then used for HS search algorithm for TK printer model.

Table 5: Performance of the HS search for 3, 6, 9 and 12 ink printer systems with the LP Printer model. The performance was compared against the linear projection method that returns the true answer. Square wave inks were used in the experiment.

Number of Inks	mean deltaE	max deltaE	min deltaE
3	0.263	1.09	0.14
6	1.09	2.39	0.04
9	1.23	2.61	1.64
12	1.58	3.39	1.69E-01

Evaluating Metamerism

Root Mean Square (RMS) difference between two reflectances is one of the common metrics used for evaluating the similarity between two spectral reflectances. However, RMS (root mean square) does not necessarily represent the difference that may be perceived by a human observer. As an alternative measure, the average colour variation calculated as $deltaE_{94}$ of the two spectral reflectances found under 11 different lights was used. The 11 illuminants used were from the Simon Fraser data base [65] shown in Table 6.

Table 6: The 11 different illuminations used in measuring the colour variation of two similar reflectance spectra. This data is from Computational Vision Lab at Simon Fraser University [65].

11 illumination types used for delta E comparison
Sylvania 50MR16Q (12VDC)---A basic tungsten bulb
Sylvania 50MR16Q (12VDC) + Roscolux 3202 Full Blue filter
Solux 3500K (12VDC)--Emulation of daylight
Solux 3500K (12VDC)+Roscolux 3202---Emulation of daylight
Solux 4100K (12VDC)--Emulation of daylight
Solux 4100K (12VDC)+Roscolux 3202---Emulation of daylight
Solux 4700K (12VDC)--Emulation of daylight
Solux 4700K (12VDC)+Roscolux 3202---Emulation of daylight
Sylvania Warm White Fluorescent (110VAC)
Sylvania Cool White Fluorescent (110VAC)
Philips Ultralume Fluorescent (110VAC)

Scene Data Base and K Means

To evaluate the effect of each ink on spectral gamut coverage, the scene reflectances from the Simon Fraser University (SFU) database were used as target reflectances to reproduce. There are 1350 individual reflectances in the database. However, time complexity of the HS ink separation method grows exponentially as the number of primaries used in the system increases. To speed up the evaluation process, the number of scene reflectances used in the experiment was reduced to a smaller set. In order to have the smaller reflectance database better represented, the original database was classified to subsets. K-means clustering was used to classify the original database to smaller subset [83]. This clustering technique includes four steps: (1) Select k initial start points as cluster centres; (2) Calculate each pixel's distance to the cluster centre; (3) recalculate each cluster's centre; (4) Repeat until converged to a stable status.

It was found that the SFU scene database can be classified to 80 disjoint classes accurately enough. One reflectance from each cluster is used to represent the cluster. All the evaluations in this section are based on the 80 selected scene reflectances. Figure 24 and Figure 25 show the complexity of the 80 selected reflectances. The figures show that in a linear system, if the primaries are selected optimally, at least 4 primaries are needed to have less than 2 deltaE_{94} colour reproduction and very similar spectral reflectances. This is assuming that the primaries can have both positive and negative reflectances (which is not realizable in real printers or displays).

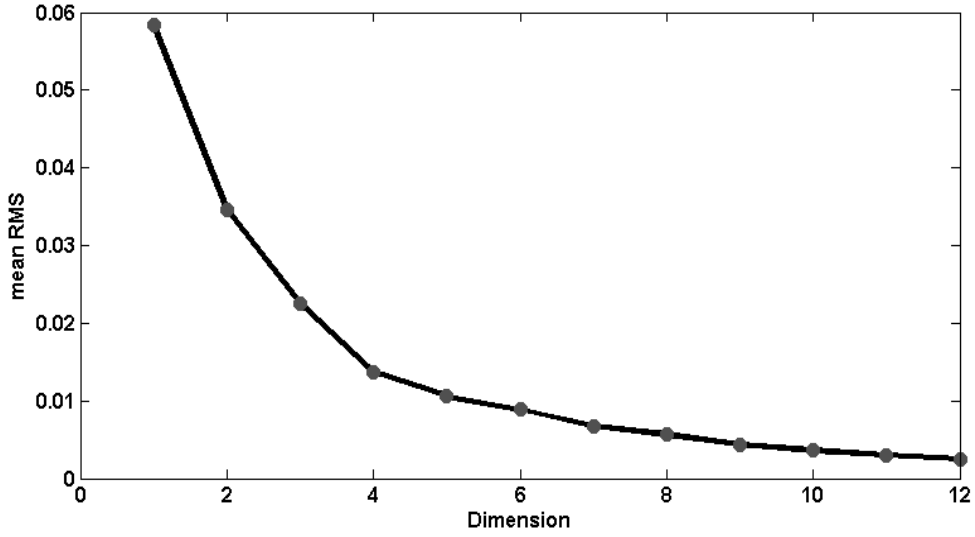

Figure 24: Mean Root Mean Square residual error as the number of PCA bases increases.

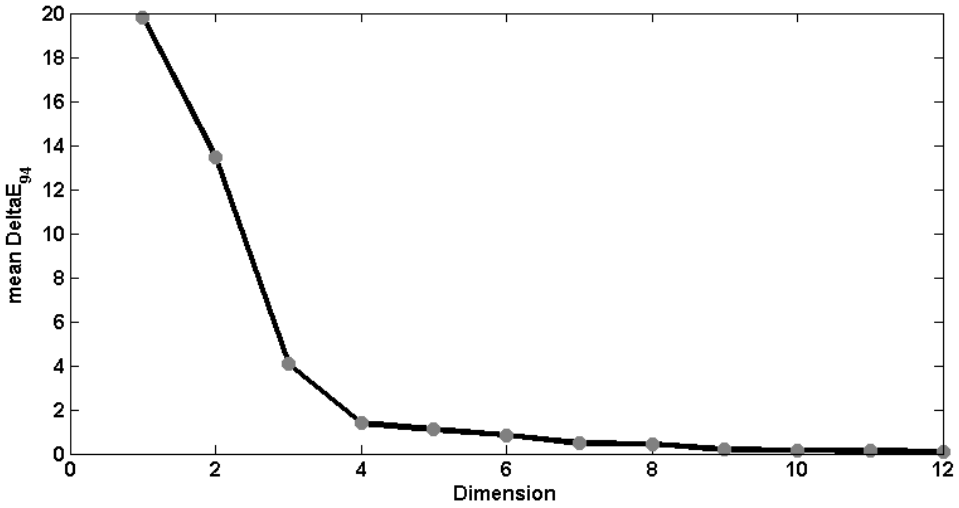

Figure 25: Mean DeltaE_{94} error between reconstructed reflectance and the database reflectance when different numbers of PCA bases used. DetaE_{94} is calculated as average detalE under 11 different illuminations provided from the SFU database.

Results

Primary Overlap

In this section, the effect of having different percentages of overlap between the primaries is evaluated. The result is repeated for each type of primary reflectance. Figure 26 shows that for the square type reflectances, as the overlap percentage increases, the accuracy of the spectral matching will decrease. Figure 27 shows similar behaviour if the performance is evaluated as ΔE_{94} colour difference under 11 different illuminations.

Figure 28 looks at one reflectance matching using 6 square waves with 0% overlap and 20% overlap. The figure shows that for square type waves, for which both the centre of the signal and the edges of the signal have similar coverage (i.e., there is no tail for the signal), having overlap on the primary reflectances causes a significant drop in reproduction accuracy. This is an indication of a drop in gamut coverage of the device.

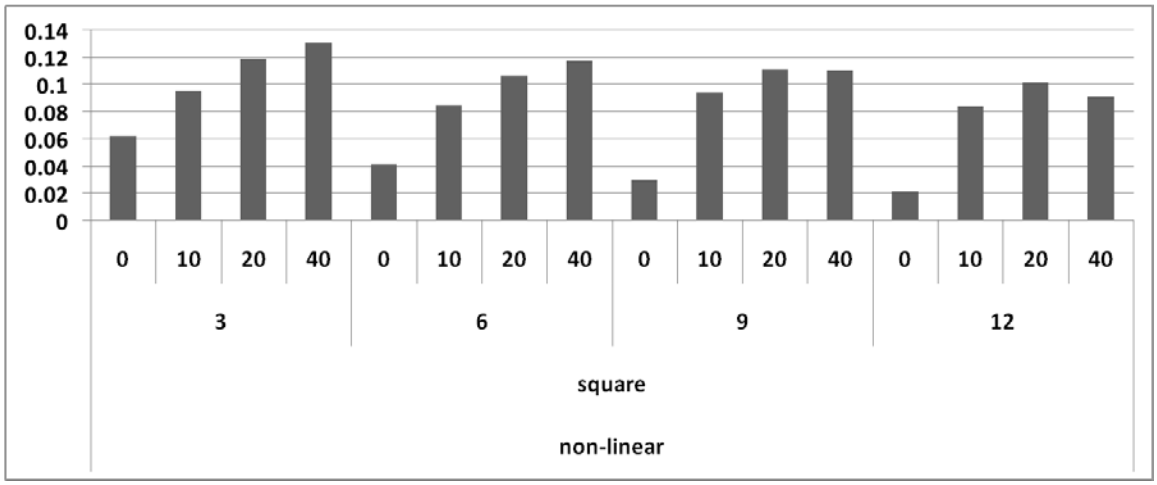

Figure 26: Spectral Gamut coverage of square wave ink given 3, 6, 9 and 12 inks evaluated as Room Mean Square difference between the database of reflectances and the closest reflectance matches that fall on the gamut. The printer model is based on non-linear (TK) model.

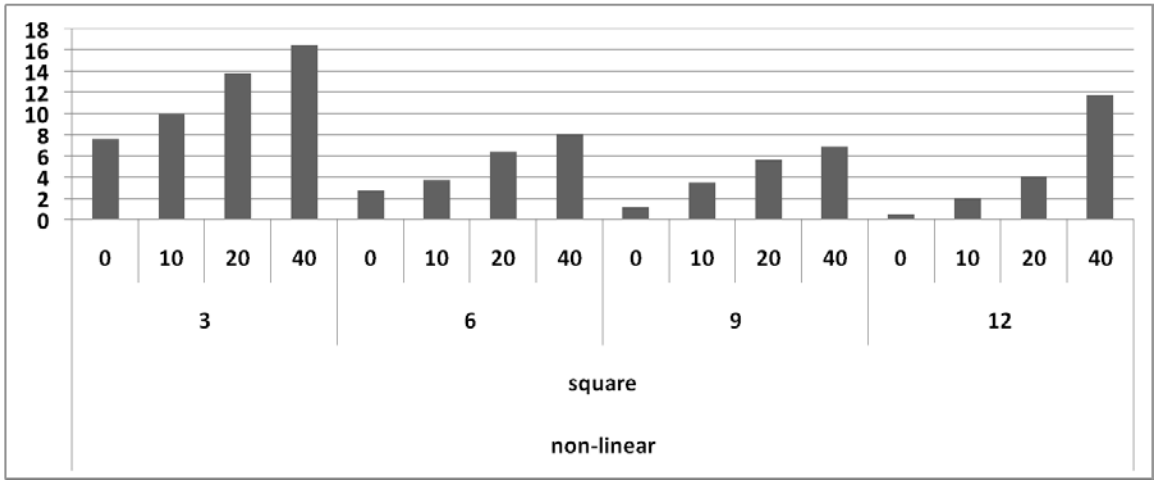

Figure 27: Spectral Gamut coverage of square wave ink given 3, 6, 9 and 12 inks evaluated as $DeltaE_{94}$ colour difference between the database of reflectances and the closest reflectance matches that fall on the gamut. The error is shown as average variation under 11 different illuminations. The printer model is based on non-linear (TK) model.

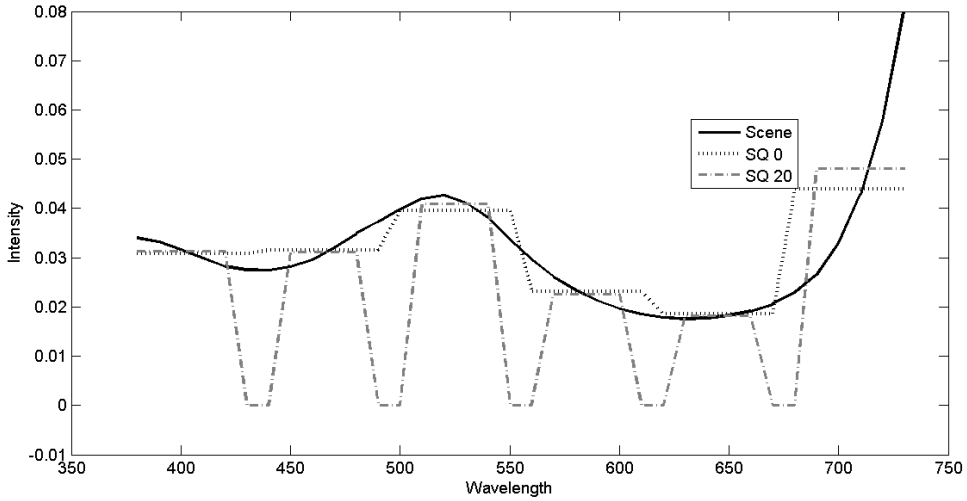

Figure 28: Input reflectance and closest match using 6 ink square waves with 0 and 20 % overlap. The printer model is based on non-linear (TK) model.

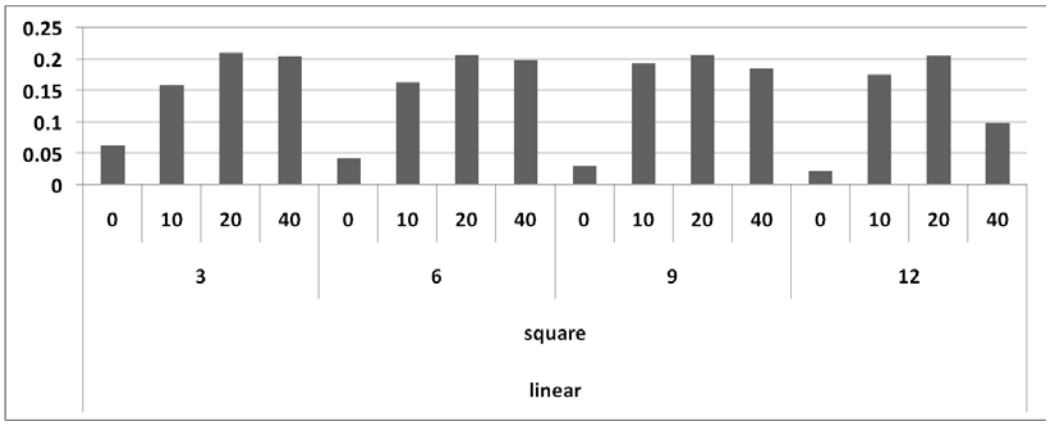

Figure 29: Spectral Gamut coverage of square wave ink given 3, 6, 9 and 12 inks evaluated as Room Mean Square difference between the database of reflectances and the closest reflectance matches that fall on the gamut. The printer model is based on linear (LP) model.

Considering trapezoidal signals (Figure 30) which have a tail (slower drop in their absorption sensitivity compared to square wave), some level of overlap improves printer spectral gamut performance. This characteristic holds for a sine wave signal as well, as shown in Figure 32 and Figure 33.

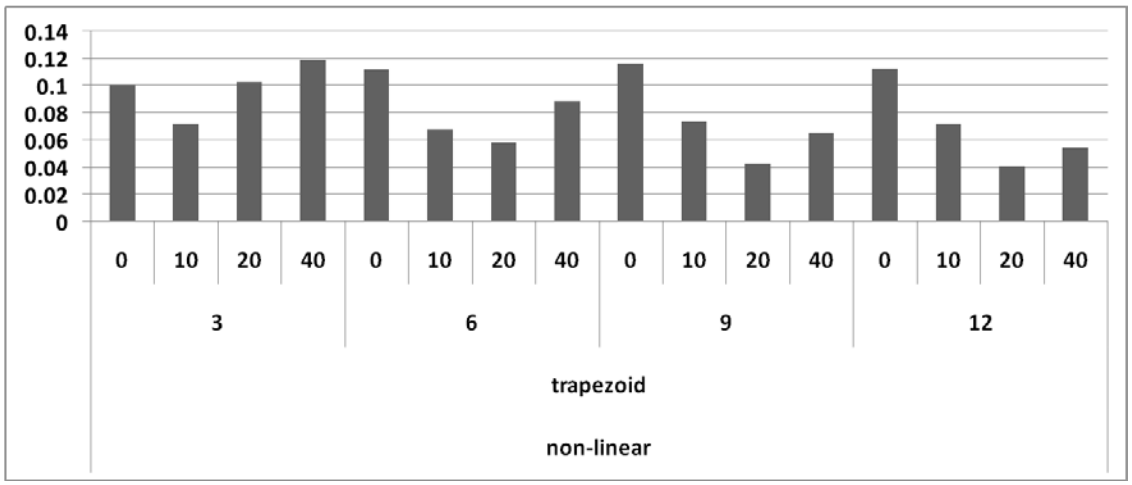

Figure 30: Spectral Gamut coverage of trapezoidal wave ink given 3, 6, 9 and 12 inks evaluated as Room Mean Square (RMS) difference between the database of reflectances and the closest reflectance matches that fall on the gamut. The printer model is based on a non-linear (TK) model.

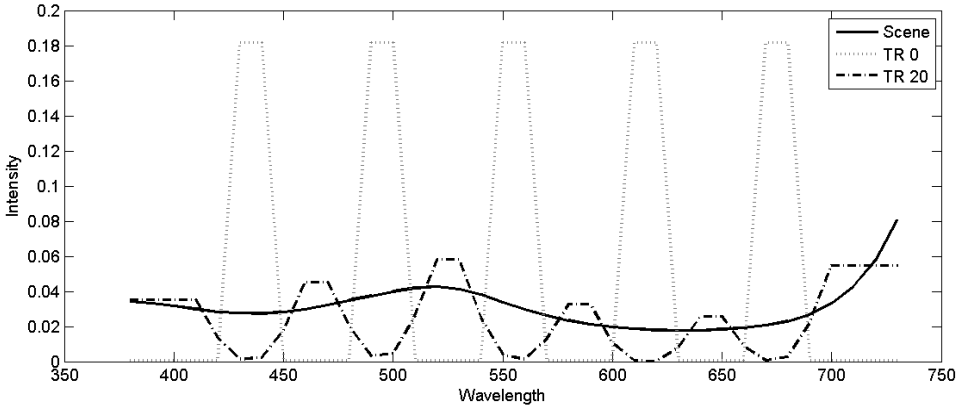

Figure 31: Input reflectance and closest match using 6 ink square waves with 0 and 20 % overlap. The printer model is based on a non-linear (TK) model.

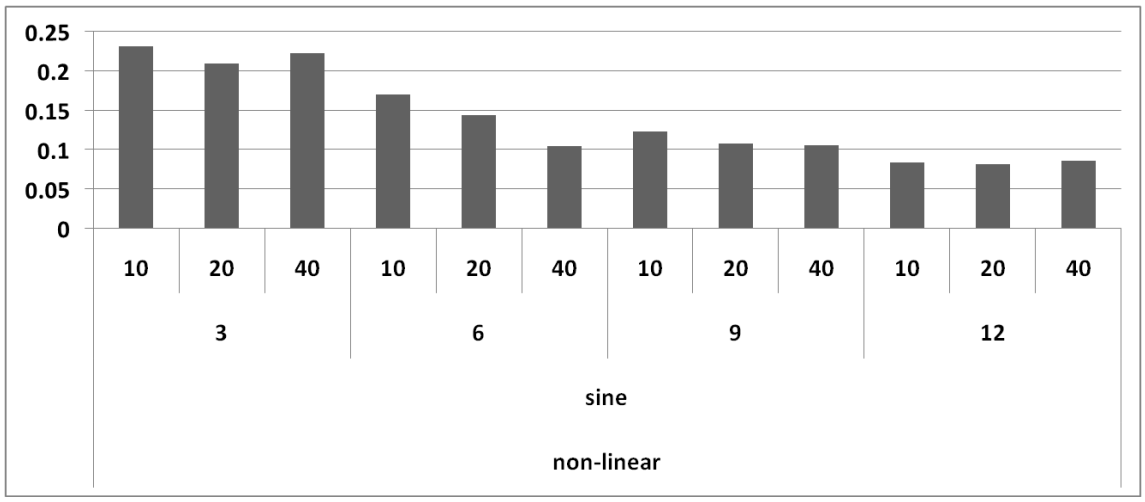

Figure 32: Spectral Gamut coverage of sine wave ink given 3, 6, 9 and 12 inks evaluated as Room Mean Square (RMS) difference between the database of reflectances and the closest reflectance matches that fall on the gamut. The printer model is based on a non-linear (TK) model.

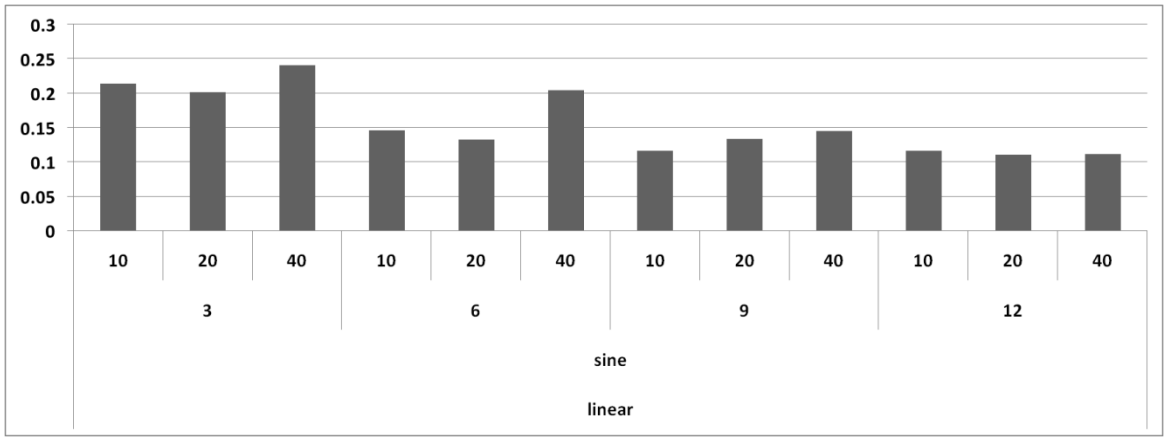

Figure 33: Spectral Gamut coverage of sine wave ink given 3, 6, 9 and 12 inks evaluated as Room Mean Square (RMS) difference between the database of reflectances and the closest reflectance matches that fall on the gamut. The printer model is based on a linear (LP) model.

Primary Interaction Model

Figure 35 Compares gamut coverage of the two primary interaction models for square waves. Previous data showed that for the square wave

functions, the more the two primaries overlap the lower the gamut coverage becomes (Figure 26). One hypothesis can be that if the primaries have optimal spectral overlap percentage, then the two interaction models (linear and non-linear) have similar gamut coverage. However, once there is more overlap between the primaries' absorption sensitivity regions than what is optimal, then a non-linear system has better performance. A possible explanation for this is that when the inks have more than the optimal overlap, there are many irregularities (non-uniformities) between the matched reflectance and the target reflectance. When a non-linear system is used, some of these irregularities are smoothed out, which can result in a more accurate reproduction as shown in Figure 34.

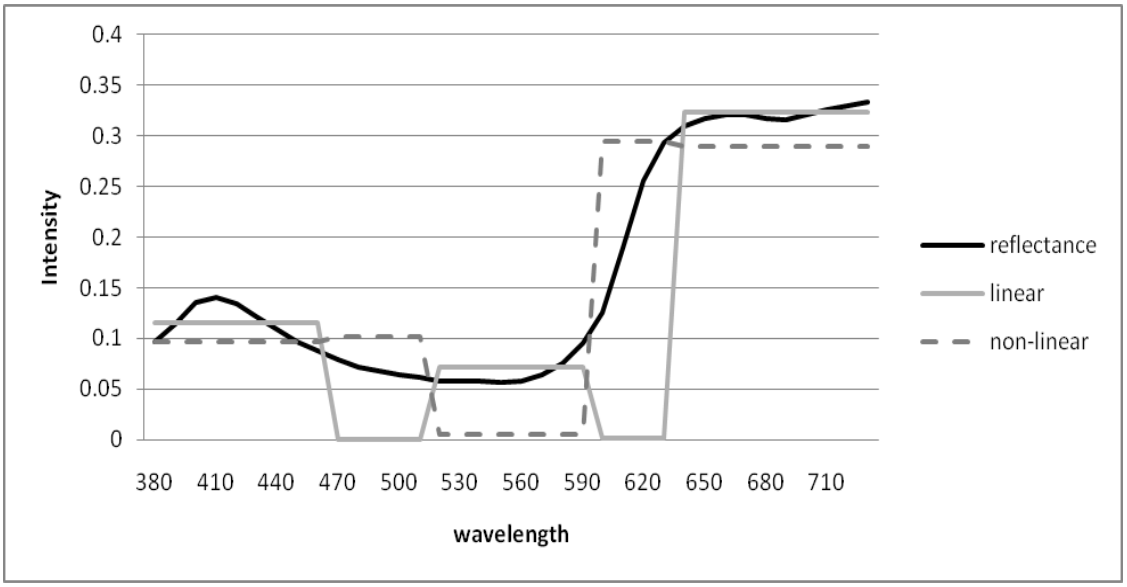

Figure 34: Spectral match of a scene reflectance using a 3-ink system with square wave inks of 20% overlap. The reproduction is shown for linear and non-linear systems. For linear system the reproduction error has RMS value of .11 and non-linear system has .065

Similar behaviour is seen for the sine and trapezoid shape signals that have longer tails. Figure 36 and Figure 37 show that for signals with not enough

overlap between the primaries, a linear model performs better. When there is enough overlap (e.g. 10% for trapezoid signal or 20% for sine wave), then both linear and non-linear models have overall similar coverage. On the other hand, when there is more than optimal overlap between signals, primaries with non-linear interaction result in a better reproduction than if they had linear interaction.

Typical inks used in the printers are a good example of primaries with long tails. Based on observations using synthetic inks, the expectation is that these inks (real inks) would have better spectral gamut coverage in a non-linear system than a linear system. Figure 38 confirms the expectation, where 3, 6 and 9 real ink reflectances were used.

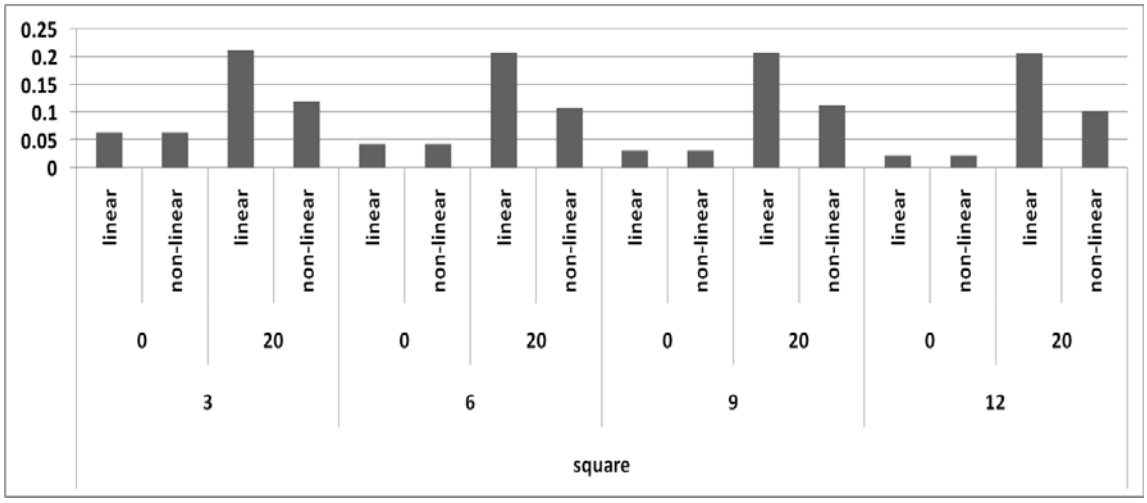

Figure 35: Performance of square wave primary evaluated as RMS of match between scene reflectance and the closest match on the system gamut.

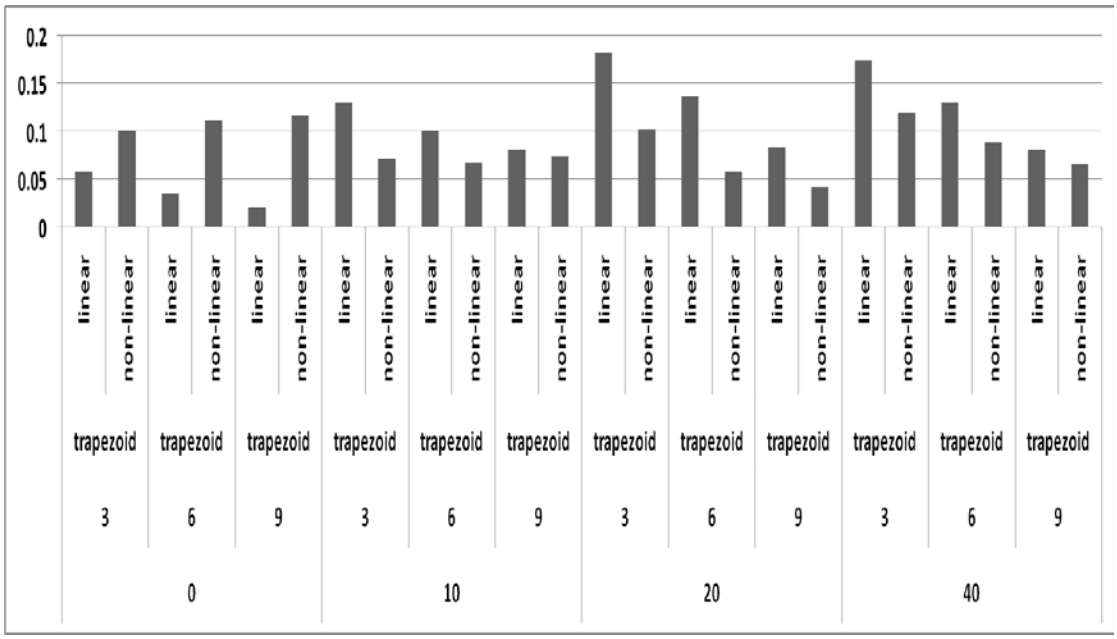

Figure 36: Performance of square wave primary evaluated as RMS of match between scene reflectance and the closest match on the system gamut.

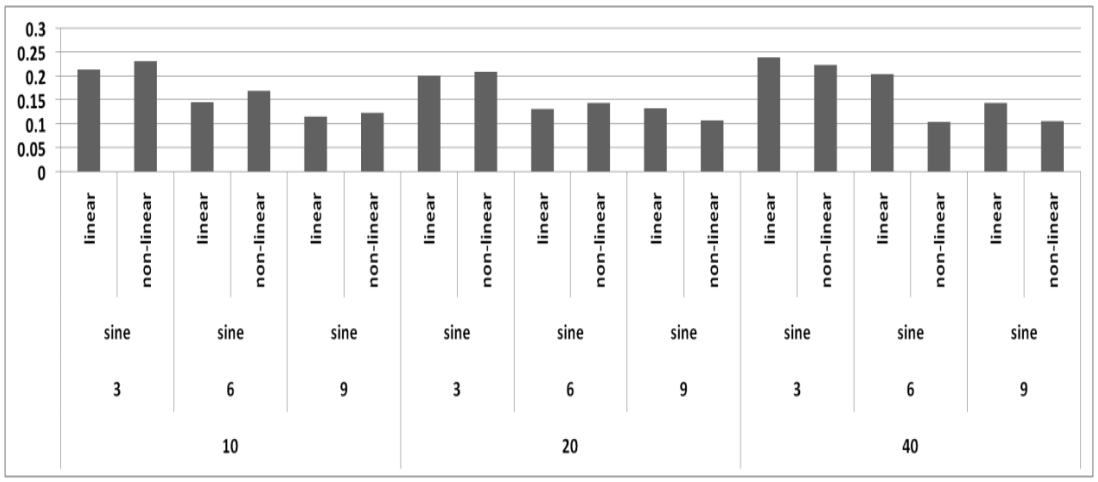

Figure 37: Performance of square wave primary evaluated as average RMS of match between scene reflectance and the closest match on the system gamut.

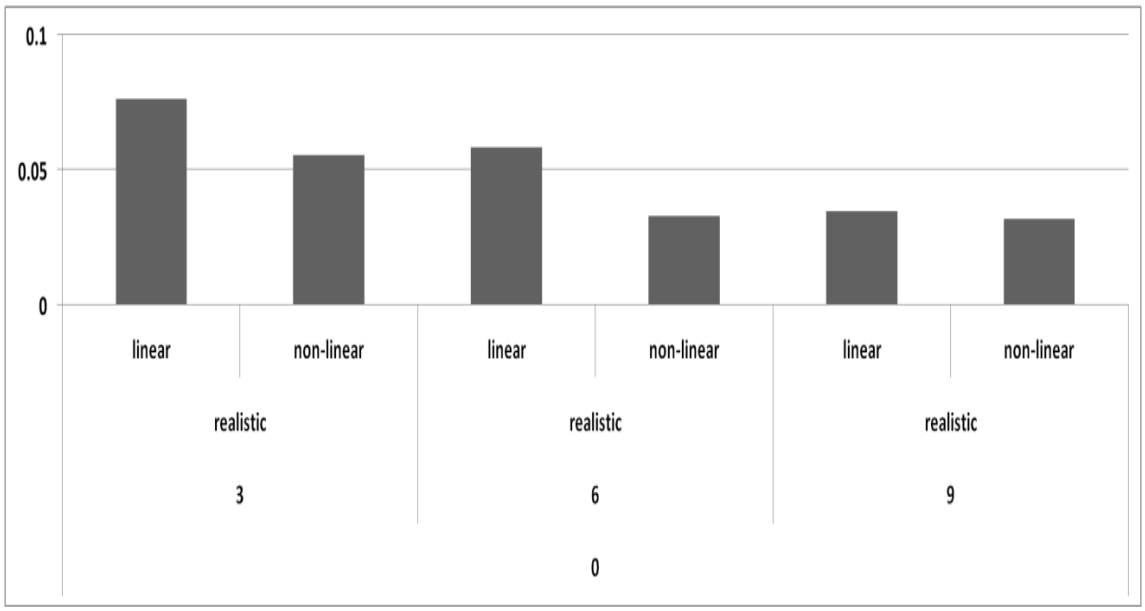

Figure 38: Performance of real ink reflectances as average RMS of match between scene reflectance and the closest match on the system gamut (both linear and non-linear models are evaluated).

Number of Primaries

The focus of this study was to understand whether the spectral gamut coverage of the device is improved when more primaries are made available in an output device.. The result in this section tries to explain how many primaries are needed in a device to get an accurate spectral colour reproduction system when the reflectance or absorption characteristics of the primaries are, or are not, optimized for reproduction purposes.

Figure 39 and Figure 40 show, for close to optimum square wave primaries, the spectral coverage of a device gamut improves noticeably as the number of primaries increases (whether the error is measured in RMS or DeltaE). On the other hand, if the overlap percentage for the same type of primaries is larger than what is desired (having non-optimum primaries), then the gamut coverage of the output device does not improve continuously as the

number of primaries increase (Figure 41 and Figure 42). The data shows that for non-optimized primaries, the gain from having a higher number of primaries (especially after 6 primaries) is cancelled by the noise in spectral reproduction from having a higher than optimized overlap amount. Similar behaviour is seen for output devices with linear primary interaction (Figure 43).

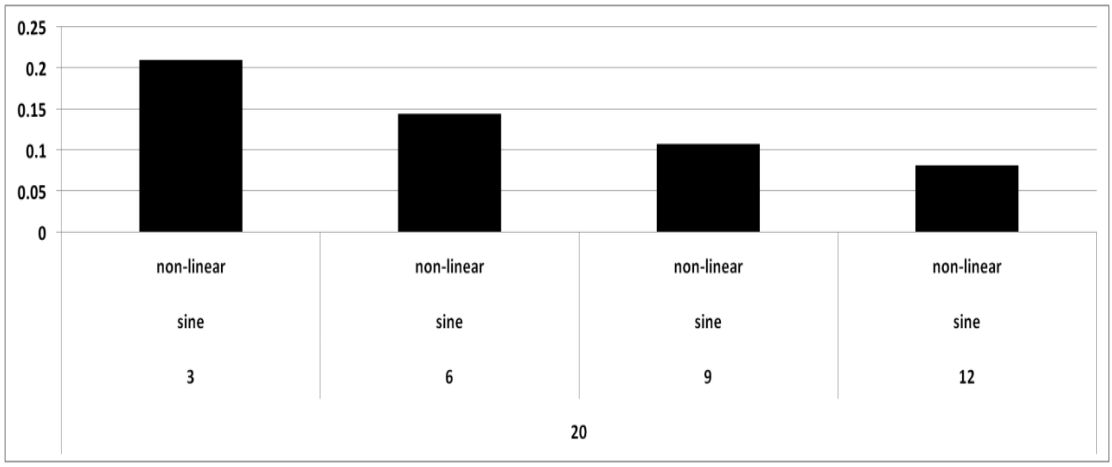

Figure 39: Spectral Gamut coverage of sine wave ink at 20% overlap (the better overlap amount) for 3, 6, 9 and 12 inks evaluated based on mean RMS difference between the closest match on gamut and the goal reflectance. Mean RMS is on Y axis.

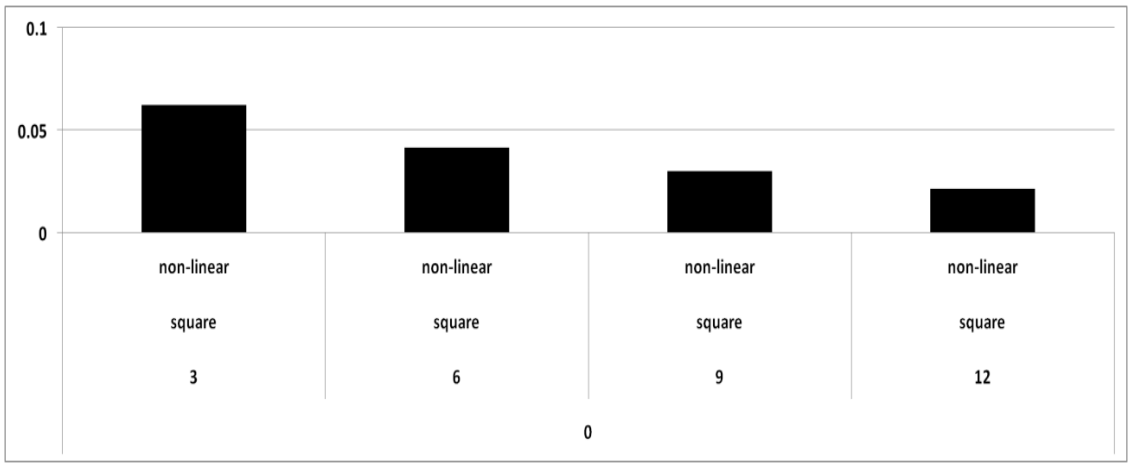

Figure 40: Spectral Gamut coverage of square wave ink at 0% overlap (the better overlap amount) for 3, 6, 9 and 12 inks evaluated based on mean RMS difference between the closest match on gamut and the goal reflectance. Mean RMS is on Y axis.

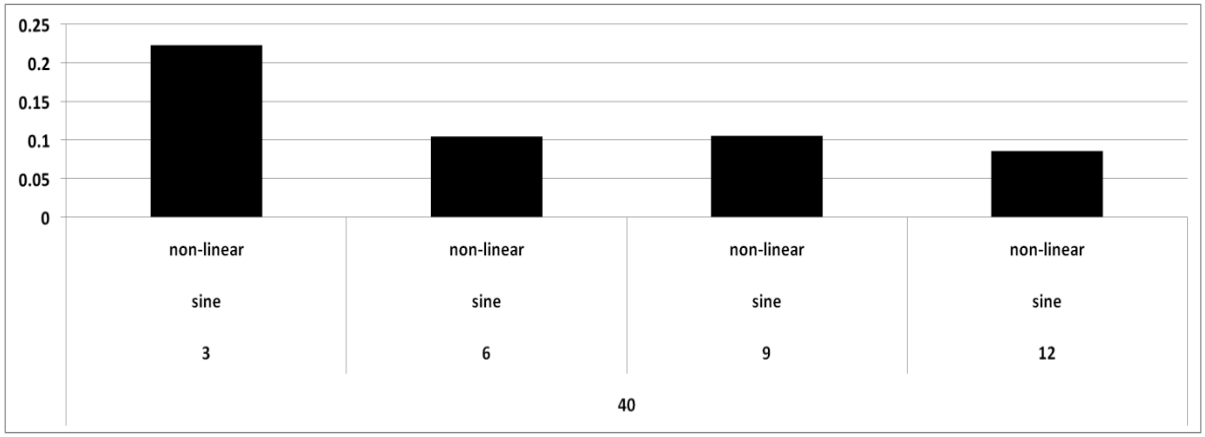

Figure 41: Spectral Gamut coverage of sine wave ink at 40% overlap (the undesired overlap amount) for 3, 6, 9 and 12 inks evaluated based on mean RMS difference between the closest match on gamut and the goal reflectance. Mean RMS is on Y axis.

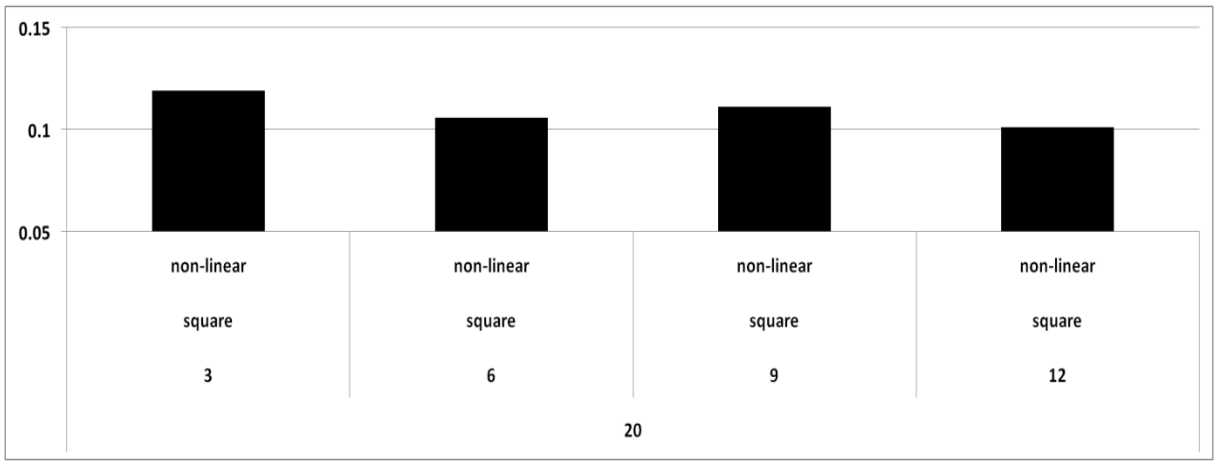

Figure 42: Spectral Gamut coverage of square wave ink at 20% overlap (the undesired overlap amount) for 3, 6, 9 and 12 inks evaluated based on mean RMS difference between the closest match on gamut and the goal reflectance. Mean RMS is on Y axis.

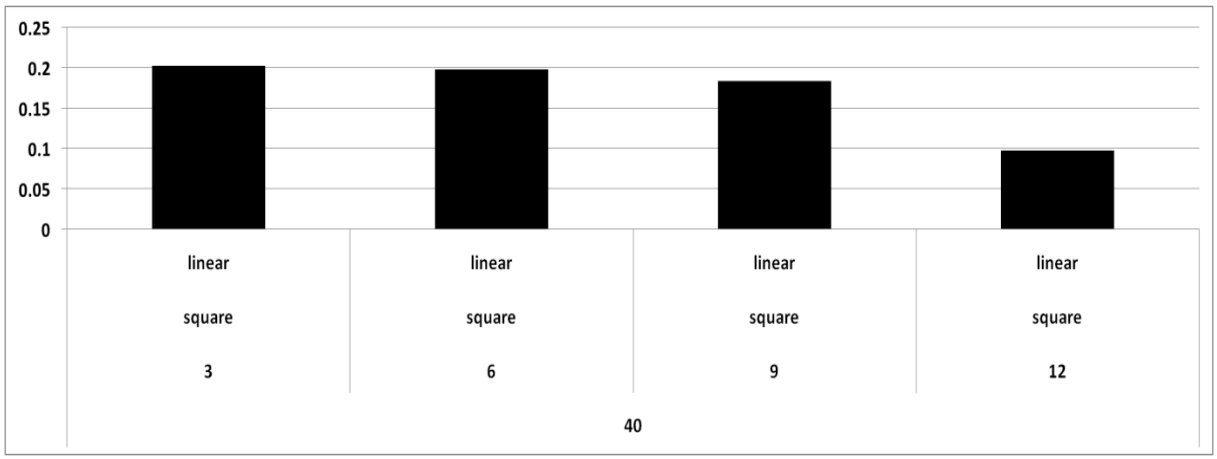

Figure 43: Spectral Gamut coverage of square wave ink at 40% overlap for a linear system. 3, 6, 9 and 12 inks evaluated based on mean RMS difference between the closest match on gamut and the goal reflectance. Mean RMS is on Y axis.

CHAPTER 5: SPECTRAL GAMUT MAPPING AND SPECTRAL INK SEPARATION

As the number of independent primaries increases in a system, the gamut coverage of the system grows. On the other hand when working with data in higher dimensions, the likelihood of some input data falling outside of the gamut increases exponentially. A similar situation applies in spectral printing, meaning that given a medium (paper) maximum reflectance constraint, non-linear interaction of the inks and wide spectral sensitivity of the inks, it is almost guaranteed that a given input spectral reflectance falls outside of the printer gamut. Because of such a high probability of an input point falling outside of the device gamut, gamut mapping becomes the base of spectral reproduction, especially for non-linear devices such as printers. This is quite different from the traditional printing approach where a considerable portion of the data falls inside the gamut. Because of this, the focus of this portion of the research is on spectral reproduction, which includes gamut mapping and primary separation (ink separation), for the printers where the non-linear interaction of inks and media increases the complexity of the reproduction algorithms substantially.

Another challenge with working in higher dimensions is the complexity of calculating the gamut. The traditional gamut mapping algorithms work in CIELAB or other three dimensional spaces. Most of these algorithms calculate the gamut boundary using methods such as convex hull [28], [45], [46], [47]. The complexity

of these methods grows exponentially with the number of dimensions, which poses another challenge to spectral reproduction.

In this section, a review of different approaches for finding the best ink combination and mapping a given reflectance on the printer gamut boundary is presented.

Spectral Reproduction Based on Interim Colour Space

ICC (International Colour Consortium) Profiles describe the colour behaviour of a particular device by defining a mapping between the source colour space and a profile connection space (PCS). Typically, this PCS is based on either CIELAB or CIEXYZ colour space. There are two common types of mappings. One approach uses look-up tables where interpolation is applied for the data points between the cells. The other mapping is based on a series of parameters for transformations, e.g. a 3x3 matrix transformation.

Several approaches have been proposed to extend the idea of ICC to spectral space. Mitchell et al. [48], [49] proposed a combination of projection plus a 6-dimensional Lookup table (LUT) PCS for a 6 ink printer. An iterative interpolation was used to invert the LUT. Their study [48] showed that using an ink-like basis improves the efficiency of the LUT compared to using orthogonal eigenvectors generated from PCA.

Berns et al. proposed a new method based on using a coarse LUT to reduce metamerism [52]. Using this method, in each cell of the LUT there are multiple ink-combination candidates that have the same colour value (CIELAB)

under one illumination but a different colour value under the second source of illumination. Knowing the colour value of an ink combination for the second illumination, we can select an ink combination that has a good match in both illuminations and thus improve colour constancy.

Following on the above research on improving colour stability across two illuminations, there are a couple of other approaches used to transfer spectral data to CIELAB colour space plus an additional 3 dimensions. Nakaya et. al. use sRGB colour space to represent the remaining 3 dimensions, [89][90]. Derhak and Rosen introduced LabPQR interim colour space [57], [58]. LabPQR is a 6-dimensional space where the first 3 dimensions represent the gamut of a printer in CIELAB under a given illumination. The remaining 3 dimensions represent the next 3 most important dimensions of the spectral gamut after the CIELAB (or CIEXYZ) data is removed. The advantage of this interim space is that a hybrid of traditional gamut mapping and spectral gamut mapping is combined with almost no additional complexity in comparison to 3-dimensional gamut mapping. Given an input reflectance, the traditional gamut mapping algorithm can be applied in CIELAB space. After the mapping, each cell represents a cluster of data points with the same colour values (CIELAB) but different PQR values, which represent different spectral reflectances. It was also shown that this interim space can represent the spectral gamut of a 6-ink printer with very high accuracy [59].

To evaluate the accuracy of the LABpqr method to meet spectral colour reproduction needs, this method was tested on five different reflectance data bases. The LABpqr values were calculated based on the 8-ink printer data

discussed in Chapter 3: Table 7 shows the round trip result of the model and the accuracy of the model in embedding spectral characteristics of the five databases. The performance was evaluated under one reference illumination (D65) and under 11 different illuminations as specified in Table 6.

The data shows that the model has a small round trip error, similar to what was reported by Derhak et al. in [57]. This result is consistent with PCA analysis of the 8-ink printer, which showed that 5 bases were sufficient to represent the printer spectral gamut accurately (Figure 12). In this experiment, out of the five databases tested, two included natural reflectances (Simon Fraser University [65] and Leeds University [82]). The other 3 databases (Leeds, Munsell, MacBeth) represent printed or painted colours, which typically have lower spatial complexity than scene reflectances because of the ink limit of the medium and the number of paints or inks used in the system.

The experiment shows that this model can be sufficient for spectral colour reproduction of paintings and prints but not for databases that include scene reflectances with higher than 6-dimensional complexity.

Table 7: LABpqr performance of an 8-ink printer system in reconstructing 5 different data sets. Leeds database represents scene reflectances provided by Leeds University [82]. Munsell database includes reflectances for a set of prints and paintings measured by Leeds university. The SFU dataset is provided by Computational Vision Lab at Simon Fraser University [65]. The last two databases include the MacBeth Colour Chart and some pigmented colours used by artists.

	Num	ΔE_{94}			RMS		ΔE_{2000}		
	Patches	mean	max	max Daylight	mean	max	mean	max	max Daylight
8-ink	6048	.18	2.6	.87	.002	.03	0.19	2.43	.91
Leeds	5682	0.96	40.8	7.22	1.77	7.31	0.80	41.32	6.93
Leeds MunSell	719	1.02	28.4	4.2362	1.64	6.92	0.84	41.32	5.82
SFU	1350	0.41	21.7	4.7257	0.02	0.09	0.45	26.47	5.28
MacBeth Colour Chart	24	0.50	7.7	1.3701	0.02	0.05	0.56	9.25	1.38
Pigment	35	0.74	6.7	1.212	0.04	0.06	0.56	9.25	1.38

There were other attempts to enable traditional gamut mapping for spectral reproduction by lowering the complexity of the gamut space using methods like PCA [56]. Bakke et al. proposed an improvement to PCA-based gamut mapping by defining the direction of projection to be towards the centre of the printer gamut in each 2D cross section of gamut created by a combination PCA basis and media vector. The 2D cross section is defined by 2 vectors – a line between the given reflectance and the gamut centre in PCA space – and a vector representing the spectral gray component of the medium (paper). The gamut boundary is found by calculating the intersection between the 2-dimensional plane and the hyper-planes that define the gamut.

Spectral Ink Separation Based on Inverting a Printer Model

As discussed earlier there are several methods proposed for modelling the printer output. Most of these models are based on a non-linear transformation and, because of that, inverting the models accurately is quite challenging. Di-Yuan Tzeng et al. [50], [51] divided a 6-ink printer model into several 4-ink printer models to reduce the complexity of inverting a printer model. The assumption is that no more than 4 inks are put down on the same location. An iterative search is used to find the closest match to a given data point in each 4-ink printer model.

Urban et al. introduced a fast method for inverting the Yule-Nielson cellular Neugebauer model [53][54]. The inversion model is based on a local search, considering one dimension (one ink) at a time. Given an input reflectance, this method finds the best ink density of the i^{th} ink given the selected ink density of the previous inks. His study showed that even though the proposed search method does not guarantee finding an optimal ink combination, it finds one that is very close to optimal.

Proposed Method I: Spectral Ink Separation using Non-Negative Least Squares

One method to simplify gamut mapping algorithms is to assume that the printer gamut is convex in spectral reflectance space and thus there is no need to have very fine sampling of the printer gamut to capture all of the concavities.

A fast gamut mapping method is introduced in this section that is based on a Non-Negative Least Square (NNLSQ) method. The Non-Negative Least

Square (NNLSQ) method tries to minimize the sum of the residuals using a non-negative combination of the available data as discussed in the Chapter 1.

Considering the gamut mapping procedure, the goal of the algorithm is to reproduce an input reflectance that is inside or on the gamut boundary shell and is closest to the input reflectance. Assuming that the gamut boundary is convex and relationship between close neighbours can be defined linearly, a point on or inside a gamut hull can be represented by a linear interpolation of the neighbouring gamut points. The equation below captures this relationship:

(18)

$$\rho = \Sigma\, \alpha_i q_i, \quad \alpha_i \geq 0, \quad \Sigma\alpha_i = 1$$

Where ρ is the input reflectance and q_i represents the set of measured points on or inside the gamut hull. The α_i's are weights, and the restrictions on the weights ensure that ρ does not lie outside the convex hull of the q_i.

For a point ρ outside a convex gamut, we can find the closest point to ρ lying on the convex hull of the gamut by finding α_i minimizing the distance e:

$$e = | \rho - \Sigma\, \alpha_i q_i |2, \quad \alpha_i \geq 0, \quad \Sigma\alpha_i = 1$$

Finlayson et al. [67] showed that the above equation can be rewritten to include a weight W as an extra dimension in the input data, and that the revised equations can then be solved by the standard NNLSQ method. Their derivation is as follows.

$$q_i' = [q_i \; W]$$

$$e' = | \rho - \Sigma \alpha_i q'_i |^2$$

Re-writing e' yields:

$$e' = e + W*(1 - \Sigma \alpha_i)$$

The advantage of the above equation is that it can be minimized by applying NNLSQ. Choosing a large value for W emphasizes the second term in *e'*, thereby enforcing the constraint $\Sigma\alpha_i = 1$.

Spectral gamut mapping means mapping a spectrum that lies outside the printer gamut onto a printable spectrum. For a spectrum represented as a point, ρ, minimizing *e'* the closest point on the gamut's surface, in other words it finds the closest printable spectrum. The spectrum is described as a linearly weighted combination of other printable spectra, spectra that are within the printer gamut.

This proposed gamut-mapping algorithm is easy to implement and the computation is relatively fast considering the dimensionality of the input spectra. The space and time requirements of the algorithm grow with the number of input data points. However, as it was shown in Chapter 3:Printer Modelling, by sampling ink space intelligently, the number of points required to represent a gamut space can be reduced by as much as 97%.

Preserving Colour for a Desired Illumination

The proposed spectral gamut mapping algorithm using the NNLSQ method maps an input reflectance to the closest printable spectrum in spectral space, but there is no guarantee that this new spectrum will have the same

colour (for a fixed illuminant) as the original spectrum. It would be preferable to have a spectral gamut-mapping technique that maps an out-of-gamut spectrum to the closest in-gamut spectrum subject to the constraint that it preserves colour under a given illumination as well.

Chau et al. [6] proposed dividing each surface reflectance into two components. One is the fundamental component that represents perceived colour under a single illumination and another is the metameric black component that is invisible to the normal human eye. Using this approach each surface reflectance, s, can be represented as:

$$s = f_s + b_s$$

where f_s represents the fundamental component or basis that represents colour, and b_s represents the metameric black of input surface reflectance. Chau proposes a gamut mapping algorithm that searches for a reflectance s' that has the same fundamental component but may have a different metameric black.

In this section an extension to the NNLSQ algorithm is introduced to include Chau's proposed method in order to preserve perceived colour while finding the closest metameric black for a given input reflectance. This can be accomplished by modifying the NNLSQ algorithm so that the projection onto the gamut is in a direction perpendicular to CIEXYZ space under a given illumination. Doing so preserves the CIEXYZ coordinates as much as possible.

The method works as follows. Let U represent the principal components basis of the x, y and z colour matching functions. If the visible spectrum is

sampled n times, then each x, y and z basis can be represented as 1xn dimensional matrix and U will be an nxn matrix, where first row in U captures the most variance in CIE XYZ colour space and the last row represents the least variance.

Let P be the set of spectra in the printer gamut *{p1, p2, …},* then the following linear projection of values in P into U

$P_u = PU$

represents the gamut in U space sorted in terms of decreasing variance in XYZ space. After this linear transformation, the first 3 coordinates of P_u represent the tristimulus values of spectra in the printer gamut. Next, weights can be applied to P_u so that applying the gamut-mapping algorithm described above to the weighted P_u yields the closest spectrum on the hull of the printer gamut that creates the least change in CIEXYZ space. The larger the weights are the more emphasize is put on preserving values in CIEXYZ dimension compared to other spectral residual variations.

Evaluation of Gamut Convexity

Many existing gamut-mapping algorithms [69], [46] and [44], including the LabPQR spectral gamut-mapping algorithm [57], map an out-of-gamut point onto the convex hull of the printer gamut. The assumption is that the gamut is convex. Is this assumption valid and how much accuracy is lost by assuming a convex printer space?

Algorithms such as Alpha Shape [70] can measure concavity of a space in a low-dimensional space (3D), but cannot be used in high-dimensional spectral space.

Comparing the NNLSQ performance to an algorithm that does not depend on the convex assumption of the gamut can explain how much inaccuracy is introduced when a printer spectral gamut is assumed to be convex.

Most mappings that do not depend on the gamut convexity assumption are based on a type of search method. It is proposed that the Hierarchical Search algorithm introduced in Chapter 3 be used.

Experiment

The printer model used for this experiment was based on the Tzeng (TK) printer model which was explained in equation 16.

Two types of inks were used, synthetic inks which are square wave based and sine wave based inks (as discussed in Chapter 2), and inks based on real pigmented ink reflectance measurements. Three different variations of square wave inks were used with 0, 10% and 20% overlap in their wavelength absorption sensitivity region. Similarly, for the sine wave ink, 10% and 20% overlaps are used.

Four different ink numbers (3, 6, 9 and 12 inks) were used to evaluate the convexity of the system spectral gamut. For the real ink data, the 3 inks considered were cyan, magenta, and yellow. For the 6-ink case, the initial 3 inks were retained, and 3 more complementary inks were added, namely, orange,

green, and violet. light cyan, black and light magenta were added to these 6 for the 9-ink case. For the 12 ink case, gray and medium gray inks along with a light red ink were added to the system.

Target reflectances were selected as the 80 scene reflectances sampled from Simon Fraser Database [65] using K-means clustering as explained in Chapter 3.

For convex hull gamut mapping, the NNLSQ implementation provided by Matlab was used. The HS search method introduced in Chapter 3 was used to evaluate concavity of the printer gamut in spectral space. The HS method was used since the method does not depend on calculating the convex hull of the printer gamut.

Results

In the previous chapter, it was shown that as the number of primaries available in the system increases, the overall spectral gamut coverage increases. The gain in the gamut coverage varies depending on the primary reflectance characteristics. Figure 44 shows that using the NNLSQ method to map the out-of-gamut reflectances onto the convex hull of the printer gamut -- similar to the non-convex mapping method -- the gamut coverage increases as the number of available primaries increases.

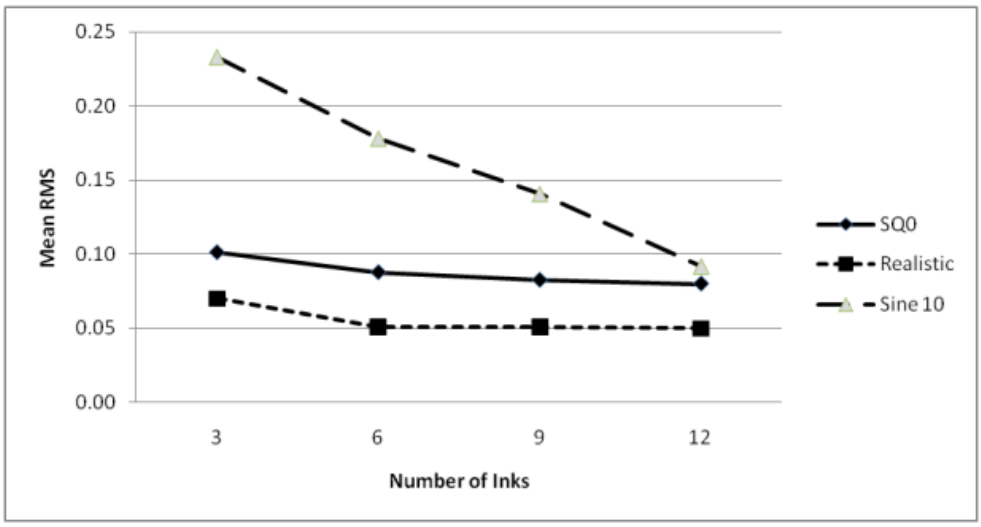

Figure 44: Gamut coverage calculated using the non-negative least square technique. The Y axis shows Root Mean Square (RMS) variation between mapped reflectance and the input scene reflectance. SQ0 represents square wave inks with 0% overlap, Sine10 represents sine wave inks with 10% overlap, and Realistic represents real ink reflectance measurements.

To evaluate the concavity of a printer gamut, the variations between the NNLSQ gamut mapping and HS (Hierarchical Search) gamut mapping were compared. HS mapping is an iterative search method that does not make any assumption about the convexity of the gamut, whereas the NNLSQ method assumes a convex space. Results from the HS method were used as the closest point on the printer spectral gamut to a given target reflectance. Figure 45 evaluates how different the gamut mapped reflectance using a convex gamut mapping based on the NNLSQ technique is from a non-convex gamut mapping. The first observation was that the variation, which indicates the concavity of the gamut, increases as the number of available inks in the system increases. Another observation was that square wave inks with a higher degree of overlap have much larger concavities in their gamuts than inks with less overlap. This is consistent with the observation from Chapter 3 that inks with a larger than optimal reflectance sensitivity overlap tend to have smaller gamut coverage. The

data in this section shows that most of the change in gamut is in its concavity rather than the coverage when the inks (more specifically square wave based inks) have larger overlap than what is optimal.

Figure 46 shows the concavity results for sine wave inks with different overlap and compares the result against real ink measurements. It shows that inks with smoother reflectance characteristics (sine wave versus square wave) have fewer concavities in their gamuts.

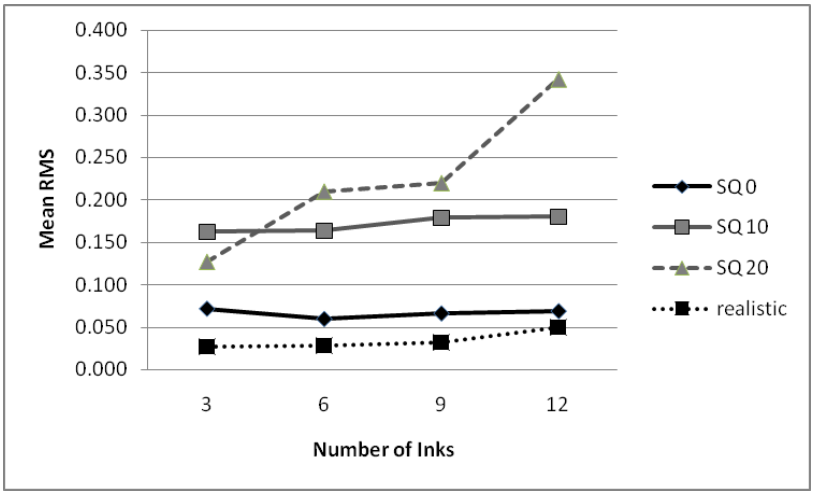

Figure 45: Variation between convex gamut mapping and concave gamut mapping. The concave gamut mapping is based on the HS iterative search algorithm and the convex gamut mapping is based on the non-negative least square algorithm. The variation is calculated as average RMS (Root Mean Square) difference between the two spectral reflectances calculated using two different mapping methods.

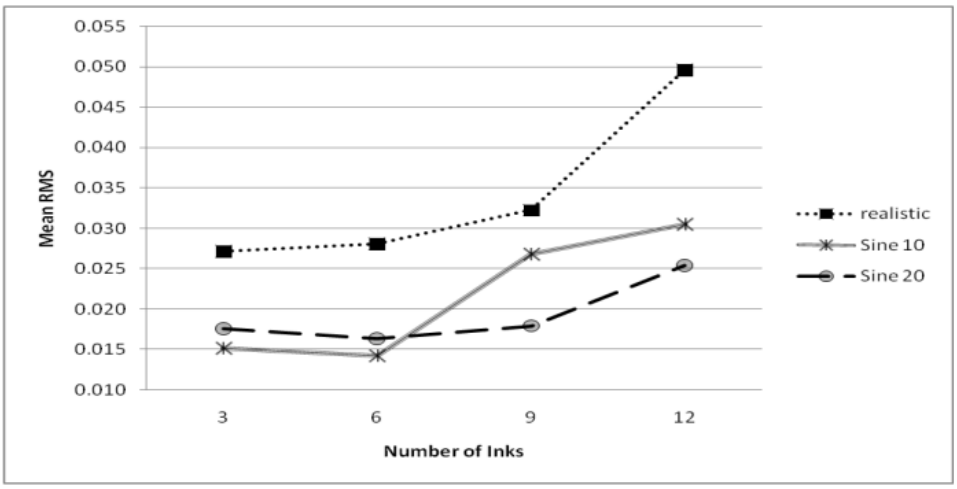

Figure 46: Variation between convex gamut mapping and concave gamut mapping for primaries with smooth variations (sine wave). The concave gamut mapping is based on the HS iterative search algorithm and the convex gamut mapping is based on the non-negative least square algorithm. The variation is calculated as the average RMS (Root Mean Square) difference between the two spectral reflectances calculated using the two different mapping methods.

Perceptual variations between convex and concave gamut mapped reflectances are presented in Figure 47, which shows the variation in $DeltaE_{94}$ colour space. The variation was calculated as the average $deltaE_{94}$ under 11 different illuminations [66].

The first observation was that the concavity assumption of the printer with sine wave inks has an acceptable variation (1 to 4 deltaE), knowing the gain that we get by using the NNLSQ technique. Knowing this, the NNLSQ algorithm can be used as a good candidate for gamut mapping of a non-linear device with a large number of primaries. The figure also shows that, despite the increase in the spectral difference between convex and concave gamut mapping as the number of inks increases, the increase is not perceptually as important. Figure 48 shows reflectance matches for 6 and 12 ink systems with sine wave inks of 20% overlap. It shows that in 12 dimensions the convex and concave gamut mapped

reflectances have small multiple variations that add up to a large spectral difference. However, multiple small variations in the spectral space are not perceptually as visible as a few large local variations in the spectral space.

On the other hand, for the real ink reflectances, there is much higher perceptual variability when the convex gamut mapping algorithm is used, compared to what the printer is actually capable of (Figure 47).

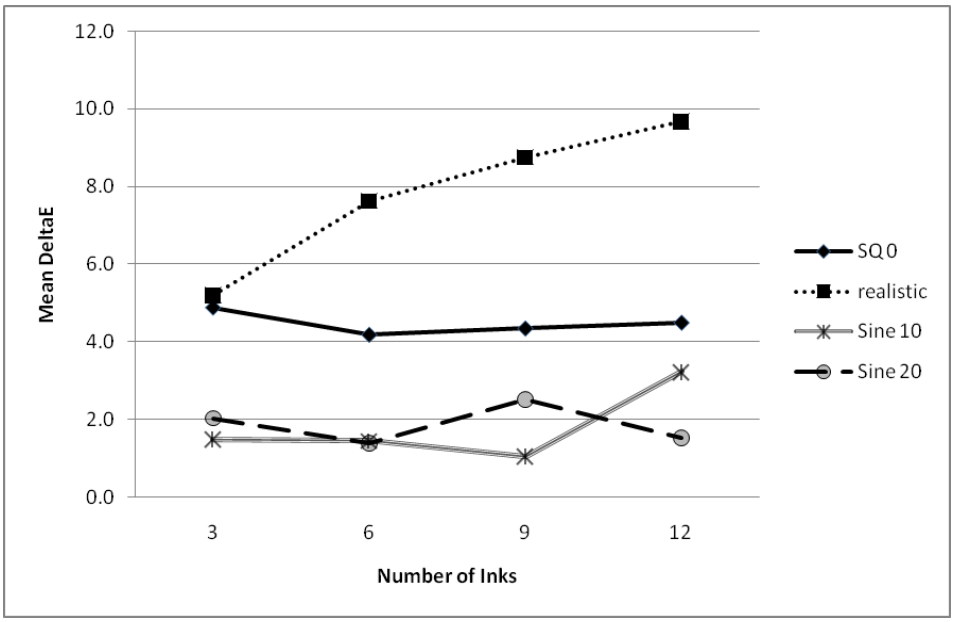

Figure 47: Variation between convex gamut mapping and concave gamut mapping for primaries with smooth variations (sine wave). The concave gamut mapping is based on the HS iterative search algorithm and the convex gamut mapping is based on the non-negative least square algorithm. The variation is calculated as average $DeltaE_{94}$ difference between the two spectral reflectances calculated using two different mapping methods.

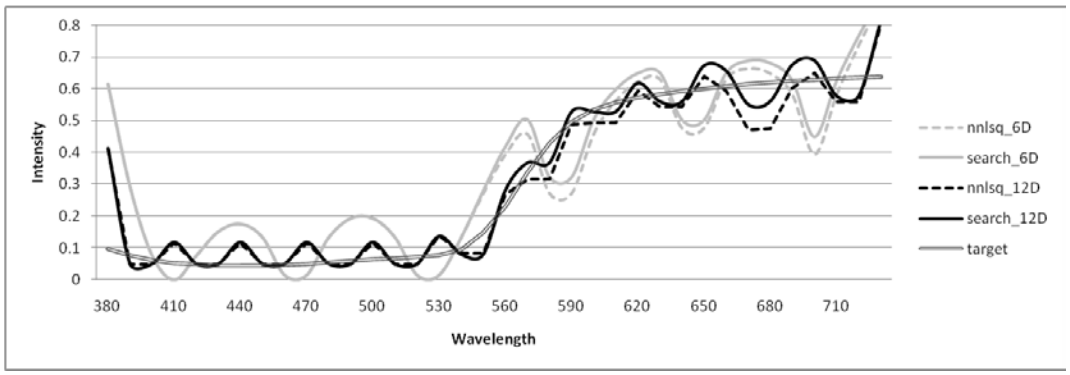

Figure 48: Reflectance characteristics of HS and NNLSQ gamut mapping for 6 and 12 ink systems. The inks are sine wave inks with 20% overlap.

Proposed Method II: Geodesic Based Ink Separation for Spectral Printing

In this section a new ink separation algorithm is introduced for printing with 6 to 9 inks. A new spectral gamut mapping algorithm is also introduced that projects an input reflectance onto the manifold of the printer spectral gamut space. Ink separation, i.e., finding the best ink combination to reproduce a given reflectance, is done by applying an interpolation between printer gamut points neighbouring a projected point's geodesic location. This algorithm was inspired by the work of McIntosh et al. [71] who suggested interpolating over geodesic distances, rather than Euclidean distances, to improve an image segmentation algorithm.

The technique finds the best manifold projection using the ISOMAP technique explained earlier. The algorithm searches for the lowest dimensionality that holds the spectral information accurately. This method will aid in finding a good ink combination given an input reflectance for 6-ink and 9-ink printer models.

Use of Thin Plate Spline Interpolation in Spectral Reproduction

For the spectral printing process, it is proposed that TPS be used to find a continuous function that maps between the set of inks and each of the output dimensions. For instance, if the output spectral reflectance of an 8-ink printer is measured from 380nm to 730nm with a 10 nm sampling, TPS is used to create 36 separate functions mapping from the 8 input dimensions to each reflectance wavelength.

Geodesic Interpolation and Ink Separation

Interpolation is a common approach to ink separation and the ink separation technique introduced in this section is also based on interpolation. In general, an ink combination is interpolated as a weighted combination of nearby experimentally measured data points. The weights typically are derived based on the distance of the point to be interpolated from its neighbours. The distance metric can be defined in many different ways. For instance, the distance between two spectral reflectances can be measured as the Euclidean distance between them. In this section, an interpolation-based ink separation algorithm based on geodesic distances over the gamut manifold is proposed.

Many spaces appear to have a high dimensionality in a linear space, but actually have lower intrinsic dimensionality. A good example is the Swiss Roll example discussed in Chapter 2.

The proposed ink separation method introduced in this chapter uses the geodesic distances between data points. The algorithm is as follows:

1. Given a set of training points (reflectances of print samples), the geodesic distances between the input reflectance (the reflectance to be printed) and all training points in the gamut are calculated

2. The geodesic distances are used in an MDS engine (Multi-Dimensional Scaling) to calculate the point locations in a space of lower dimension.

3. Thin Plate Spline interpolation is used based on the data point locations in the new space

3a. Weights for the interpolation are calculated based on the distance of the point from the neighbouring points in the lower dimensional space.

Steps 1 and 2 are part of the standard ISOMAP algorithm [62]. ISOMAP makes the assumption that the Euclidean distances to points within the local neighbourhood of a given point, P, approximate the corresponding geodesic distances. The geodesic distance to a point, Q, outside the local neighbourhood is calculated as the sum of the distances between neighbouring points along the shortest path from P to Q.

Spectral Gamut Mapping based on Manifold Projection

In this section, a possible spectral gamut mapping algorithm based on manifold projection is presented. Figure 49 represents an example where gamut mapping in Euclidean space may not result in the closest point in the gamut.

However, mapping based on the geodesic location of the gamut points can result in a closer (true) mapped location (Figure 50).

The proposed mapping algorithm has the following steps:

1. Given a printer gamut space, calculate the data point's geodesic location using ISOMAP
2. Transfer the input spectral reflectance using the same transformation
3. After the transformation, gamut mapping is applied in the (lower dimensional) transformed space
    a. The Non-Negative Least Square gamut mapping algorithm introduced in the previous section is used for mapping the transformed input reflectance onto the printer gamut
4. The projected value in the lower dimensional space is inverted back to the spectral space using an interpolation method
    a. Thin Plate Spline interpolation is used for the inverse transformation

Another advantage of applying gamut mapping based on the manifold projection is that the mapping can be done in a much lower dimensional space. Because of reduce dimensionality, the time and space complexity of the gamut mapping can be reduced significantly.

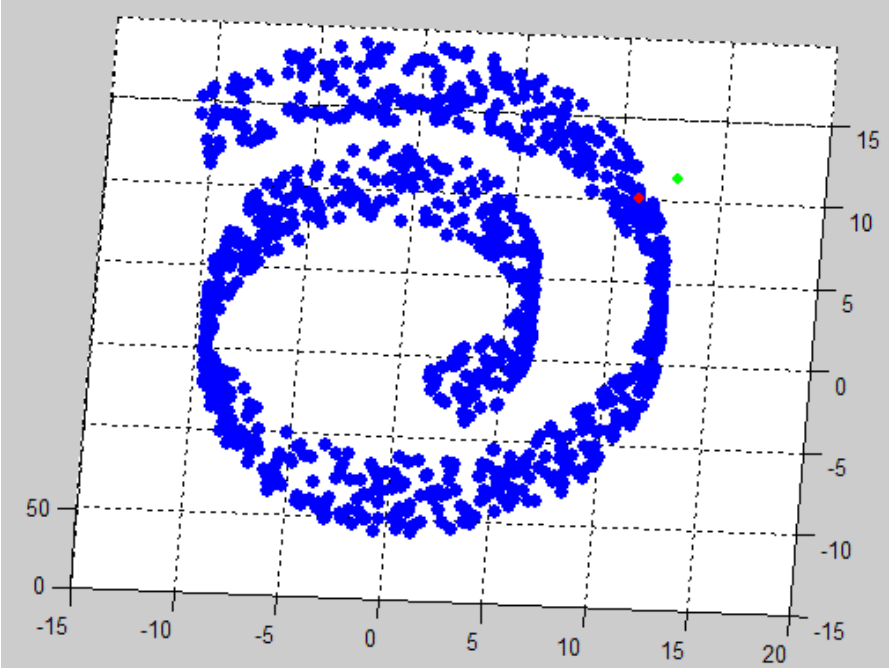

Figure 49: Example of the gamut mapping algorithm in Euclidean Space. Blue lines (Swiss roll) represent a device gamut and the green point represents an out of gamut point.

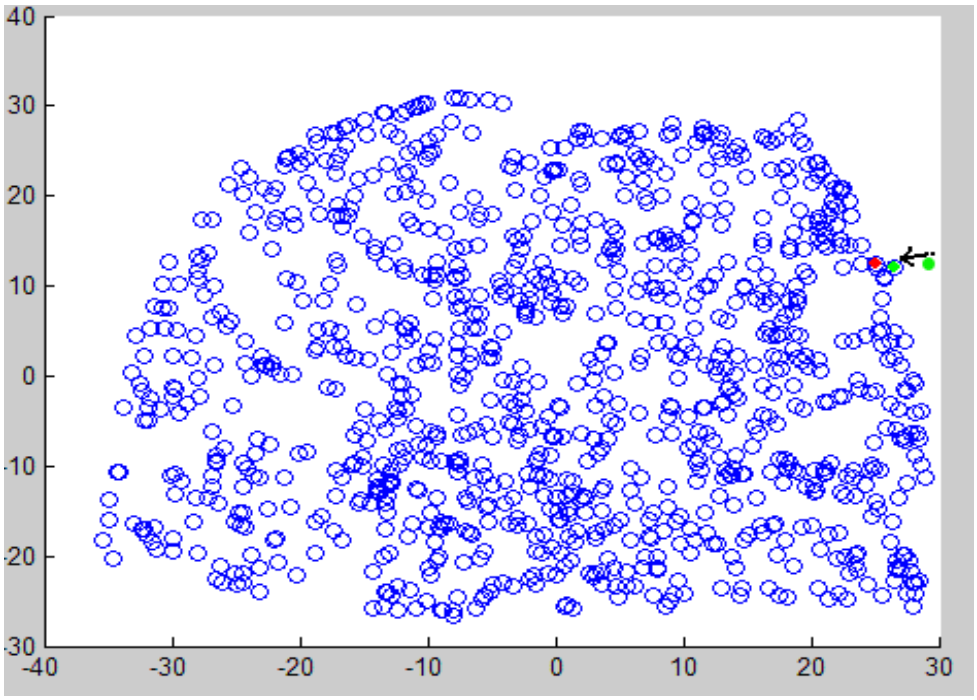

Figure 50: Gamut mapping method using ISOMAP where the projections are applied in a lower dimensional space.

Evaluation Method

Similar to the previous gamut mapping algorithm (NNLSQ), the accuracy of the manifold projection algorithm is evaluated by comparing the result of the mapping algorithm against what the Hierarchical Search (HS) mapping finds. Details of HS gamut mapping are explained in Chapter 3.

Performance of the manifold projection method was evaluated by comparing the RMS (Root mean square) differences of the mapped reflectance using this technique with the HS search method results. In addition to RMS, average deltaE_{94} colour difference of the mapped reflectances using the proposed method and HS search method under 11 different illuminations is presented.

To evaluate the difference between the projected reflectance and the results from the HS search algorithm the manifold projected value needs to be projected back to the spectral colour space. Thin Plate Spline interpolation, which is defined in the previous chapter, is used for inverting the ISOMAP transformation.

Time and Space Complexity

There are several methods to calculate Geodesic distances between points given the distances between neighbouring points. Most commonly, Dijkstra's algorithm is used to find the shortest path between each point in the data set [2]. If there are M_p points representing the printer gamut, and M_D input points for ink separation, the time complexity of Dijkstra's algorithm based on the Fibonacci heap algorithm is $O(E + (M_p+M_D)Log(M_p+M_D))$, where E represents the number of edges between the points. The number of edges varies with the data set characteristics and diameter of the neighbourhood around each data point. In practice, it takes around 2.5 seconds to calculate the geodesic distances for 2000 points on an average computer.

Experiments

Printer Gamut

To evaluate the gamut complexity of the printer, two printer gamuts were evaluated. The first one was based on spectral measurements of 1350 patches printed with an 8-ink printer. This gamut is referred to as a "realistic" printer gamut since the measurements were based on the real printer gamut

measurements. The second printer gamut was based on the synthetic printer model introduced by Tzeng explained in Chapter 3. The model was used to predict the spectral reflectance resulting from a given ink combination.

Ink Choices

Two sets of ink selections were used in this study. The first set was based on real ink measurements as discussed in previous chapters. The inks were orange (O), cyan (c), magenta (m), yellow (y), green (Gr), violet (V) and black (K), light magenta (LM) and light cyan (LC) for the 9-ink printer. Orange (O), cyan (c), magenta (m), yellow (y), green (Gr) and violet (V) were used for the 6-ink printer, and the 3-ink printer model used cyan (c), magenta (m) and yellow (y).

The second set of inks had synthetic ink reflectances with a square wave shape and 0% overlap in their absorptions sensitivity region.

Printer Spectral Gamut Intrinsic Dimensionality

What are the intrinsic dimensionalities of the gamuts of the two printers? In terms of a linear model, Principal Component Analysis (PCA) provides one answer. However, in terms of a non-linear model, ISOMAP provides a second answer. If the answers differ, then it can be conclude that the printer gamuts bend in a way that is analogous to the Swiss Roll example. Figure 51 and Figure 52 compare how the residual variance changes with increasing dimensionality for both PCA and ISOMAP. If PCA shows a higher dimensionality for the data set than what ISOMAP finds, then we can conclude that the underlying structure of

the gamut is a lower-dimensional data set. Figure 51 and Figure 52 are based on the realistic gamut; Figure 53 and Figure 54 are for the synthetic gamut.

The analysis shows that the printer gamuts are of lower (3 or 4 versus 5 or 6) intrinsic dimensionality than can be determined by linear PCA. In addition, the weights used for the interpolation based on the new proposed method are calculated using geodesic distances of the points in lower dimension. As a result, it should be possible to obtain more accurate ink separations using interpolation based on the distances between the ISOMAP-embedded locations of the reflectances.

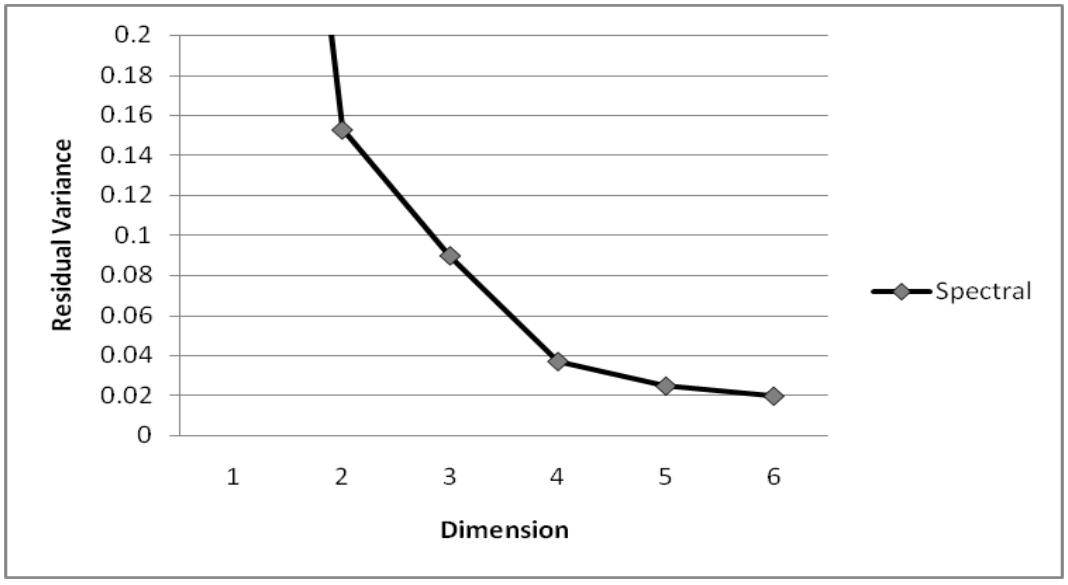

Figure 51: PCA residual variance for the realistic printer gamut space. The plot shows that the dimensionality of the 7-ink printer is around 5 dimensions.

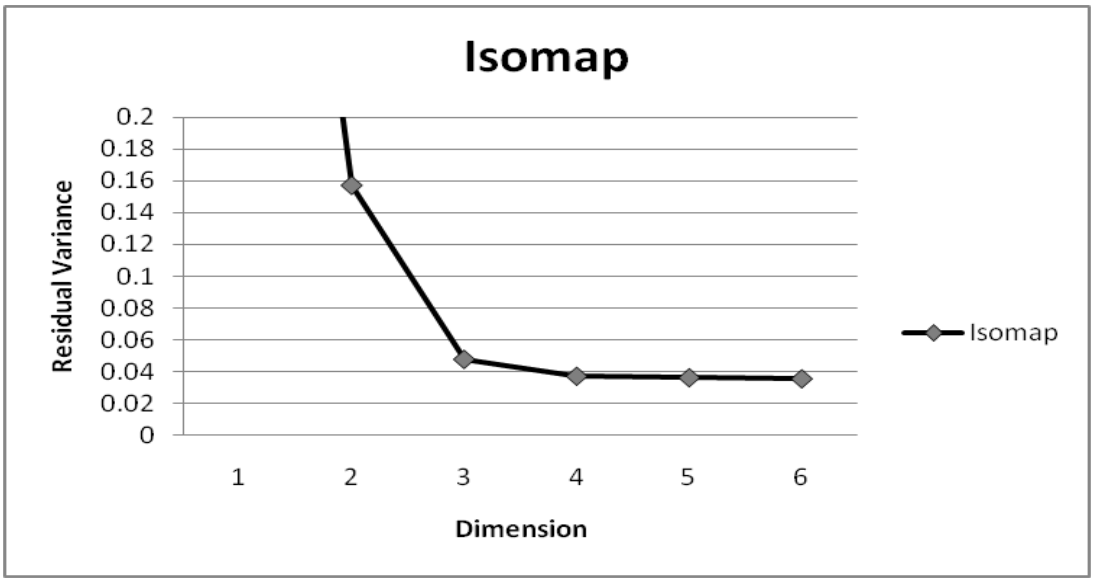

Figure 52: ISOMAP residual for the realistic gamut. The data shows that the underlying dimensionality of the gamut is around 3.

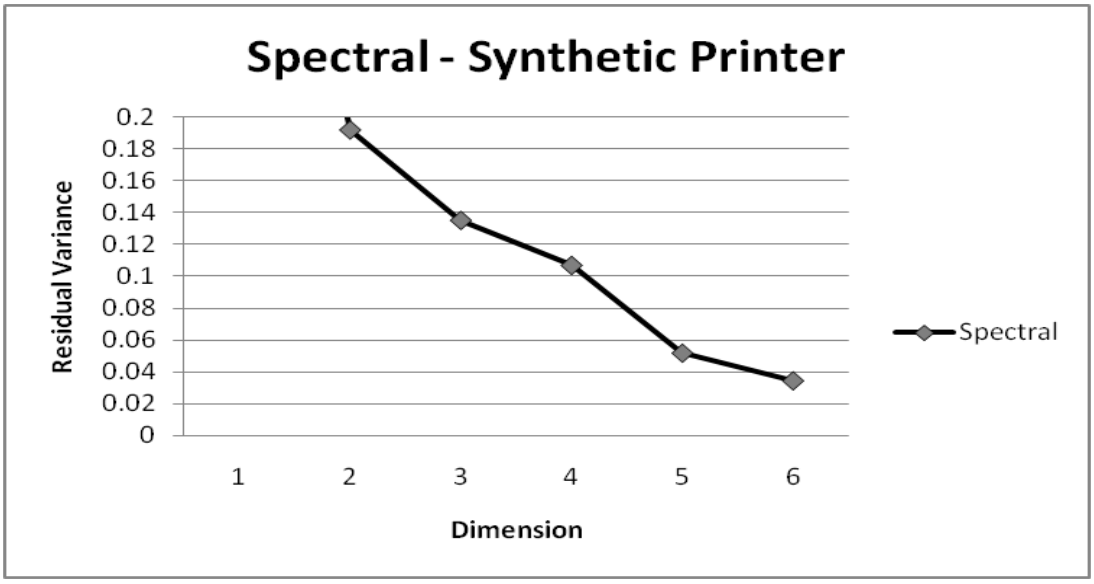

Figure 53: PCA residual variance for the synthetic printer gamut space. The scores show that the dimensionality of the 6-ink printer is around 6 or 7 dimensions.

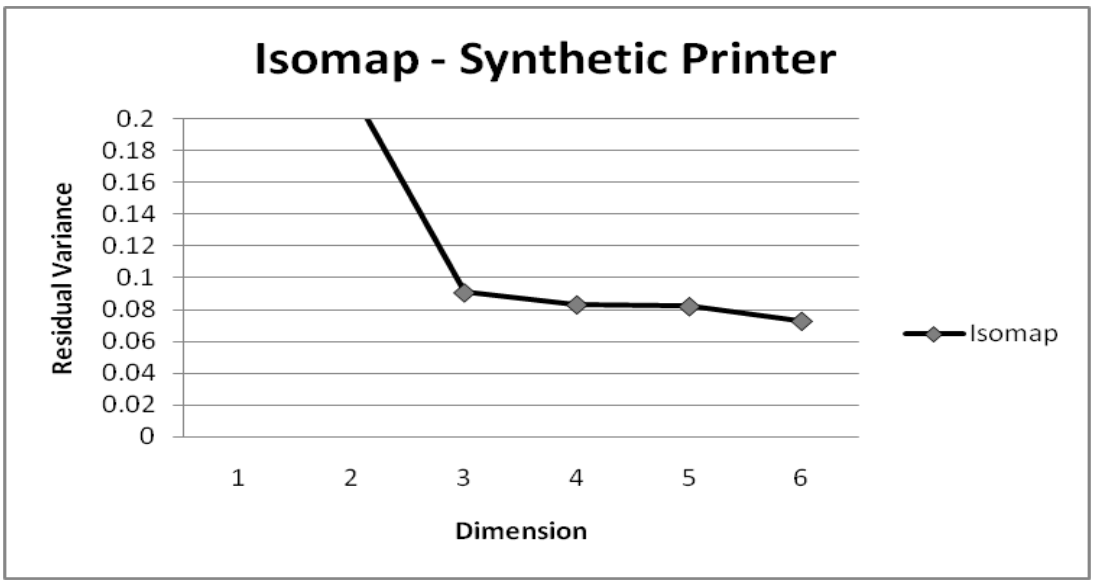

Figure 54: ISOMAP residual for the synthetic gamut. The data shows that the underlying dimensionality of the gamut is around 3 to 4.

Results

To evaluate how well the ink separation technique works, the synthetic printer gamut was sampled uniformly in ink space, obtaining 2300 data points as a training data set. An additional 250 data points from inside the printer gamut were selected to represent the test sample. The test and training sets were disjoint.

The 250 test points were processed through the ink separation algorithm. The predicted ink combinations were then run through the printer model to predict the corresponding spectral reflectances. The predicted reflectances were then compared to the original input reflectances.

To evaluate the performance of the geodesic ink separation model, its results were compared to those obtained by doing the separation in linear space. Table 8 shows that there is a gain when the interpolation is based on the geodesic distances instead of the Euclidean distances.

Table 8: Ink separation evaluation based on geodesic location and linear space locations. The errors reported are the minimum, mean, and max ΔE_{94} that occur under the 11 different illuminations, and the RMS difference between the spectra.

		Geodesic		Linear	
Inks		**RMS**	**ΔE_{94}**	**RMS**	**ΔE_{94}**
3	min	0.0011	0.236	0.0078	1.204
	mean	0.034	3.068	0.0335	6.33
	max	0.134	8.2	0.0717	24.78
6	min	0	0.005	0	0.006
	mean	0.0089	2.843	0.0298	3.379
	max	0.0541	18.29	0.1339	20.45
9	min	0	0.004	0	0.014
	mean	0.0081	2.617	0.0179	3.051
	max	0.0487	14.1	0.1238	20.05

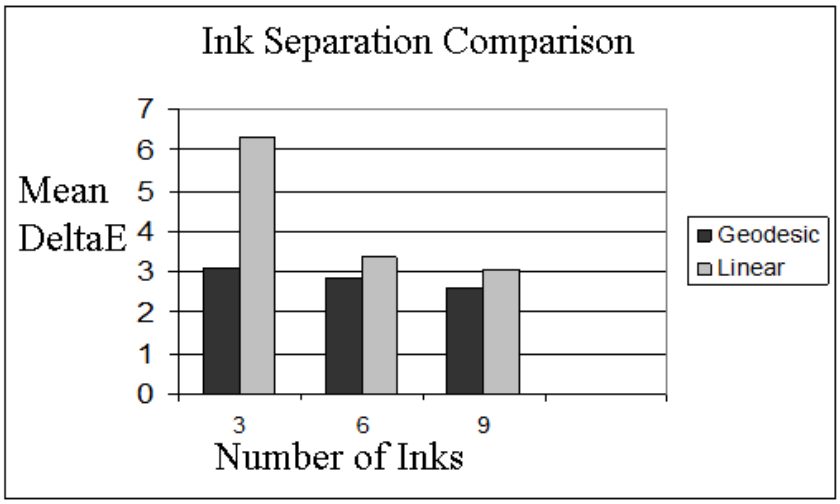

Figure 55: Ink separation methods evaluated in ΔE_{94} under 11 different illuminations. The data above shows average ΔE_{94} for the 11 illuminations

Spectral Gamut Mapping Evaluation

Test Data

To test the gamut mapping algorithm, the scene reflectances from the SFU database were used [65]. There are 1350 individual reflectances in the

database. Figure 56 and Figure 57 show the accuracy of the spectral reproduction when the proposed spectral gamut mapping algorithm is used compared to the hierarchical search method to map the out-of-gamut points onto the gamut hull. The table shows that the proposed gamut mapping algorithm is as accurate as, or better than, the hierarchical search algorithm.

It is important to keep in mind that the hierarchal search algorithm has some inaccuracy as well which can add to the overall evaluation comparison. Some of the inaccuracy of the hierarchical search algorithm comes from the sampling resolution of each ink axis. The higher the sampling resolution, the more accurate the model. For these experiments, the hierarchical search had 6 levels, and at each level the sampling resolution for each axis was 5. For instance, for a 3-ink system, at each search level there are 5^3 different ink combinations to choose from. Once the closest ink combination was selected (P_a), 5^3 samples were selected close to the point P_a. This process was repeated for 6 levels.

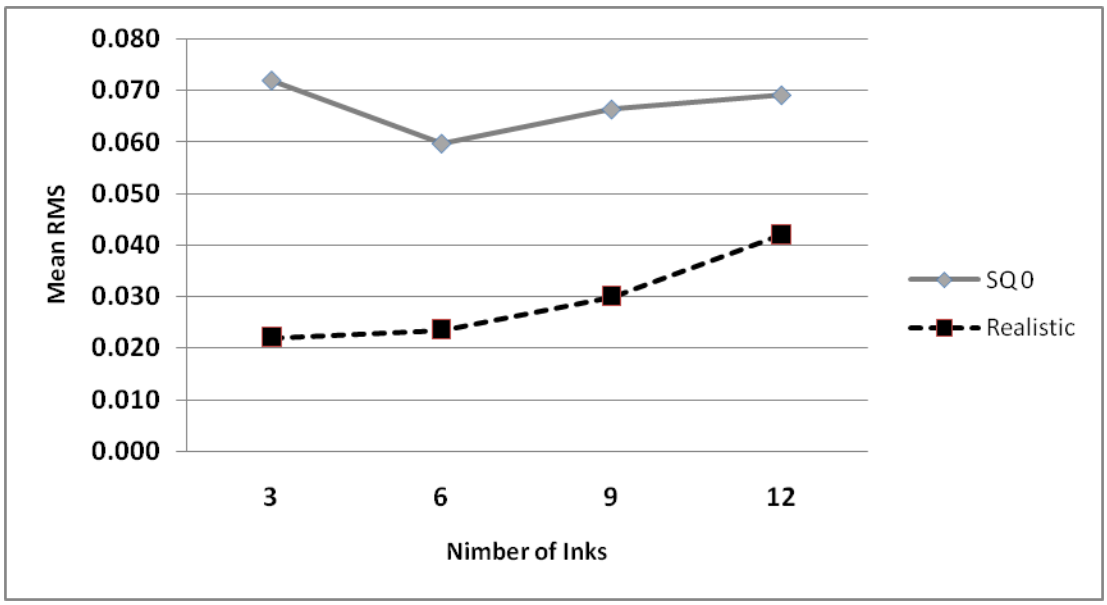

Figure 56: Comparison between ISOMAP-based gamut mapping and HS gamut mapping for realistic and synthetic ink reflectances. The variation is calculated as the average RMS difference between the two spectral reflectances calculated using the two different mapping methods.

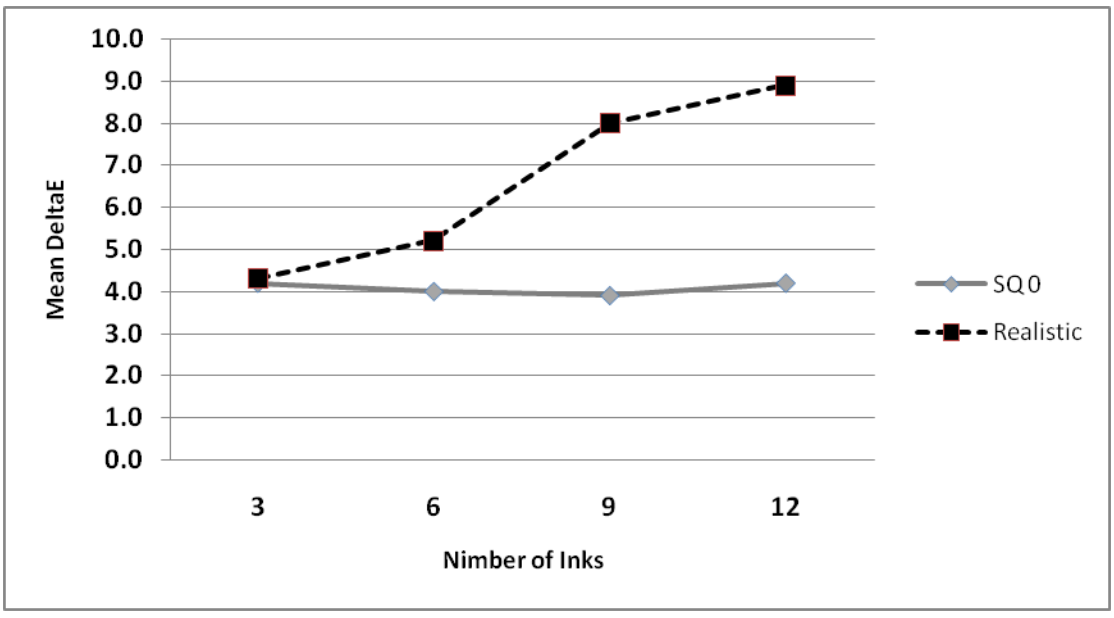

Figure 57: Comparison between ISOMAP-based gamut mapping and HS gamut mapping for realistic and synthetic ink reflectances. The variation is calculated as average $DeltaE_{94}$ difference between the two spectral reflectances calculated using the two different mapping methods.

Figure 58 compares accuracy of gamut mapping based on Isomap technique versus NNLSQ (non-linear least square) method. Two types of inks

were used in the comparison: square wave inks with no overlap and real ink measurements. Figure 59 and Figure 60 compare performance of the two mapping algorithm in $DeltaE_{94}$ colour space. The two figures show that NNLSQ gamut mapping has similar performance to the ISOMAP method. This means that, not much of printer gamut concavity is reduced by transforming the printer gamut using ISOMAP technique.

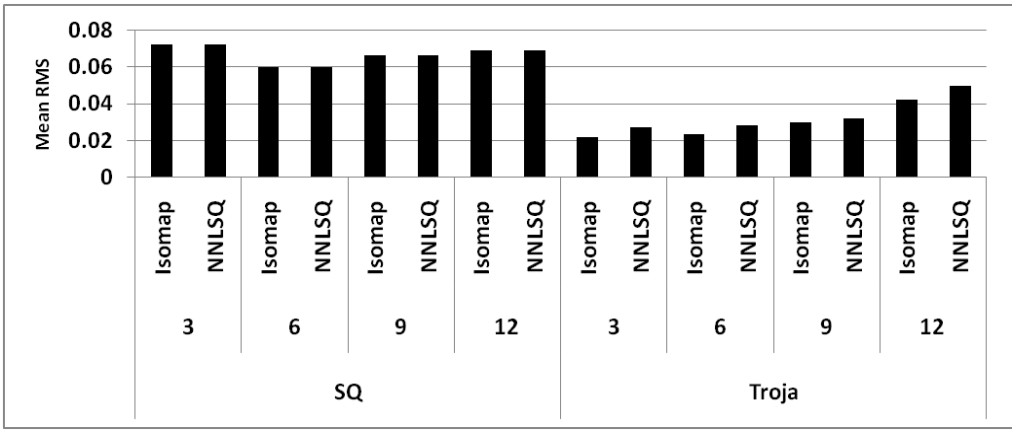

Figure 58: Comparison between accuracy of ISOMAP-based gamut mapping and NNLSQ gamut mapping measured in mean RMS. Accuracy is defined as variation between how the gamut mapping performs compared to HS gamut mapping

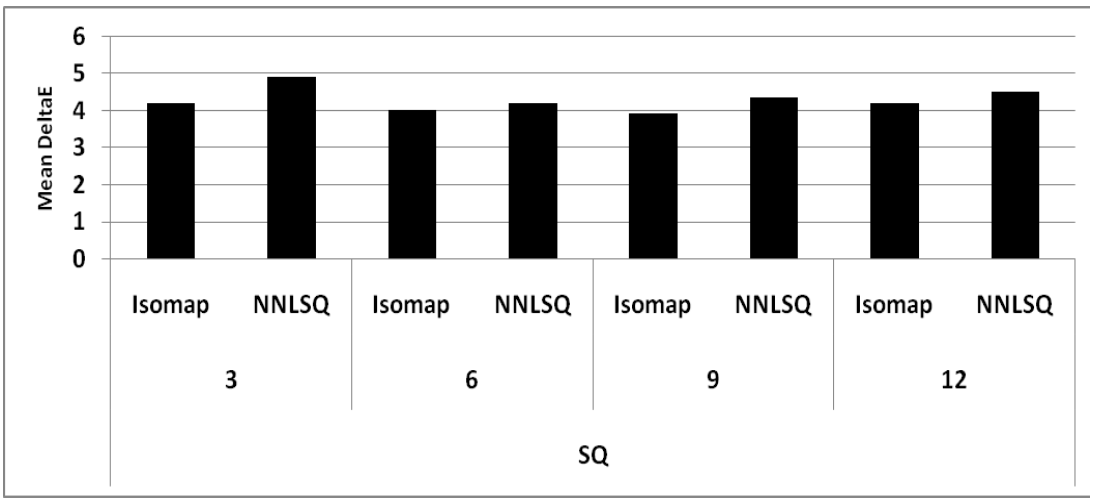

Figure 59: Comparison between accuracy of ISOMAP-based gamut mapping and NNLSQ gamut mapping measured in mean $DeltaE_{94}$ for square wave ink with 0% overlap. Accuracy is defined as variation between how the gamut mapping performs compared to HS gamut mapping

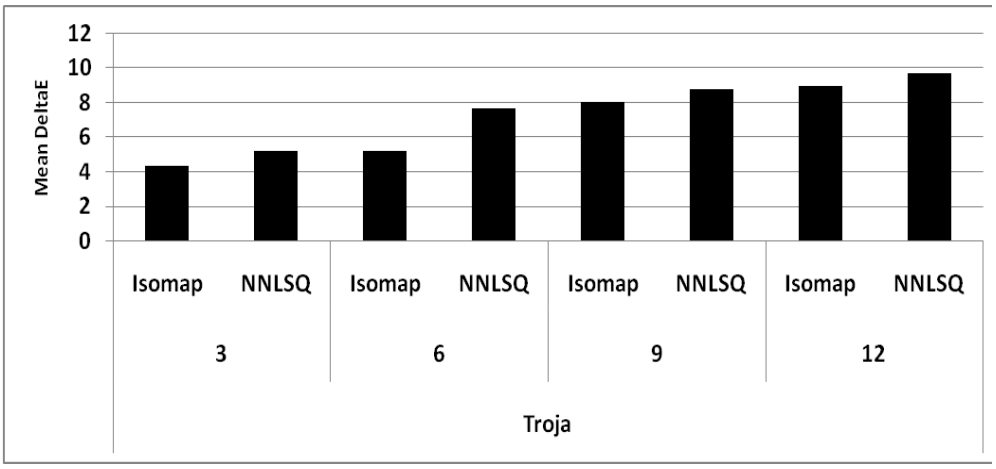

Figure 60: Comparison between accuracy of ISOMAP-based gamut mapping and NNLSQ gamut mapping measured in mean DeltaE94 for real inks. Accuracy is defined as variation between how the gamut mapping performs compared to HS gamut mapping

Conclusion

A spectral ink separation algorithm is introduced based on interpolation using the geodesic distances between neighbouring points. A spectral gamut mapping algorithm is also introduced which uses ISOMAP.

The performance of the ink-separation model was evaluated for 3-ink, 6-ink and 9-ink printers using a synthetic printer model. The experimental results show that the accuracy of interpolation, and thus of the resulting ink separation, improves if the calculation is done using geodesic distances.

In addition, a new spectral gamut mapping algorithm is introduced based on manifold transformation of the printer gamut.

CHAPTER 6: EVALUATION OF SPECTRAL COLOUR REPRODUCTION

Introduction

In this section, an experiment with real inks is presented to evaluate how closely a sample colour can be reproduced using available real inks, and whether the accuracy of spectral reproduction is noticeably better than traditional tri-chromatic colour reproduction.

Target Samples

Two sets of target samples were used. The first set was based on the MacBeth colour checker shown in Figure 61. To have a more focused evaluation of spectral reproduction given a limited set of inks, 3 colour tiles with similar reflectance characteristics were used in the experiment (as shown in Figure 61). Figure 62 shows the reflectance of the 3 colour patches and Table 9 represents the colour variation for each patch under 11 different illuminations from the Simon Fraser database.

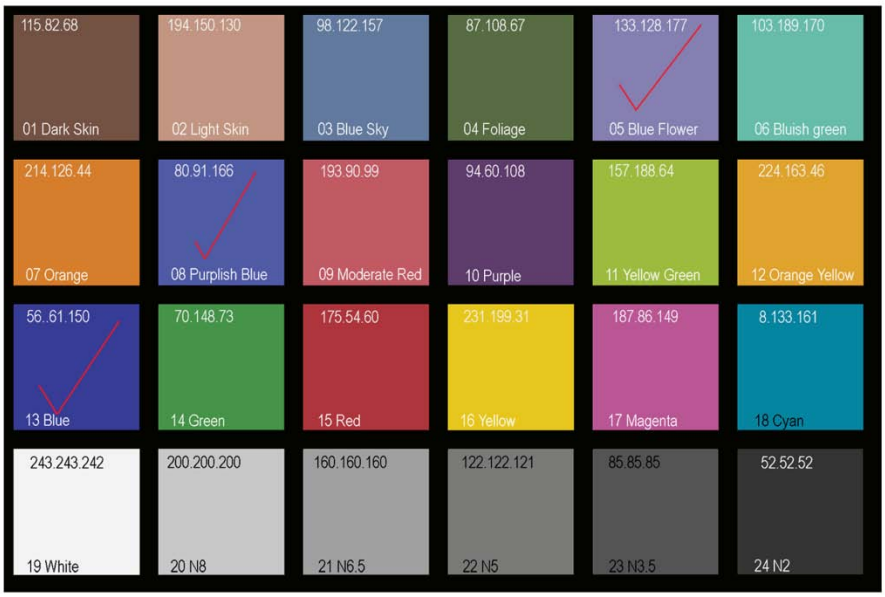

Figure 61: The 3 colour tiles used from the MacBeth Colour Checker for spectral colour reproduction testing. The colour tiles used were the 5th, 8th and 13th colour tiles as indicated by the red mark.

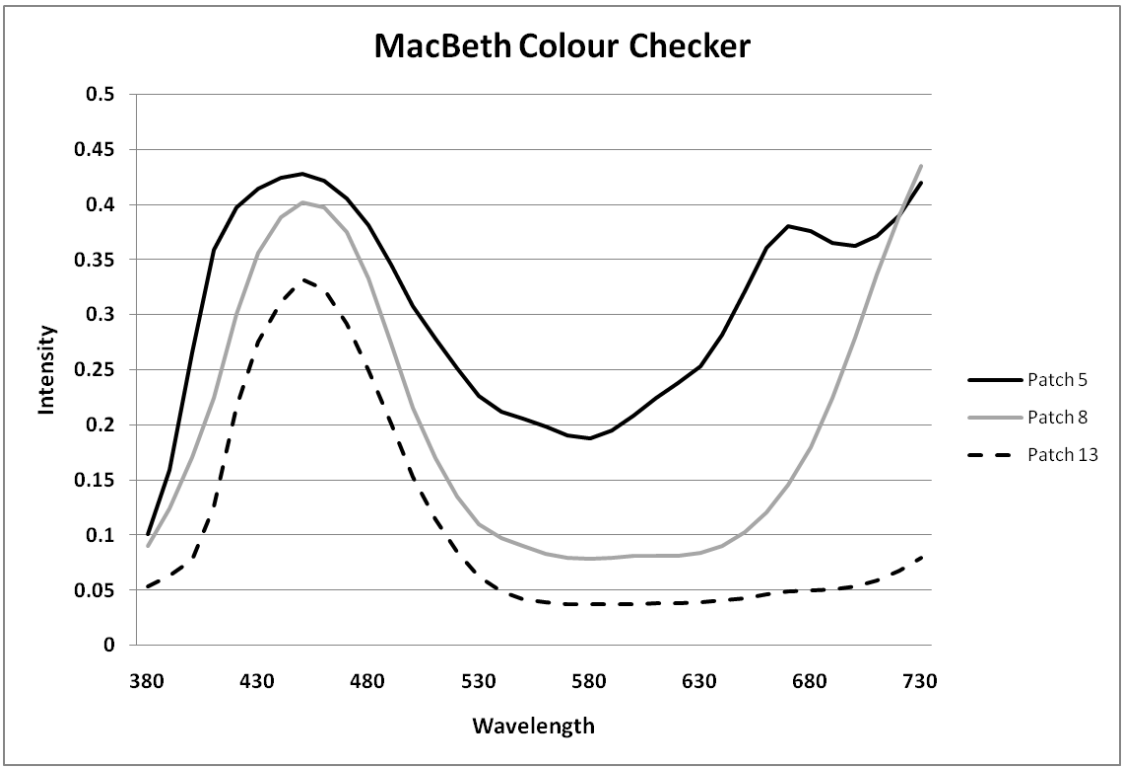

Figure 62: Reflectance characteristics of the 3 colour patches selected from the MacBeth Colour checker as target reflectances for reproduction.

Table 9: Average Colour variation (inconsistency) of each patch under 11 different illuminations. Mean DeltaE_{94} column represents average colour variation from target patch

Patch Number	Mean DeltaE_{94}
5	2.1
8	3.2
13	5.8

The next set of test targets was based on real paint samples that are specifically hard to reproduce. For the purpose of this study, 2 yellow paint samples were selected with the reflectance and colour inconsistency variations shown in Figure 60 and Table 10.

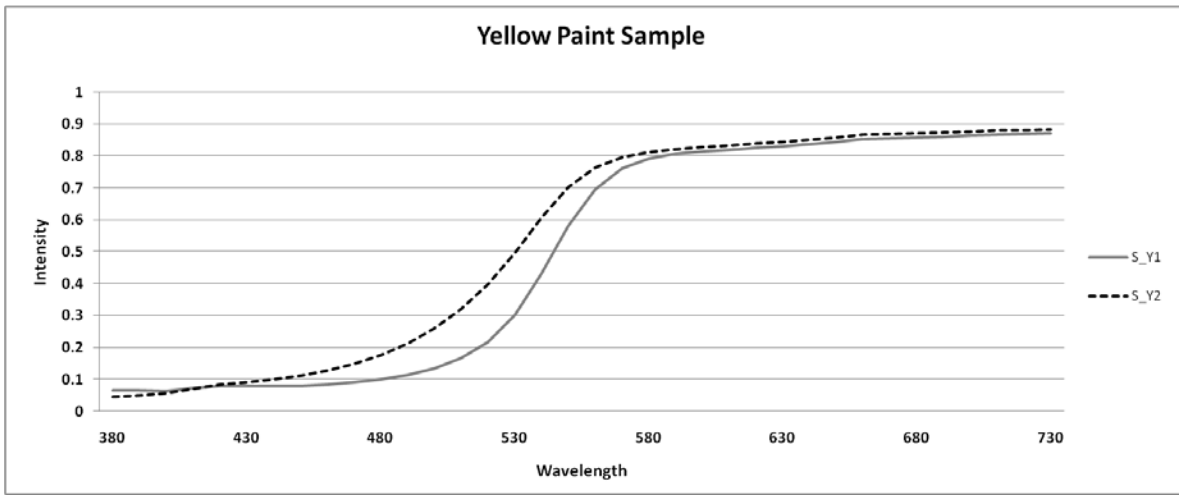

Figure 63: Reflectance characteristics of the 3 yellow paint samples selected as targets.

Table 10: Colour variation (inconsistency) of the 2 yellow paint patches under 11 different illuminations.

Patch Number	$DeltaE_{94}$
S_Y1	3.7
S_Y2	6.6

Experiment Setup

A 9-ink printer with 3 different magenta inks (Figure 64), 2 red inks (Figure 65) and 2 different yellow inks (Figure 66) plus a cyan and a black ink was setup to reproduce the selected target samples. The selection of the 9 inks is based on limited set of available inks during the experiment and also the colour range of the target samples. The printed patches were optimized for typical lighting condition found in viewing light booths as shown in Table 11.

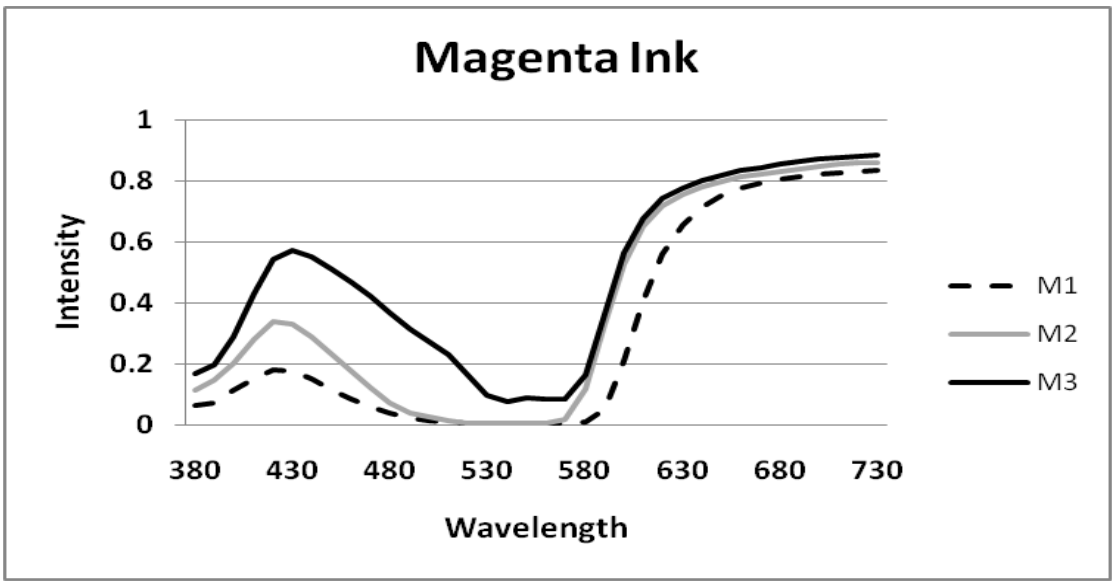

Figure 64: Reflectance characteristics of the 3 different magenta inks used for the experiment.

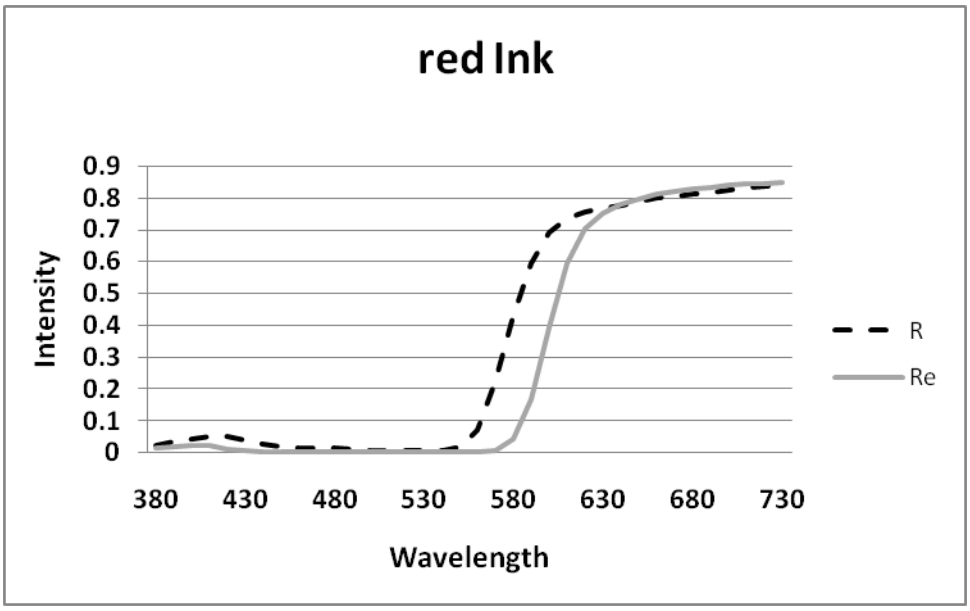

Figure 65: Reflectance characteristics of the 2 different red inks used for the experiment.

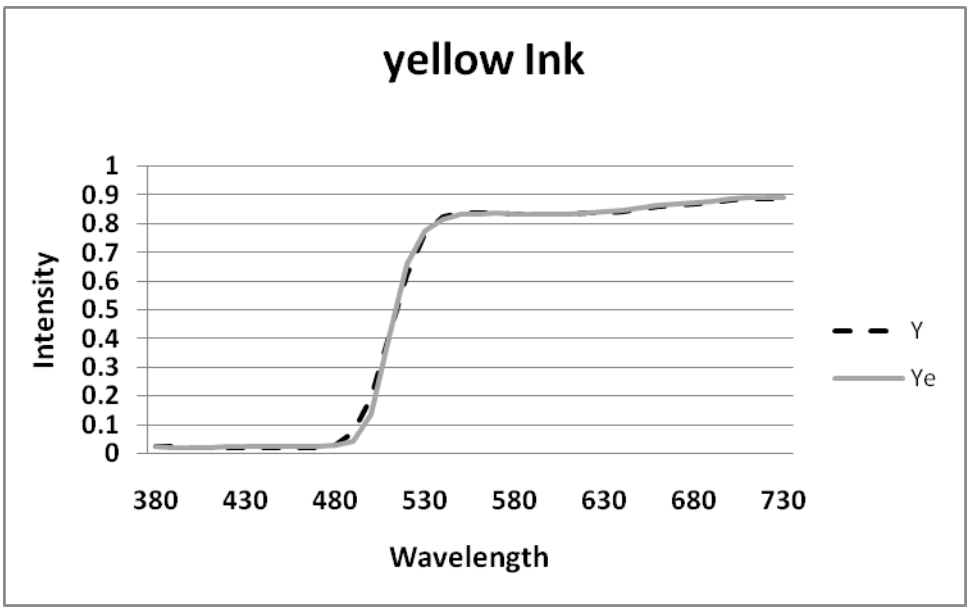

Figure 66 Reflectance characteristics of the 2 different yellow inks used for the experiment.

Table 11: 4 Light sources available in the viewing light booth

Light Sources
Daylight D65
Incandescent light A
Cool White Fluorescent CWF
Department store light - TL 84

Implementation Details

To evaluate spectral colour reproduction, each target colour patch was printed using spectral printing and traditional colour reproduction which matches a colour in CIELAB colour space (trichromatic matching).

For CIELAB colour reproduction, an illumination was selected from the available 4 choices that had the most colour variability from the other 3. This was done to magnify the effect of spectral printing given the limited number of available inks. Because of this, the same light source was not used for the entire target under trichromatic (CIELAB) colour reproduction.

The printer modeling used for the experiment was based on the modified YNCN model explained in Chapter 2. To reduce the number of training patches needed for the application, the printer gamut was divided into two parts; one part focuses on the yellow part of the printer gamut and the other focuses on the blue region.

For trichromatic colour reproduction, a convex-hull gamut mapping was implemented to map out-of-gamut points onto the printer gamut. For the ink separation process, the Hierarchical Search algorithm was implemented to find the best ink combination given the mapped input reflectance.

Since the ISOMAP technique has a better performance than NNLSQ technique for gamut mapping, the gamut mapping and ink separation algorithms are both based on the ISOMAP technique (explained in Chapter 4).

Results

For the MacBeth Colour Checker samples, patches number 5 and 8 were matched under Cool White Florescent light. Patch number 13 was matched under Daylight illumination. Figure 67, Figure 68 and Figure 69 show the accuracy of colour reproduction under CIELAB colour space and spectral space for the 3 selected MacBeth colour patches.

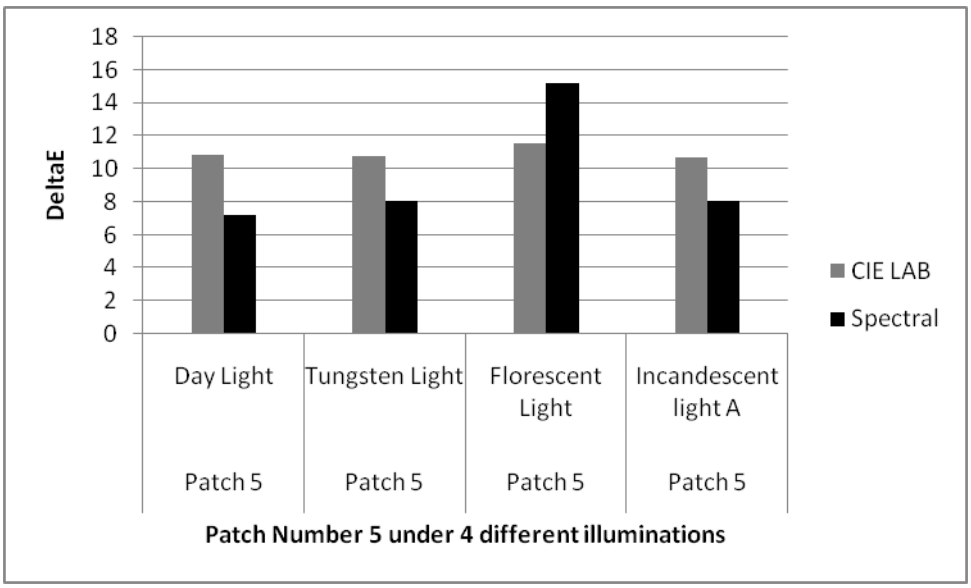

Figure 67: Accuracy of reproduction of patch number 5 under 4 different illuminations using trichromatic matching versus spectral colour reproduction. [84]

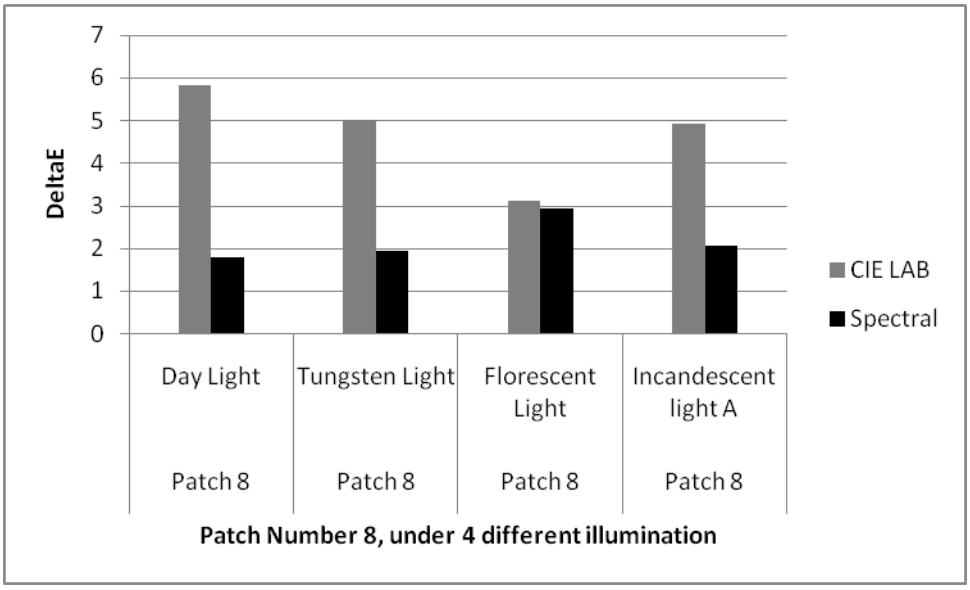

Figure 68: Accuracy of reproduction of patch number 13 under 4 different illuminations using trichromatic matching versus spectral colour reproduction.

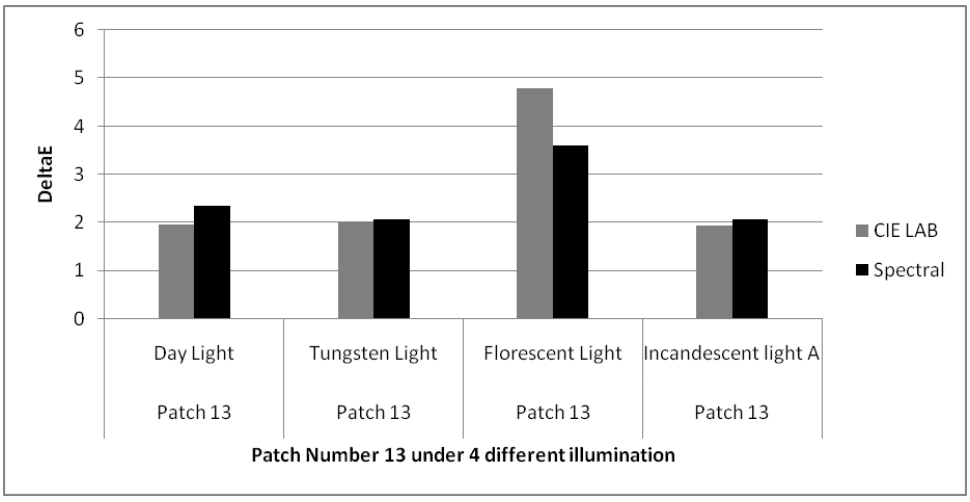

Figure 69: Accuracy of reproduction of patch number 13 under 4 different illuminations using trichromatic matching versus spectral colour reproduction.

For the yellow patch, S_Y1, given the available two yellow inks, spectral reproduction could not find an ink combination that has better metamerism than that of trichromatic matching.

For S_Y2, an illumination was selected as the reference lighting for the trichromatic matching. Figure 70 shows the accuracy of each reproduction process measured as $DeltaE_{94}$ colour variation. The figure shows that when trichromatic matching is used, the selected ink combination can reproduce a closer result to the target patch under one illumination. However, spectral colour reproduction on average produced closer reproduction than trichromatic matching.

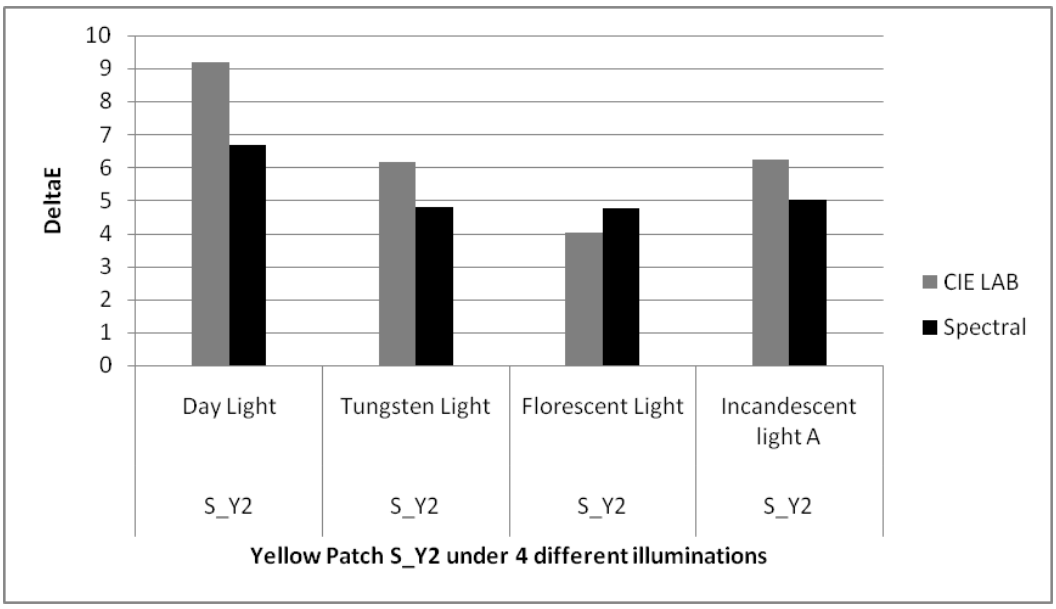

Figure 70: Accuracy of reproduction of the yellow patch S_Y2 under 4 different illuminations using trichromatic matching versus spectral colour reproduction. The trichromatic matching was done under Incandescent light A illumination.

CHAPTER 7: SPECTRAL ANALYSIS OF BRONZING

Introduction

Until now the focus of this study has been on improving metamerism as one of the main advantages of spectral reproduction. In this section, another use of spectral colour reproduction, understanding and optimizing Bronzing, is discussed. Bronzing has recently been identified as one of the important factors in improving the colour reproduction process.

Bronzing is caused by reflection of light from the ink when the printed image is viewed at a particular angle. Bronzing is pronounced with pigmented inkjet inks because the pigments do not penetrate into the ink-receiving layer of the print medium. Rather, the pigments form a film or layer on top of the ink-receiving layer. One common type of bronzing is caused by interference between the light reflected from the top surface of the inkjet film and the light reflected from the interface between the inkjet film and the ink-receiving layer. This type of bronzing is typically observed with black-pigmented inkjet inks and varies with the thickness of the inkjet medium coating. Therefore, bronzing is more pronounced on glossy, photo-based print media than on paper-based print media [72].

To reduce bronzing, different colour mappings (dot placement algorithms) [72] and different ink selections are used. Some works have focused on use of composite colours instead of primary colours [73] or adding a gloss optimizer to

the printer system. Currently, most methods available for measuring and evaluating bronzing are based on an subjective evaluation where engineers compare reflectance variations of prints under different viewing angles.

The focus of this section is to show another application of spectral analysis aimed at improving the colour reproduction process, something that is not feasible using traditional tri-chromatic analysis. The proposed algorithms try to address the issue of detecting and measuring the bronzing defect, knowing that, at this time, there is no subjective metric for measuring bronzing. The proposed models are based on automating measurement of the bronzing. A new metric to evaluate this defect is also proposed.

In the first part of this section, a new method of understanding and measuring bronzing is proposed based on variations in spectral reflectance of an ink under a range of viewing angles. In the second part of this section, a modeling method is proposed to predict the reflectance of a given ink under certain angles. This method permits the evaluation of bronzing without the need to measure a print under a large range of viewing angles. This algorithm then is extended to model bronzing of an ink at different densities.

Using this technology, a subjective metric to evaluate bronzing can be designed. The second advantage of this algorithm is that industries can quickly evaluate how the bronzing profile of an ink changes under different densities of the given ink.

Data Measurement

For bronzing evaluation, a Gonio-spectrophotometer was used to measure spectral reflectance of a patch under different viewing angles in 2 dimensions. An initial calibration against a perfect diffuse white was performed.

Based on precise control on the incident and acceptance angle by the computer, a Gonio Spectrophotometer measures the spectral distribution of every pair of illumination/detection angles individually. After calibration and mounting of the samples, the settings for measurement conditions are made.

Bronzing Evaluation based on Spectral Reflectance Characteristics

In this section a method for evaluating bronzing based on the spectral reflectance variation of a printed plot under different viewing angles (assuming the illumination incident angle is constant) is introduced. Figure 71 shows the spectral reflectance of a black ink patch at viewing angles of 10 to 15 degrees in steps of 0.5 degrees. The incident angle was kept constant at 20 degrees. The prints were made on photo paper.

The photo paper medium has a coating that scatters light much less than typical paper. Since the energy reflected from a photo medium increases at its specular angle, where incident angle equals viewing angle, it is necessary to remove any artefacts that are due to shininess of the media, which do not represent ink and media colour variation. One proposal is to normalize the measurement data by the measurement of the white of the media at the same angle (Figure 72). The normalization process divides the spectral measurement

of a patch by the reflectance measurement of the same paper (medium) without any ink on it. For normalization, the white medium was measured at the same angle as the printed patch.

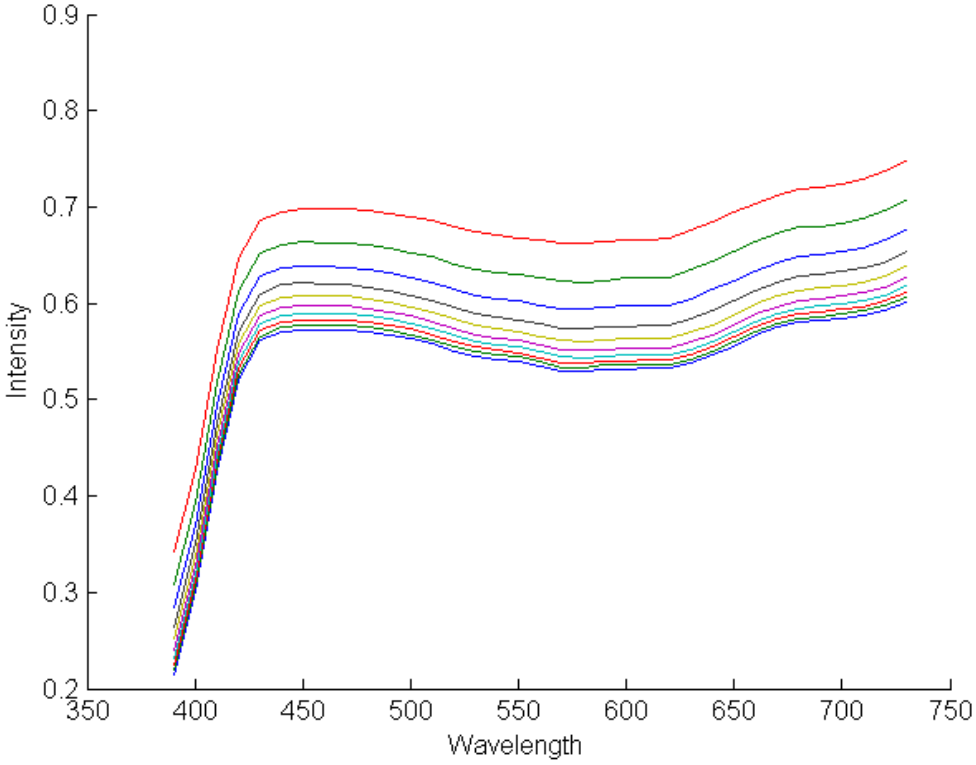

Figure 71: Spectral Reflectance Variation of black ink (K1) as viewing angle changes (keeping incident angle constant).

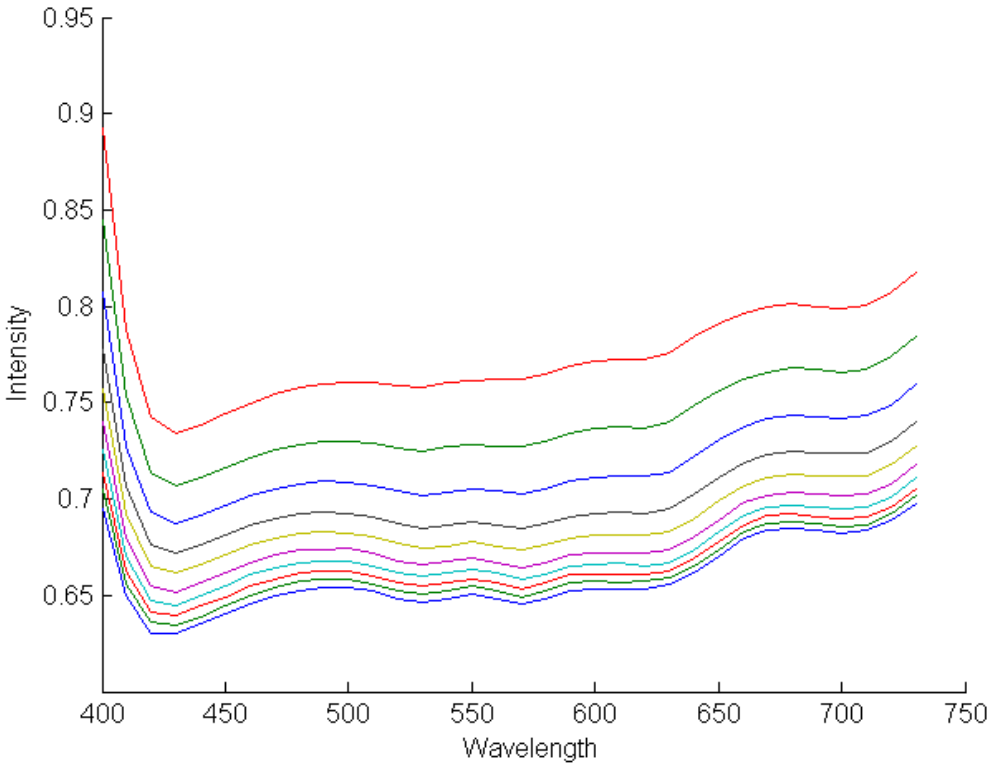

Figure 72: Spectral reflectance variation of the black ink (K1) under different viewing angles normalized by reflectance of the white paper under the same angles.

Another observation is that reflectance characteristics of inks are a function of the difference between the viewing and incident angles in 2 dimensions. Figure 73 shows this difference, which is typically referred to as phase angle, is highly correlated to the reflectance variation. Through the rest of this paper, phase angle rather than incident or viewing angle is used as the main parameter for evaluation reflectance variation of a target.

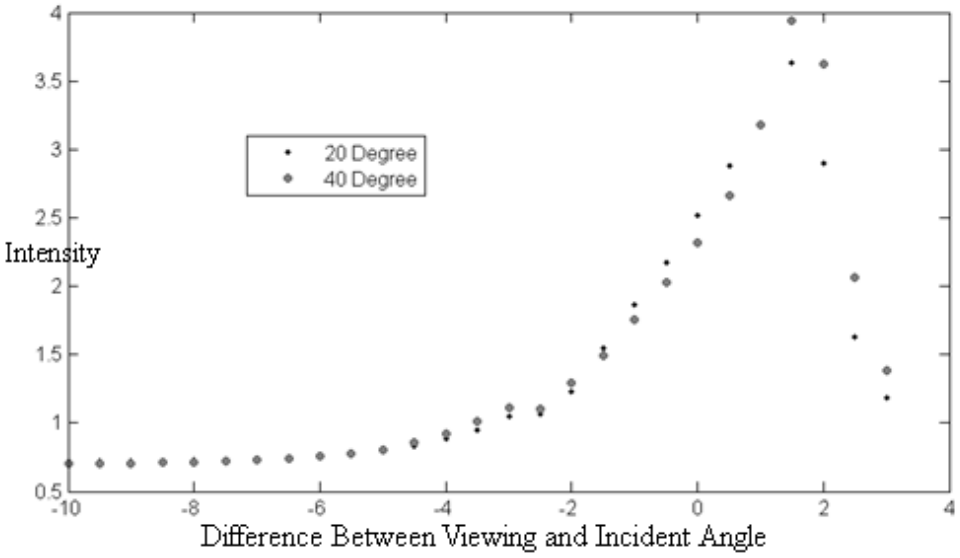

Figure 73 Reflectance of K1 ink measured at two different viewing angles. The data is plotted against the difference between the viewing and incident angles.

Through a visual evaluation of plots and their normalized reflectance variation under different phase angles, a metric is proposed to evaluate bronzing based on reflectance variation characteristics of a target. The theory behind the metric is that the plots related to higher bronzing levels will have larger, more non-uniform spectral variation at different phase angles. Figure 74 shows a type of black ink that tends to have a large degree of bronzing at high densities and not much bronzing when little ink is put down.

The proposed bronzing metric is based on variations in spectral reflectance of the target under different viewing angles as given in equation (19).

(19)

$$Spectra_{normalized} = Spectra_{ink} / Spectra_{mediaWhite}$$

$$Range(\sum_{i=1}^{n} Spectra_{i,normalized})$$

where Range calculates the maximum value minus minimum value of the reflectance taken over all wavelengths.

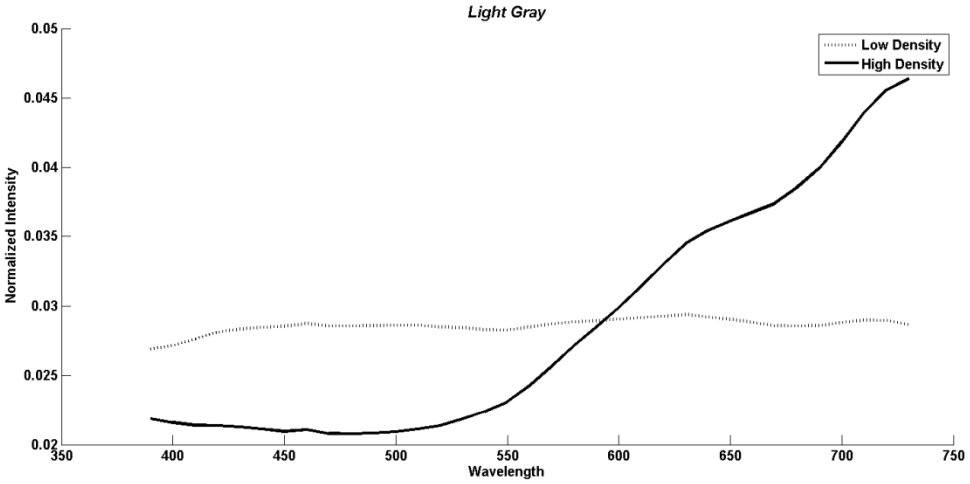

Figure 74: Maximum reflectance variation of an ink under two different densities when considered under a set of viewing angles (keeping incident angle constant). The selected set of viewing angles are+- 10 degrees of incident angle.

Results

In the experiments, the 5 different inks shown in Figure 75 were used. Some inks, such as magenta and K3, are known to have little bronzing, whereas, the others do show a significant level of bronzing. Since inks are known to have different behaviours for bronzing under different densities, two density levels were considered in the experiment (Low and High densities).

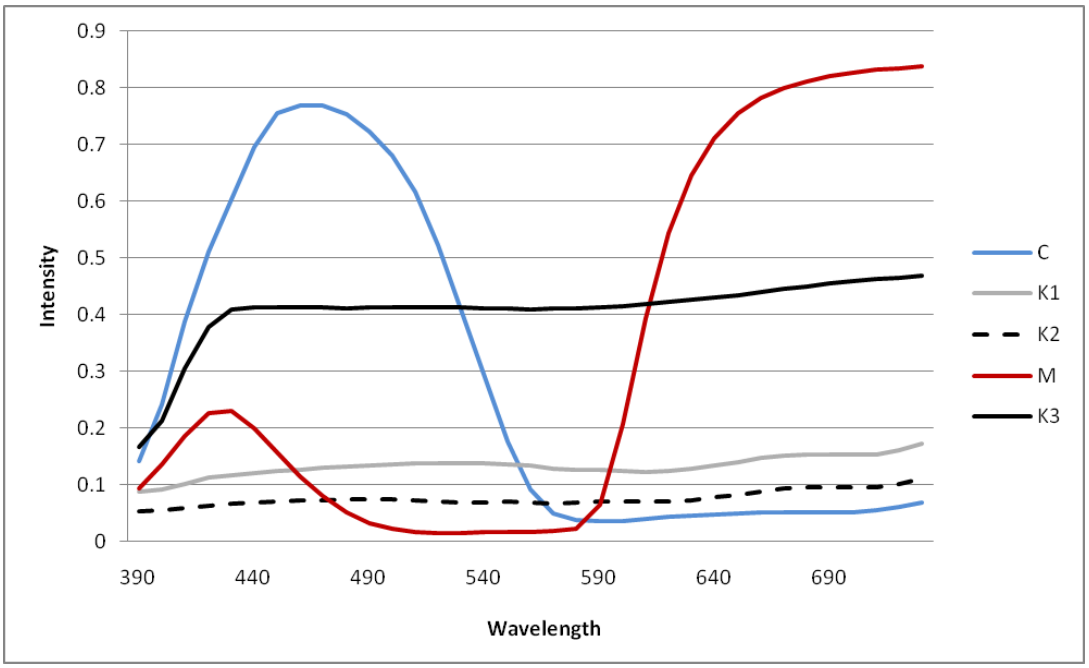

Figure 75: Spectral characteristics of the 5 inks used in the study. K1, K2 and K3 represent 3 different types of black ink tested. C represents cyan ink and M represents magenta ink.

Each patch was printed and measured using a Goni-Spectrophotometer at a 20 degree incident angle. The viewing angle was changed from 10 degrees to 30 degrees in 0.5 degree increments. All the measurements were captured in spectral colour space and normalized by the white reflectance of the medium at the same viewing and incident angles.

Figure 76 shows the bronzing metric calculated based on the proposed method. The figure shows that using the proposed metric, K1 and K2 inks have a large level of bronzing at different densities which agrees with what is generally known about the bronzing characteristics of the two inks.

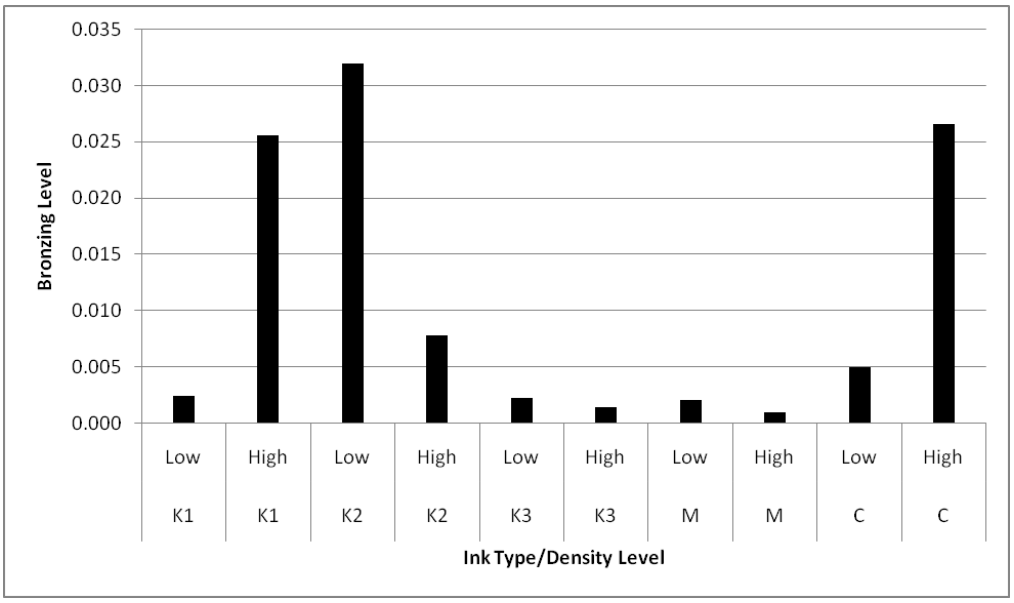

Figure 76: Bronzing level calculated based on the proposed bronzing metric. K1, K2 and K3 represent 3 different types of black ink tested. C represents cyan ink and M represents magenta ink.

Modeling Bronze

In this section, the existing printer output modelling techniques are extended to model other quality metrics such as bronzing.

Predicting Reflectance under Different Viewing Angles

Figure 77 shows the reflectance variation of a given ink at the example wavelength of 480nm as the viewing angle changes, while the incident angle is held constant. The figure shows that an interpolation technique can be used to predict reflectances under different incident angles. The proposed method interpolates between measurements of reflectances under different incident angles in order to predict a patch's reflectance as a function of viewing angle. The equation below captures the process:

(20)

$$R_{\lambda,\theta} = F(R_{\lambda,\theta 1}, R_{\lambda,\theta 2}, R_{\lambda,\theta 3}, ...)$$

where F represents the continuous function created using an interpolation method and $R_{\lambda,\theta 1}$ represents the measured reflectance at wavelength λ and angle Θ_1.

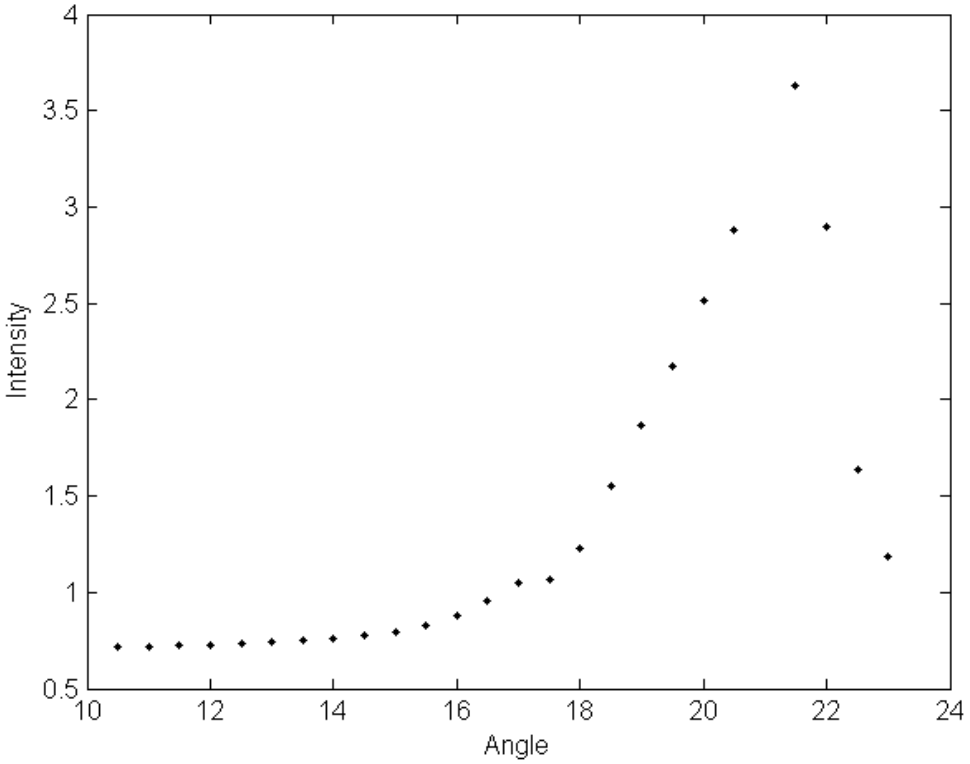

Figure 77: Variation of the black ink (K1) reflectance at 480 nm wavelength under different viewing angles. The incident angle was kept constant at 20 degrees.

Using this model to predict the reflectance variation of an ink under any phase angle, a process to measure bronzing with much fewer input data points can be created.

Modelling Bronze for Different Ink Densities and Phase Angles

Printer output models such as the Yule-Nielson Cellular Neugebauer model or the ISOMAP based model try to predict reflectance of a printed patch by running an interpolation method for each of the wavelengths. In this section, the printer output modelling algorithms are extended to predict the reflectance characteristics of an ink under different phase angles for different densities.

In the previous section, it was shown that using an interpolation method, it is possible to predict the reflectance of an ink under any phase angle for a given ink density. The problem that is addressed in this section is whether the interpolation can be further extended to predict the reflectance of an ink under any phase angle for any ink density.

Figure 78 shows reflectance variation of a black ink at 3 different ink densities. It shows that, considering each phase angle for each wavelength, the spectral variation of an ink as density varies can be predicted.

Based on this observation, a more sophisticated model can be created by combining the printer modelling algorithms introduced in Chapter 2 with an interpolation to predict reflectance variation of fixed ink density under different phase angles. This new method can enable the researcher to predict the bronzing amount of an ink for different ink densities.

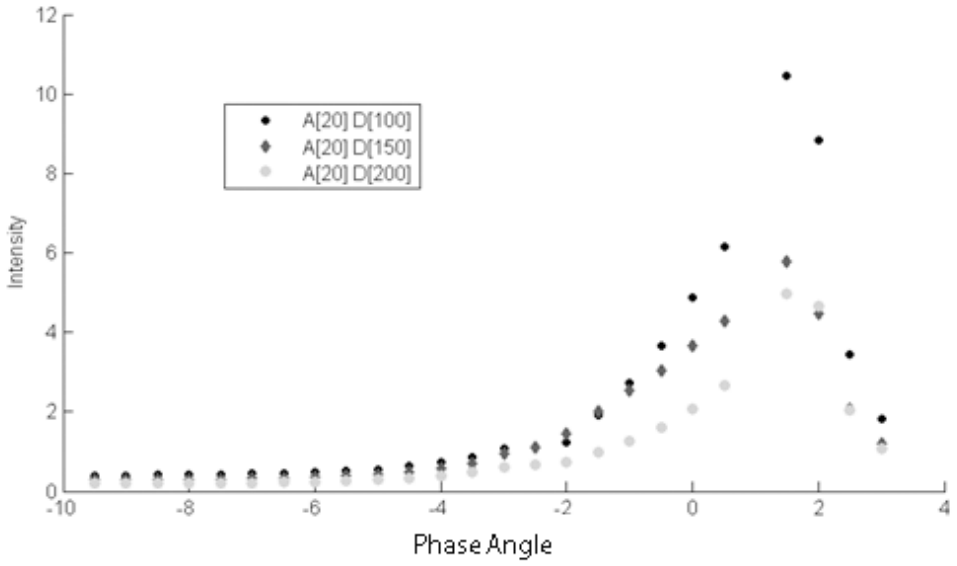

Figure 78: Reflectance variation of 3 different ink densities at 480 nm wavelength.

The equation below captures the proposed algorithm for measuring bronzing for different ink densities, where F is an interpolation function, Θ is the phase angle, λ wavelength, and D is the density of the ink being studied.

(21)

$$R_{\lambda,\theta,D} = F(R_{\lambda,\theta,D1}, R_{\lambda,\theta,D2}, R_{\lambda,\theta,D3}, \ldots.)$$

What can be learned from this model?

One of the common techniques for reducing bronzing is to adjust the ink separation table within the printer to optimize the ink combination, knowing that some inks have less bronzing at specific ink densities. For instance, consider a printer system that has cyan, magenta, light cyan, light magenta, yellow, light gray and black inks available. In this system, the medium gray ink may have the

lowest bronzing for having a neutral gray colour at 20 CIE L*; whereas, for darker regions using a composite ink, (cyan+magenta+yellow) might reduce the bronzing significantly.

Knowing this information, the ink separation table can be modified to minimize bronzing, which is very similar to the process for reducing metamerism.

Experiment Setup

Two different black inks (K1 and K2) were measured. For training purposes, 6 different densities for each ink were printed. The printed patches were measured at -10,-8,-4,...10 phase angles. Figure 79 shows the reflectances of the two inks used in the study. The two black inks have a high level of bronzing.

Five ink densities, not including the training ink densities, were used for the test purposes and their spectral reflectance was predicted at -10 to 10 phase angles with steps of 0.5 degrees. Since the reason for designing this modelling algorithm is to be able to predict reflectances accurately enough in order to better understand bronzing behaviour of the patches, the Bronzing Metric, introduced in the previous chapter, was used for comparison purposes. For interpolation, weighted Locally Linear Interpolation (LLI) was used and, for printer modelling, the Yule-Nielson Neugebauer model was selected.

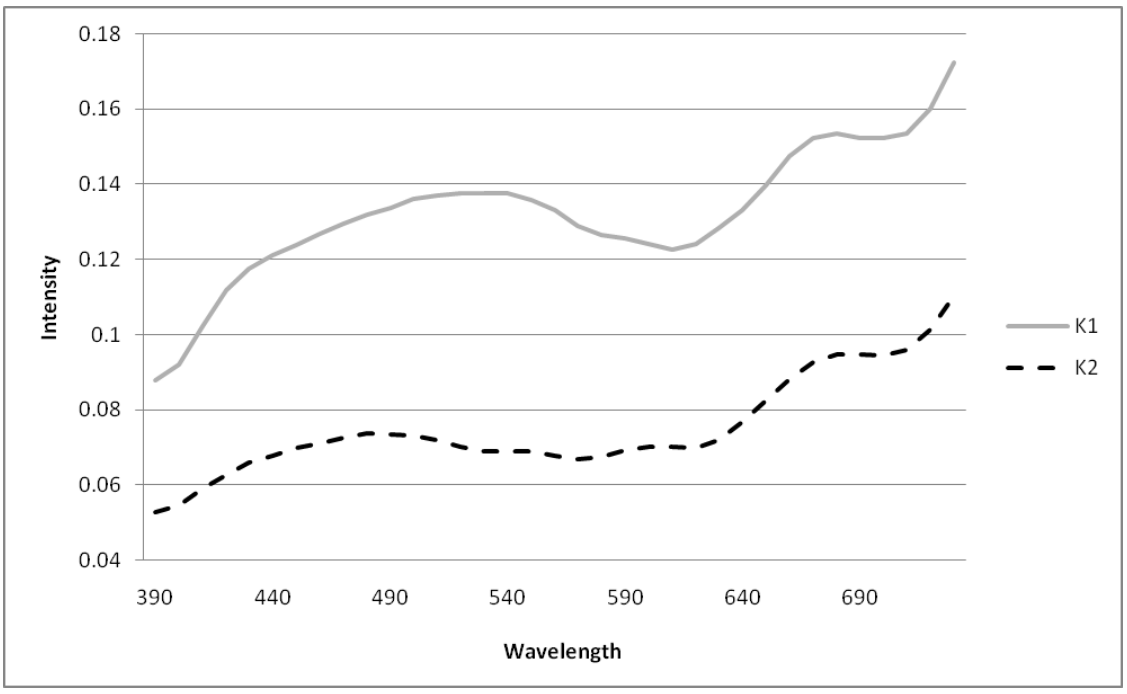

Figure 79: Spectral characteristics of the 2 black inks used in this study. The measurements were collected using an eye-1 spectrophotometer at 2 degrees observer angle.

Results

Using the proposed model, the spectral reflectance of each patch was predicted under 40 different phase angles (-10 degrees to 10 with increments of 0.5 degrees). The proposed bronzing metric introduced in the previous chapter was used to predict the bronzing metric. The predicted bronzing metric was compared to a calculated bronzing metric based on real measurements in Figure 80. Equation 19 combined with 21 was used to calculated bronzing. The figure shows that the modelling algorithm can be used to decide which inks, at which densities, have lower or higher levels of bronzing.

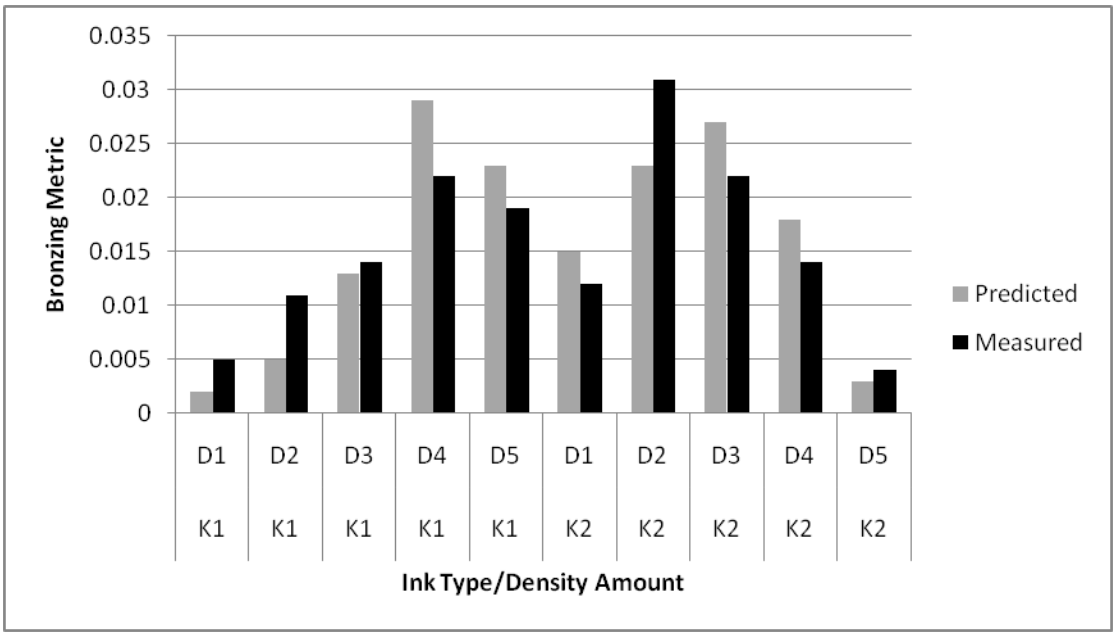

Figure 80: Performance of the bronzing model compared to real measurements. The vertical axis represents the bronzing metric that was proposed in the previous section. D1 to D5 show the 5 different densities used for each ink density. D1 is lightest ink density and D5 is the highest ink density. K1 and K2 are the 2 black inks used.

CHAPTER 8: SUMMARY

When primaries interact with each other non-linearly as in a printer system, modelling the system output becomes complicated. The Yule-Nielson Cellular Neugebauer (YNCN) model is known to have the highest accuracy in predicting any ink combination relative to other existing models. The drawback of YNCN is that it requires significantly more measurement points than other models. In this thesis, two models were proposed for improving the YNCN model. The first one takes advantage of the paper (medium) constraints, such as ink limiting, to reduce the necessary number of measurements substantially (by as much as 97%). A better, smarter sampling method based on the linearization curves can relax the required number of measurement points even further. The second proposed model is based on using a non-linear transformation, ISOMAP, to reduce the complexity of the output system before any interpolation is applied. Two conference papers are published for these proposed methods ([68], [78]).

Finding the optimal spectral characteristics for each primary and the number of primaries needed for a given system is another focus of spectral reproduction research. Hardeberg [30] showed that in a real system, due to the noise associated with each primary, the accuracy of the system does not always improve when more primaries are added.

The effect of different system behaviours (linear or non-linear) and the reflectance characteristics of the primaries on the accuracy of spectral colour

reproduction were evaluated. In particular, the spectral characteristics of each primary and the number of primaries to use were both studied. The results will be useful to a researcher in deciding how an existing output device (printer, projector, scanner or a camera) might be improved by introducing an additional light source or ink with specific reflectance or absorption characteristics. Another important finding of the study was the effect of overlap between reflectance characteristics and their smoothness on spectral colour reproduction accuracy. Two models, one linear and one non-linear, were used and a hierarchical search algorithm was implemented to evaluate the system. The results are published in NIP23 paper [76] and NIP25 [85] .

The next topic addressed in the thesis is that of an algorithm to determine the best primary combination to reproduce a given spectrum. The majority of the mapping algorithms in this field are based on calculating the convex hull of the gamut, and using the hull to determine if an input spectrum is out of gamut. To reduce the complexity of these algorithms when applied for spectral analysis, some researchers have proposed using a lower-dimensional space to make spectral gamut mapping more manageable. Other methods attempt to invert forward device models, but these tend to have high time complexity and low accuracy.

Two gamut mapping and two ink separation methods are proposed in this thesis. The first gamut mapping algorithm proposes a new approach to calculate the convex hull for only the relevant portion of the gamut space. This model also calculates the best ink separation assuming a convex output gamut. The main

advantage of this algorithm is that the complexity of the algorithm grows linearly with the number of available points in the system, which is a great improvement compared to the other convex hull based approaches in which their time complexities grow at a polynomial rate. The results of the work are published in the CIC 2006 conference [77].

The second gamut mapping algorithm is based on mapping the gamut in a low-dimensional space using a non-linear transformation before any known gamut mappings are applied. There are two main advantages to this method. First, the model maps the printer spectral gamut space to a lower dimensional space more accurately than other linear approaches (e.g. PCA or ICA). Second, after the mapping the spectral gamut space has fewer concavities compared to linear dimensional reduction methods.

The second proposed ink separation method is based on multi-dimensional interpolation from the input spectral gamut to output ink combination. This interpolation approach uses geodesic distances to calculate weights used in the interpolation instead of standard Euclidean distances [79].

Also, real experimental results were used to evaluate the performance of the proposed model against one of the conventional tri-chromatic printing models. The setup has a printer with 9 inks with different colours, some with similar hue angle: magenta1, magenta2, magenta3, Red1, Red2, yellow1, yellow2, cyan and black. The experiment is aimed to reproduce the colour of some tiles from a Macbeth Colour Checker, and some yellow painting patches as accurately as possible in spectral space. The forward printer model used is

based on a modified Yule Nielson Neugebauer model. The spectral gamut mapping algorithm is based on the proposed mapping after a non-linear transformation. The ink separation algorithm is also based on the proposed technique of using Geodesic distances in the interpolation process.

In the last section of this study, we model the reflectance variation of a printed patch under different phase angles. A metric to evaluate bronzing is proposed based on the reflectance variation. The metric is based on the spectral reflectance variation of a patch under different phase angles. This can be a great advancement in measuring bronzing where there is no simple objective method exists at this time. Lastly, a method to predict how bronzing varies as a function of ink density is proposed. It combines the proposed bronzing measurement with existing spectral printer modelling. Knowing this model, the spectral colour reproduction process can be improved to consider both metamerism and bronzing effects.

Detailed Contributions

Two spectral modelling algorithms for printer output were introduced. The first algorithm is based on optimizing the Cellular Neugebauer Model, which takes advantage of ink limiting and linearization information to minimize the number of ink combinations to measure. A modification to the model is proposed to handle missing measurement points due to ink limiting. The second spectral modeling method is based on using the ISOMAP technique to map the printer gamut into a space where the primaries have less non-linear interaction between one other.

The effects of absorption or reflectance sensitivity for each type of primary and the number of primaries on the accuracy of spectral colour reproduction were evaluated. A study was performed for output devices with both linear and non-linear interactions between the primaries. Four different types of synthetic primaries and three different overlap amounts for each primary type were used in the study. Finally, the effectiveness of the existing inks was compared against the optimized synthetic inks for spectral colour reproduction. The results from this study helps engineers, when designing inks, filters or other types of primaries, to improve the existing spectral reproduction accuracy of their output device, whether the device is a projector or a printer. The study also helps engineers to better understand the gain in spectral gamut of a device if an additional primary is added to the system.

Since spectral gamut mapping is an important part of the spectral colour reproduction process and the mapping algorithm is more complex for non-linear output devices, two spectral gamut mapping algorithms were introduced for printers. One of the algorithms is based on calculating the convex hull for only regions of interest in a printer gamut. The proposed method has a time and space complexity that grows linearly with the number of data points representing the printer gamut. The algorithm is also used to evaluate the concavity of the printer gamut in spectral space as the number of primaries increases.

The second spectral gamut mapping algorithm is based on gamut mapping in a lower dimension space as calculated using ISOMAP. The accuracy of the proposed gamut mapping algorithm is comparable to running an

exhaustive search in the printer gamut. In addition, an ink separation algorithm was proposed based on interpolation using Geodesic distances between gamut points. Both of the proposed algorithms are flexible and can handle printer gamuts with different level of complexities. This is the main advantage of these algorithms over existing techniques such as LABpqr where the complexity of the device output gamut is assumed not to be larger than 5 or 6 dimensions.

To evaluate the feasibility of the proposed methods using the existing printers and inks, an actual spectral colour reproduction was compared against colour reproduction in CIELAB colour space for a real 9-ink printer system. The results showed that, given the limited number of available inks, using spectral colour reproduction method, metamerism could be reduced by around 40%.

Lastly, another application of analysis in spectral colour space was presented. It was shown that using spectral analysis of a printed patch, a bronzing metric can be defined. The metric can also be extended to assist engineers to minimize bronzing in colour reproduction.

REFERENCES

[1] R. S., Burns, “Methods for Characterizing CRT displays”, *Displays*, Volume 16, Issue 4, 1996; 173-182

[2] Tamura N, Tsumura N, Miyake Y. “Masking Model for Accurate Colorimetric Characterization of LCD”. Proc*. IS&T/SID 10th Color Imaging Conference* 2002; 312-316.

[3] D., Wyble, M., Rosen, “Color Management of DLP Projectors”, *Proc. IS&T/SID 12th Color Imaging Conference* 2004, 228-232

[4] B.V. Funt, B. Bastani, X R. Ghaffari, “Optimal Linear RGB-to-XYZ Mapping for Color Display Calibration”, *Proc. IS&T/SID 12th Color Imaging Conference* 2004; 223-227

[5] *Xrite*, < http://www.xrite.com/documents/literature/gmb/en/spectrolino_serial_5_en.pdf >, *Xrite,* Spectralino SpectraScan, 2009

[6] W. Chau, and W.B. Cowan, “Gamut Mapping Based on the Fundamental *Components of Reflective Image Specifications”*, *Proceedings of 4th IS&T/SID Color Imaging Conference*, 67-70.

[7] Ian E. Bell, Ian Bell Consulting, Simon K. Alexander, “A Spectral Gamut-Mapping Environment with Rendering Parameter Feedback”, *Eurographics*, 2004

[8] Arne M. Bakke, Ivar Farup, and Jon Y. Hardeberg , “Multispectral gamut mapping and visualization: a first attempt”, *SPIE, Color Imaging X: Processing*, Hardcopy, and Applications, Reiner Eschbach, Gabriel G. Marcu, Editors, 193-200, 2005

[9] L. Yang and S.J. Miklavcie, “Theory of Light Propagation incorporating scattering and absorption in turbid media”, *Opt. Lett.,* 30, 792-794, 2005

[10] <http://www.answers.com/topic/principal-components-analysis>, *Mathworld*, Principal Component Analysis, 2009

[11] < http://mathworld.wolfram.com/LeastSquaresFitting.html>, *Mathworld*, Least Square Fitting, 2009

[12] <http://www.bibl.liu.se/liupubl/disp/disp97/tek492s.htm>, *Dot Gain in Colour Halftones*, 2007

[13] <http://en.wikipedia.org/wiki/Radial_basis_function>, *Wikipedia*, Radial Basis Functions, 2009

[14] P. Kubelka and F. Munk, “Ein beitrag zur optik der farbanstriche”, *Z. Tech. Phys.* 12, 593–601, 1931

[15] Di-Yuan Tzeng, “Spectral Based Color Separation Algorithm Development for Multiple Ink Color Reproduction”, *PhD Thesis*, Rochester Institute of Technology, 1988

[16] Li Yang, Ink-Paper Interaction, “A Study in Inkjet Color Reproduction”, *PhD Thesis*, Linkiping University, 2003

[17] Murray, A., “Monochrome Reproduction in Photoengraving”, *J. Franklin Inst.* 221,721-744, 1936

[18] Neugebauer, H. E. J., “Die Theoretischen Grundlagen des Mehrfarbenbuchdrucks”, (German) *Zeitschrift für Wissenshaftliche Photographie Photophysik und Photochemie* 36:4, 73-89 (1937) [Reprinted in Proc. SPIE 1184: Neugebauer Memorial Seminar on Color Reproduction, 194-202, 1989

[19] Demichel, M. E., *Procédé* 26, 17-21, 26-27, 1924

[20] Yule, J. A. C., “Principles of Color Reproduction”, *John Wiley & Sons, Inc,* 255, 1967

[21] Wyble, D., Berns, RS., “A Critical Review of Spectral Models Applied to Binary Color Printing”, *Rochester Institute of Technology*, 1999

[22] Yule JAC, Nielsen WJ. “The penetration of light into paper and its effect on halftone reproduction,” *Proc. TAGA*, 1951

[23] Balasubramanian R. “A printer model for Dot-on-Dot halftone screens.”, Proc SPIE, *Color hard copy and graphic arts IV*, Vol, 2413, p. 356-364, 1995

[24] Heuberger KJ, Jing ZM, Persiev S. “Color transformations and lookup tables”. *TAGA/ISCC Proc*; p 863–881, 1992

[25] Kohler. T., Berns, RS., “Reducing metamerism and increasing gamut using five or more colored inks”, *Proc. of IS&T Third Technical Symposium on Prepress, proofing and Printing*, pg. 24, 1993

[26] Tzeng, DY., Berns, RS., “Spectral-Based Six-Color Separation Minimizing Metamerism”, Proc. CIC, *The Eighth IS&T/SID Color Imaging Conference*, 2000

[27] DY. Tzeng and R. Berns, “Spectral-Based Ink Selection for Multiple-Ink Printing I. Colorant Estimation of Original Objects”, Proc*. IS&T/SID Seventh Color Imaging Conference: Color Science*, Systems and Applications, Scottsdale, pg. 106-111, 1998

[28] DY. Tzeng and R. Berns, “Spectral-Based Ink Selection for Multiple-Ink Printing II. Optimal Ink Selection”, *Proc. IS&T/SID Seventh Color Imaging Conference: Color Science, Systems and Applications*, Scottsdale, pg. 182-187, 1999

[29] DY. Tzeng., “Spectral-based color Separation algorithm development for multiple-ink color reproduction”, *Ph.D. Dissertation*, Rochester Institute of Technology, 1999

[30] David Connah, Ali Alsam, Jon Hardeberg, “Multi-Spectral Imaging: How many sensors do we need”, *Proc. IS&T/SID Twelfth Color Imaging Conference*, pg 53-58, 2004

[31] H. F. Kaiser, “The varimax criterion for analytical rotation in factor analysis”, *Psychometrika*, 23, 187, 1958

[32] P. D. Burns, “Analysis of image noise in multispectral color acquisition,” *Ph.D. thesis, Center for Imaging Science*, Rochester Institute of Technology 1997

[33] F. K¨onig andW. Praefcke, “A multispectral scanner”, in L.W. MacDonald and M. R. Luo, editors, *Colour Imaging: Vision and Technology*, John Wiley and Sons Ltd, pp. 129-144, 1999

[34] H. Sugiura, T. Kuno, N. Watanabe, N. Matoba, J. Hayashi and Y. Miyake, “Development of high accurate multispectral cameras”, *in Proceedings of the International Symposium on Multispectral imaging and Color Reproduction* for Digital Archives, Chiba University, Japan, pp. 73-80, 1999

[35] J. K. Eem, H. D. Shin and S. O. Park, “Reconstruction of surface spectral refectances using characteristic vectors of Munsell colors”, in *Proceedings of IS&T and SID's 2nd Color Imaging Conference: Color Science, Systems and Applications*, Scottsdale, Arizona, pp. 127–31, 1994

[36] L. T. Maloney, “Evaluation of linear models of surface spectral reflectance with a small number of parameters”, *Journal of the Optical Society of America* - A, 3(10), 1673, 1986

[37] J. Parkkinen, J. Hallikainen and T. Jaaskelainen, “Characteristic spectra of Munsell colors, *Journal of the Optical Society of America* - A, 6, 318, see http://cs.joensuu.fi/spectral, 1989

[38] W. Wang, M. Hauta-Kasari and S. Toyooka, “Optimal lters-design for measuring colors using unsupervised neural network”, *in Proceedings of the 8th Congress of the International Colour Association*, AIC Color 97, Kyoto, Japan, vol. I, pp. 419-422, 1997

[39] J. Y. Hardeberg, “On the spectral dimensionality of object colors”, in *Proceedings of CGIV'2002, First European Conference on Colour in Graphics*, Imaging, and Vision, Poitiers, France, pp. 480-485, 2002

[40] A. Johnson and D. W. Wichern, “Applied Multivariate Statistical Analysis”, *3rd Ed. Prentice Hall*, New York, 459-486, 1992

[41] J. L. Simonds, “Application of Characteristic Vector Analysis to Photographic and Optical Response Data”, *Journal of Optical Society of America*. 53, No. 8, 968-974, 1963

[42] D. B. Judd, D. L. MacAdam, and G. Wyszecki, “Spectral Distribution of Typical Daylight as a Function of Correlated Color Temperature”, *Journal of Optical Society of America*, 54, No. 8, 1031- 1040, 1964

[43] N. Ohta, “Estimating Absorption Bands of Component Dyes by Means of Principal Component Analysis”, *Analytical Chemistry,* 45, 553-557, 1973

[44] J. Morovic, M. Lou, "The fundamental of Gamut Mapping: A Survey", *Journal of Imaging Science and Technology*, vol. 45, no. 3, 2001

[45] McDonald, L.W., “Gamut Mapping in Perceptual Color Space”, *Proceeding 1st IS&T/SID Color Imaging Conference*. Springfield, VA, 1993, 193-196

[46] R. S. Gentile, E. Walowitt and J. P. Allebach, “A comparison of techniques for color gamut mismatch compensation”, *Journal of Imaging Technology*, vol. 16, pp. 176-181, 1990

[47] E. D. Montag and M. D. Fairchild , “Gamut mapping: Evaluation of chroma clipping techniques for three destination gamuts*.” IS&T/SID Sixth Colour Imaging Conference*, Scottsdale, 1998, p. 57-61

[48] Mitchell Rosen, N. Ohta, “Spectral Color Processing using an Interim Connection Space”, *IS&T/SID Twelfth Colour Imaging Conference*, Scottsdale, 2004, p. 187-192

[49] Mitchell Rosen, F. Imai, X. Jiang, N. Ohta, “Spectral Reproduction from Scene to Hardcopy II: Image Processing”, *Proceedings of SPIE, the International Society for Optical Engineering*, 33-41, 2001

[50] L. Taplin, R. Berns, “Spectral Color Reproduction Based on a Six Color Inkjet Output System”, *Proc. IS&T/SID Ninth Color Imaging Conference*, 209-213, 2001

[51] DY. Tzeng, R. Berns, “Spectral Based Six Color Separation Minimizing Metamerism”, *Proc. IS&T/SID Eighth Color Imaging Conference*, pg 342-347, 2000

[52] Y. Chen, R. Berns, L. Taplin, F. Imai, “A Multi-Ink Color Separation Algorithm Maximizing Color Constancy”, *Proceeding of IS&T/SID Eleventh Color Imaging Conference*, 277-281, 2003

[53] P. Urban, R. Grigat, “Spectral Based Color Separation Using Linear Regression Iteration”, *Wiley Periodical*, Vol. 31, No. 3, 229-238, 2006

[54] P. Urban, M. Rosen, R. Berns, “Fast Spectral-Based Separation of Multispectral Images”, *Proceeding of IS&T/SID Fifteenth Color Imaging Conference*, 2007

[55] A. Bakke, Ivar Farup, J. Hardeberg, ”Multi-Spectral Gamut Mapping and Visualization – A first attempt”, SPIE, *Color imaging X : processing, hardcopy, and applications,* Vol 5667, 193-200, 2005

[56] H. Haneishi and Y. Sakuda, “Representing Gamut of Spectral Reflectance by a Polyhedron in High Dimensional Space,” *in Proceedings of the Third International Conference on Multispectral Color Science* (MCS’01), pp. 5–8, 2001

[57] M. Derhak, M. Rosen, “Spectral Colorimetry Using LabPQR – An Interim Connection Space”, *Proceeding of IS&T/SID Twelfth Color Imaging Conference*, 246-250, 2004

[58] S. Tsutsumi, M. Rosen, R. Berns, “Spectral Reproduction Using LabPQR: Inverting the Fractional-Area-Coverage-to-Spectra Relationship”, *Proceeding of IS&T/SID Fourteenth Color Imaging Conference*, 107-110, 2006

[59] S. Tsutsumi, M. Rosen, R. Berns, “Spectral Color Reproduction Using an Interim Connection Space-Based Lookup Table”, *Proceeding of IS&T/SID Fifteenth Color Imaging Conference*, 184-189, 2007

[60] B. Bastani, B. Funt, J. Dicarlo, “Spectral Reproduction – How many primaries are needed?”, *Proceeding of NIP23, 23rd International Conference on Digital Printing Technologies and Digital Fabrication*, Anchorage, Alaska, 410-413, 2007

[61] Xiong, W., Shi, L., Funt, B., "Illumination Estimation via Thin-Plate Spline Interpolation", *Proceeding of IS&T/SID Fifteenth Color Imaging Conference*, 2007

[62] J. B. Tenenbaum, V. de Silva, J. C. Langford (2000). "A global geometric framework for nonlinear dimensionality reduction", *Science* 290 (5500): 2319-2323, 22, 2000

[63] G.A.F. Seber, *Multivariate Observations”*, *Wiley*, 1984

[64] B. Bastani, B. Cressman, B. Funt, "Calibrated Color Mapping Between LCD and CRT Displays: A Case Study", *Color Research and Application*, Volume 30, Issue 6, Date: December 2005, Pages: 438-447

[65] Barnard, K. Martin, L., Funt, B.V. and Coath, A., "A Data Set for Color Research", *Color Research and Application*, vol. 27, no. 3, pp. 140-147, 2002. (Data from: www.cs.sfu.ca/~colour)

[66] J. Ferguson , P. A. Staley, “Least squares piecewise cubic curve fitting”, *Communications of the ACM*, Volume 16 , Issue 6, 1973

[67] G. Finlayson, S. Hordley and I. Tastl, "Gamut Constrained Illuminant Estimation", *International Journal of Computer Vision*, vol. 67 , no. 1, 2006

[68] B. Bastani, B. Cressman, M. Shaw, "Sparse Cellular Neugebauer Model for N-ink Printers," *Proceeding of IS&T/SID Fourth Color Imaging Conference: Color Science, Systems and Applications*, Scottsdale, pp. 58-60, 1996

[69] N. Katoh and M. Ito, "Applying Non-linear Compression to the Three-dimensional Gamut Mapping", *The Journal of Imaging Science and Technology*, vol. 44, no. 4, pp. 328-333, 1999

[70] T. Cholewo and S. Love, "Gamut Boundary Determination Using Alpha-Shapes," *Proceeding of IS&T/SID Seventh Color Imaging Conference: Color Science, Systems and Applications*, Scottsdale, pp. 200-204, 1999

[71] C. McIntosh and G. Hamarneh "Is a Single Energy Functional Sufficient? Adaptive Energy Functionals and Automatic Initialization", *In Lecture Notes in Computer Science, Medical Image Computing and Computer-Assisted Intervention (MICCAI)*, pp. 503-510, 2007

[72] Z. Ma, Y. Bi, Inventor; Hewlett-Packard Company, "Inkjet Inks Having Reduced Bronzing", *International Patent PCT/US2006/017315*, 2005

[73] L. Tsang, J. Moffatt, M. Austin, Inventor; Hewlett-Packard Company, "Additives to eliminate bronzing of inkjet ink formulations on specialty quick-dry inkjet photographic media", *United States Patent US 7052535*, 2006

[74] < http://www.aviangroupusa.com/MCRL_GCMS.php> , Murakami *GonioSpectrophotometer*, 2008

[75] Li Yang, "Light Media Interaction in print color reproduction", *Proc. NIP22, 22nd International Conference on Digital Printing Technologies and Digital Fabrication*,, Tutorial, 2006

[76] Bastani, B, Funt, B, Dicarlo, J, "Spectral Reproduction- How Many Primaries Are Needed?", *Proc. NIP23, 23rd International Conference on Digital Printing Technologies and Digital Fabrication*, Alaska, p. 410-413, 2007

[77] Bastani, B, Funt, B, "Spectral Gamut Mapping and Gamut Concavity", *Proceeding of IS&T/SID Fourteenth Color Imaging Conference: Color Science, Systems and Applications,* Albuquerque, NM, p. 218-221, 2007

[78] Bastani, B., Funt, B., "Spectral Modeling of an n-Ink Printer via Thin Plate Spline Interpolation", *Proc. NIP24, 24th International Conference on Digital Printing Technologies and Digital Fabrication*, 2008

[79] Bastani, B., Funt, B., "Geodesic Based Ink Separation for Spectral Printing", *Proceeding of IS&T/SID Sixteenth Color Imaging Conference: Color Science, Systems and Applications*, 2008

[80] <http://www.mathreference.com/ca-int,simp.html>,*Mathreference*, The Volume of a Simplex, 2008

[81] Sharma G, editor, “Digital Color Imaging Handbook”, *CRC Press*, Boca Ranton, FL, 2003

[82] Li, X., Li, CJ, Luo, M. R., Pointer, M., Cho, M. and Kim, J., “A New Colour Gamut for Object Colours”, *Fifth Colour Imaging Conference*, pages 283-287, 2007

[83] Han J, Kamber M, "Data Mining: Concepts and techniques*", Chapter 8*, pp335-485, Morgan Kaufmann, 2001

[84] < http://www.cis.rit.edu/mcsl/online/cie.php >, *RIT Useful Color Data*, 2009

[85] B. Bastani, B. Funt, “Spectral Gamut Characteristics Based on Number of Primaries and Their Characteristics”, *Proc. NIP25, 25rd International Conference on Digital Printing Technologies and Digital Fabrication*, Louisville, Kentucky, 410-413, 2007

[86] Joshua B. Tenenbaum, Vin de Silva, and John C. Langford, “A Global Geometric Framework for Nonlinear Dimensionality Reduction”, *Science 22* 2319-2323, 200

[87] R. Balasubramanian, “Optimization of the spectral Neugebauer model for printer characterization”, *Journal of Electronic Imaging*, Vol. 8, 156, 1999

[88] < http://mathworld.wolfram.com/DijkstrasAlgorithm.html>, Wolfram Mathworld, 2009

[89] F. Nakaya and N. Ohta, “Spectral encoding / decoding using LabRGB”, *Fifteenth Colour Imaging Conference,* 2007

[90] F. Nakaya and N. Ohta, “Applying LabRGB to Real Multi-Spectral Images”. , *Sixteenth Colour Imaging Conference,* 2008

[91] <http://en.wikipedia.org/wiki/Thin_plate_spline>, *Wikipedia*, Thin Plate Spline, 2009

[92] < http://www.mathworks.com/support/tech-notes/1500/1508.html>, *Matlab*, Curve Fitting